EFFECT OF CHROMOSOMAL COPY NUMBER VARIATIONS ON CONGENITAL BIRTH DEFECTS AND HUMAN DEVELOPMENTAL DISORDERS

APPROVED BY SUPERVISORY COMMITTEE

Andrew R. Zinn, M.D., Ph.D

Christine K. Garcia, M.D., Ph.D

Orson Moe, M.D., Ph.D

Ralph DeBerardinis, M.D., Ph.D

DEDICATION

Many many people have given me love, support, advice, and caffeine over the course of my graduate research to which I am eternally grateful. To Andrew, my mentor for many years and scientific guide- if someday I become half the researcher you are, I will have turned out. There aren't enough words- thank you, thank you, thank you.
To my thesis committee- thank for your insightful comments, direction and criticism and most for your genuine desire to see me succeed.
To my collaborators, Vidu Garg and Linda Baker- thank you for sharing your research with a lowly grad student. I would literally have nothing to research without your generosity.
To the lab-thanks for listening to boring mitochondrial results each week. I will miss you terribly.
To Miguel- No puedo poner a las palabras la profundidad de mi amor para usted. Usted es mi amigo, mi amor, mi corazón, mi amante, mi ayuda y mi ancla. Con usted por mi lado puedo lograr las cosas magníficas que no podría solamente. Te amo.
To Justin- the talk of complex four late at night was worth it. Love you.
To Kim, Kristen and Adriane- my absolute favorite people- thank you for believing even when I did not. Thank you for listening to me when I needed it most.
To my family, (Maman, Daddy, Adriane, Salvador, Grandmother, Aunt E, Kathy, Don, Aaron, Tracy, Amy, Tim, Ellen, Greg, Jack, Emma, Zoë, Courtney, Chris, Carol, Ken, Jim, Grace, Ann, Robert, Joanie, Magikhana, Julie and Mike) thank you for your constant love and reassurance. Your confidence in my abilities continues to amaze me. I know you all individually believe I will change the world and make it a better place from the research I will do. I do not take this lightly and will work very hard not to disappoint.
To the Santos clan (Beto, Carmen, Beto, Elizabeth, Stacy, Tatan and too many others to name) thank you for accepting a science nerd into the family and taking my ambitious scientific pursuits in stride and with grace. To the dead but not forgotten: Granddaddy, Grandma and Grandpa- I know you were here, too.

~Thank you~

EFFECT OF CHROMOSOMAL COPY NUMBER VARIATIONS ON CONGENITAL BIRTH DEFECTS AND HUMAN DEVELOPMENTAL DISORDERS

by

LANE JOHANNA JAECKLE SANTOS

DISSERTATION

Presented to the Faculty of the Graduate School of Biomedical Sciences

The University of Texas Southwestern Medical Center at Dallas

In Partial Fulfillment of the Requirements

For the Degree of

DOCTOR OF PHILOSOPHY

The University of Texas Southwestern Medical Center at Dallas

Dallas, Texas

June, 2009

EFFECT OF CHROMOSOMAL COPY NUMBER VARIATIONS ON CONGENITAL BIRTH DEFECTS AND HUMAN DEVELOPMENTAL DISORDERS

Lane Johanna Jaeckle Santos, Ph.D.

The University of Texas Southwestern Medical Center at Dallas, 2009

Andrew Robert Zinn, M.D. /Ph.D.

Congenital birth defects are the leading cause of death in the first year of life and the majority of severe congenital anomalies are the result of changes in chromosomal number or structure. The genetic basis of several different congenital malformations including heart defects and urogenital/anorectal defects were explored. A critical region for hypospadias, penoscrotal transposistion and imperforate anus commonly seen in chromosome 13q deletion syndrome was refined, implicating loss of *EFNB2* as a possible cause of their formation. Array comparative genomic hybridization was used to show that a significant number of children with congenital heart defects harbor cryptic chromosomal copy number variants, and patients presenting with additional neurological anomalies such as developmental delay highly increase the likelihood of discovering such copy number variants. A novel microdeletion syndrome was discovered using array comparative genomic hybridization that deletes 260 kb on chromosome Xq24 and includes the mitochondrial adenine nucleotide translocase, ANT2. This is the first described mitochondrial disorder characterized by both mitochondrial dysfunction and congenital heart defects and implicates mitochondrial dysfunction as the basis for certain congenital birth defects.

TABLE OF CONTENTS

PRIOR PUBLICATIONS

Garcia NM, Allgood J, **Santos LJ**, Lonergan D, Batanian JR, Henkemeyer M, Bartsch O, Schultz RA, Zinn AR, Baker LA (2006) Deletion mapping of critical region for hypospadias, penoscrotal transposition and imperforate anus on human chromosome 13. J Pediatr Urol 2: 233-242

Jenkins D, Bitner-Glindzicz M, Thomasson L, Malcolm S, Warne SA, Feather SA, Flanagan SE, Ellard S, Bingham C, **Santos L**, Henkemeyer M, Zinn A, Baker LA, Wilcox DT, Woolf AS (2007) Mutational analyses of UPIIIA, SHH, EFNB2 and HNF1beta in persistent cloaca and associated kidney malformations. J Pediatr Urol 3: 2-9

Richards AA*****, **Santos LJ***, Nichols HA, Crider BP, Elder FF, Hauser NS, Zinn AR, Garg V (2008) Cryptic chromosomal abnormalities identified in children with congenital heart disease. Pediatr Res
***** *authors contributed equally*

Jaeckle Santos LJ, Xing C, Barnes RB, Ades LC, Megarbane A, Vidal C, Xuereb A, Tarpey PS, Smith R, Khazab M, Shoubridge C, Partington M, Futreal A, Stratton MR, Gecz J, Zinn AR (2008) Refined mapping of X-linked reticulate pigmentary disorder and sequencing of candidate genes. Hum Genet 123: 469-76

Jaeckle Santos LJ, Baker LA, Garg V, Zinn AR (2009) Life without ANT2: oxidative stress and apoptosis. Manuscript in preparation.

LIST OF FIGURES

LIST OF TABLES

LIST OF APPENDICES

LIST OF DEFINITIONS

aCGH – array comparative genomic hybridization

CNV – copy number variation

FISH – Fluorescence in situ hybridization

bp – base pairs of DNA

CHD – congenital heart disease

XLPDR – X-linked Reticulate Pigmentary Disorder

IP- Incontinentia Pigmenti

Mb – Mega bases, 1,000,000 base pairs of DNA

Kb- kilo bases, 1,000 base pairs of DNA

XLMR – X-linked Mental Retardation

LOH- loss of heterozygosity

RT-PCR – Reverse Transcriptase Polymerase Chain Reaction

OXPHOS- Oxidative Phosphorylation

BAC- Bacterial artificial chromosome

BrDU- Bromodeoxy uridine

FACS- fluroscence activated cell sorting

PBS- phosphate buffered saline

CCCP- carbonyl cyanide *m*-chlorophenylhydrazone

NAO- nonyl acridine orange

DHE- dihydroethidium

PI- propidium iodide

FBS- fetal bovine serum

NADH- Nicotinamide adenine dinucleotide

ND1- NADH dehydrogenase subunit 1

ND4- NADH dehydrogenase subunit 4

mtDNA- mitochondrial DNA

JC-1- 5,5',6,6'-tetrachloro-1,1',3,3'-tetraethylbenzimidazolylcarbocyanine iodide

CPEO- chronic progressive external opthalmoplegia

ASD/VSD- atrial septal defect, ventricular septal defect

ANT2- Adenine nucleotide translocase 2, also known as SLC25A5

ANT1- Adenine nucleotide translocase 1, also known as SLC25A4

UBE2A- ubiquitin conjugating enzyme E2 , 1A

NKRF- NFκB repressing factor

CXorf56- chromosome X open reading frame 56

EFNB2- ephrin B2

RB- retinoblastoma 1

ZIC2- zinc finger protein of the cerebellum 2

SHH- sonic hedgehog preproprotein

BMP- bone morphogenetic protein

FGF- fibroblast growth factor

HOXA13- homeobox A13

GLI- glioma-associated oncogene 1

NEMO- nuclear factor κB kinase (IKKγ)

NFκB- nuclear factor kappa B

SNP- single nucleotide polymorphism

ACOT9- acyl-Coenzyme A thioesterase 2, mitochondrial

SAT1- spermidine/spermine N1-acetyltransferase

GRPR- gastrin-releasing peptide receptor

PRDX4- thioredoxin peroxidase

LOD- logarithm (base 10) of odds

SMS- spermidine aminopropyltransferase, aka spermine synthase

RFLP- restriction fragment linked polymorphism

ACA12- SCARNA23, small Cajal body-specific RNA 23

POLA- polymerase (DNA-directed), alpha

DKC1- dyskerin

snRNA- small nucleolar RNA

CHAPTER ONE
Introduction

The work presented in this thesis is the result of studies aimed at resolving the genes responsible for various congenital birth defects as well as a congenital inflammatory disorder. Chapter 2 details the investigation of the genetic basis of urogenital and anorectal malformations in patients with deletions of the long arm of chromosome 13, by refining a critical region of the chromosome necessary for the formation of these defects. Chapter 3 presents studies that narrowed the location of the genetic cause of X-linked reticulate pigmentary disorder (XLPDR), a chronic disease of unchecked cutaneous and visceral inflammation with unknown genetic etiology. Chapter 4 studies the prevalence of cryptic chromosomal abnormalities found in patients with congenital heart disease, which are responsible for the largest number of fatalities in the first year of life. Chapter 5 presents a novel contiguous gene deletion syndrome found in a patient with multiple congenital anomalies which arise at least in part from mitochondrial disease.

The studies herein are strategically designed to take advantage of rare and unusual patients and families seen at UT Southwestern Medical Center/Children's Medical Center of Dallas by a number of clinical collaborators, especially Dr. Linda Baker, a pediatric urologist, Dr. Vidu Garg, a pediatric cardiologist, and Dr. Robin Carder, a pediatric dermatologist. A constant theme throughout my thesis is the use of recent and even state of the art genetic technologies to study the genetic basis of human congenital disease, including microsatellite genotyping, large scale resequencing, and array comparative genomic hybridization all of which is made possible by the Human Genome Project. The remainder of chapter 1 is an introduction to the genetics of congenital birth defects. X-linked reticulate pigmentary disorder does not involve a specific birth defect, and as such, an introduction to my studies of this disease is presented only in chapter 4.

Causes of congenital birth defects

Both environmental and genetic factors have roles in the development of any human disease. Genetic disease originates from deleterious changes to an individual's genome that in disease and perturbed normal functioning. The most common kind of disease causing genetic changes are chromosomal, and affects the number or structure of the 46 human chromosomes. These changes vary from entire chromosomes to several thousand base pairs in length.

Each year, about 1 in 150 babies are born with a chromosomal abnormality affecting the size or structure of the chromosomes (Carey 2003). There are many different chromosomal abnormalities that have been described, and most children with a chromosomal abnormality also have mental and/or physical birth defects. Studies of chromosomal aberrations in patients with congenital defects have provided extremely valuable insight into the progression of congenital malformations and the genes that regulate these developmental processes.

Birth defects in the general population

About 3% of babies (1 in 33) in the United States are born each year with congenital birth defects (Kumar 2005) which are defined as an abnormality of structure, function or metabolism present at birth that results in physical or mental disabilities and often death. Anomalies can be macroscopic or microscopic, and present on the surface or within of the body. Additional defects sometimes manifest after birth, which increases in incidence to 8% by 5 years of age (Nelson and Holmes 1989).

Congenital malformations are the leading cause of death in the first year of life, and contribute significantly to morbidity and mortality throughout the early years of life (Martin et al. 2005). Recognized causes of congenital anomalies are genetic, environmental and multifactorial, but genetics accounts for the largest percentage and most are the result of chromosomal abnormalities (Nussbaum Robert L. 2007). The high rate of mortality, coupled with obvious genetic involvement, makes the study of chromosomal anomalies associated with congenital malformations both appealing and critical to the understanding of human embryonic development and future treatment options for children born with congenital birth defects.

Several thousand different birth defects have been identified, but can generally be divided into four main categories of malformations: congenital defects of the heart, neural tube defects, gastrointestinal and urogenital defects or limb defects. All other physical anomalies have a combined incidence of 6 per 1000 live births (Kumar 2005). The most common malformations are listed below in Table 1-1.

Malformation	Frequency per 10, 000 total births
Clubfoot without CNS anomalies	25.7
Patent ductus arteriosus	16.9
Ventricular septal defects	10.9
Cleft lip with or without cleft palate	9.1
Spina bifida without anencephalus	5.5
Congenital hydrocephalus without anencephalus	4.8
Anencephalus	3.9
Reduction deformity (musculoskeletal)	3.5
Rectal and intestinal atresia (includes imperforate anus)	3.4

Frequency of the more common congenital malformations in the United States. Adapted from (James 1993).

Cardiovascular defects

Congenital anomalies of the heart account for 28% of infant deaths due to congenital anomaly, and have the highest risk of death in infancy (Kumar 2005). Seventy years ago, less than 30% of children with severe congenital heart defects survived to adulthood. Today, more than 85% of affected children now reach adulthood due to advances in surgical intervention (Leong et al. 2009). Transposition of the great arteries is the most common congenital heart defect and affects about 1,900 newborns a year. This serious heart defect results when the spatial arrangement of any of the great vessels is disrupted. Slightly less common heart defects include atrioventricular septal defects, which involve deficiencies of the atrioventriculum of the heart and hypoplastic left heart syndrome which is characterized by underdevelopment of the left side of the heart (CDC 2006). Many more infants are born with other serious heart defects including Tetralogy of Fallot, which is diagnosed by the presence of four heart anomalies which present together (Higgins and Reid 1994). While advances in surgery have dramatically improved the outlook for affected newborns, heart defects remain the leading cause of birth defect-related infant deaths (Kochanek et al. 2004).

Gastrointestinal and urogenital defects

The most prevalent gastrointestinal defects are esophageal atresia or tracheoesophageal fistula. More common are a spectrum of anorectal malformations that range from simple anal stenosis to persistence of cloaca (CDC 2006). Anorectal malformations have an incidence of 1 in 4000 to 5000 live births (Kumar 2005) and are slightly more common in boys. The most frequent defect is imperforate anus, which is caused by a malformation of the rectum that leaves no opening for the passage of feces. Imperforate anus is often present as a component of VACTERL syndrome, which involve vertebral, anorectal, cardiac, tracheoesophageal, renal and limb defects (Walsh et al. 2001). Hypospadias is the most common form of abnormal openings either ventrally or dorsally in the penis. It occurs in approximately 1 in 300 live male births, and is often associated with failure of normal descent of the testes (cryptorchidism) and with malformations of the urinary tract (Miller et al. 2009).

Other common birth defects include musculoskeletal defects, such as club foot and reduction defects of the upper and lower limbs (CDC 2006). Club foot is a common birth defect of the ankle and foot, occurring in about one in every 1,000 live births. Approximately 50% of cases of clubfoot are bilateral, and treatments include orthotic braces and or surgery. This condition, while common, is not thought to be life threatening (Morcuende and Weinstein 2003).

Genetic causes of specific birth malformations

Virtually all chromosomal syndromes are characterized by congenital anomalies and chromosomal aberrations that result in specific birth malformations are now discussed. (Nussbaum Robert L. 2007). Karyotypic anomalies are present in approximately 10-15% of patients with congenital birth defects but only trisomy 21 approaches a birth frequency of 1 in 1000 total births. Trisomy 21, also called Down Syndrome (47,XX or XY +21), is the result of three copies of part or all of chromosome 21. The medical consequences of the DNA copy number variation seen in Down syndrome are highly variable and may affect the function of many organ systems. Affected persons exhibit characteristic facial features, cognitive impairment, congenital heart disease, hearing deficits, short stature, Alzheimer's disease and reduced life expectancy (Moore 2008).

The next most common chromosomal anomalies are Klinefelter syndrome (47, XXY) and Turner syndrome (45, X). Klinefelter syndrome is caused by the presence of an additional X chromosome in males. It is the most common sex chromosome disorder and the second most common chromosomal disorder caused by the presence of extra chromosomes (Kumar 2005). Klinefelter syndrome affects 1 in 500 men resulting in reduced fertility and small testicles, and is thought to be a common cause of male infertility (Paduch et al. 2008). Turner syndrome is caused by monosomy of the X chromosome in females. The overall incidence of Turner syndrome is 1 in 2500 females and results in a diverse clinical phenotype. Affected females have short stature, webbing of the neck, reproductive sterility, severe heart defects and cognitive deficits (Nijhuis-van der Sanden et al. 2003).

DiGeorge syndrome is the most common chromosome microdeletion syndrome (1 in 4000 live births) and results from the loss of 3 Mb of DNA from chromosome 22q11, causing haploinsufficiency of approximately 40 genes (Leong et al. 2009). The mnemonic CATCH 22 can be used to describe the spectrum of anomalies commonly seen in DiGeorge syndrome patients: **C**ardiac defects, **A**bnormal facies, **T**hymic aplasia, **C**left palate, **H**ypocalcemia and chromosome **22**. One gene found in the deleted region, *Tbx1*, has been found to be chiefly responsible for the cardiovascular, craniofacial, thyroid and otic manifestations seen in DiGeorge syndrome patients (Bassett et al. 2005; Cohen et al. 1999; Yagi et al. 2003).

Chromosome 13q deletion syndrome is a chromosomal disorder with deletions of the distal portion of chromosome 13. The phenotype of 13q deletion syndrome includes growth retardation, developmental delay, microcephaly and other central nervous system malformations, eye abnormalities, dysmorphic facies, congenital heart defects, gastrointestinal anomalies, vertebral, limb and anorectal defects (Walsh et al. 2001). Specific breakpoints are associated with specific phenotypes, and distal deletions which include the 13q31.3-q32 region are associated with the most severe extra-CNS malformations (Brown et al. 1993; Brown et al. 1995; Fryns et al. 1980; Walsh et al. 2001).

Single gene mutations of large effect may underlie major congenital anomalies, which follow mendelian inheritance, and are thought to be responsible for 2-10% of congenital malformations. The study of chromosomal aberrations in persons with specific congenital birth defects allows for the identification of new candidate genes involved in development. However, more than 70% of congenital malformations have no known cause and despite excellent research attempts, many facets of embryonic development are not well characterized.

Genetic screening techniques

Genetic analysis by karyotype is standard when a patient presents with problems of early growth and development, including developmental delay, dysmorphic facies, and multiple malformations or mental retardation. G-banding karyotype is a well established method and has been used for many years to discern changes in chromosomal number or size (Nussbaum Robert L. 2007). When stained with Giemsa stain, each chromosome set exhibits a characteristic light and dark staining pattern that can be examined using microscopy. G-banding requires an expert cytogeneticist to analyze the karyotype and determine if chromosomal anomalies are present. If changes are found in chromosomal size or number, fluorescence in situ hybridization (FISH) can be preformed to confirm the presence of such perturbations using sequence and chromosome specific fluorescent probes.

The limit of resolution of G-banding is 5Mb, which is often not sensitive enough to identify smaller pathogenic deletions or duplications (de Ravel et al. 2007). Array comparative genomic hybridization (aCGH) has revolutionized clinical cytogenetics by enabling the detection of genome-wide DNA copy number alterations as small as 5 kb (Edelmann and Hirschhorn 2009). Array based methodology relies on the comparison of a reference genomic DNA isolated from a control subject to a test (patient) sample. Both samples are differentially labeled with fluorescent dyes and competitively hybridized to glass slides arrayed oligonucleotides, and analyzed for copy number variation between the two genomes based on changes in fluorescence.

Array CGH has been successfully used to discover copy number variations strongly associated with many diseases, largely due to the 1,000 fold increased sensitivity over standard karyotyping. However, the sensitivity of the assay has also led to the discovery of many copy number variants which appear to be present in the general population and are non-pathogenic. The challenge for researchers is then to discern which variants are likely disease causing and which are not, and is a continual issue when employing array based methodologies (Edelmann and Hirschhorn 2009).

When aCGH is used in conjunction with traditional karyotyping methods, it has proven very effective in revealing the presence of cryptic microdeletions or duplications that would otherwise have been missed, and thus has been instrumental in identifying and characterizing new genetic syndromes (Selzer et al. 2005; Urban et al. 2006). In patients with an unusual clinical presentation that includes developmental delay (Richards et al. 2008; Thuresson et al. 2007) there is a strong likelihood of discovering chromosomal copy number variants using aCGH.

Many of the patients described in this body of research are the result of an open collaboration between campus clinicians and the laboratory of Andrew Zinn. Essentially, when a collaborating clinician sees a patient who presents with a spectrum of anomalies including developmental delay, short stature, multiple affected organ systems or congenital defects, all of which indicate the likelihood of a chromosomal anomaly, DNA is collected and chromosomal integrity is assayed using karyotyping and aCGH. This method has resulted in the identification of several novel copy number variants that contribute to disease (Bhoj et al. 2009; Holder et al. 2004), aided in refinement of critical regions of deletions necessary for development of disease (Garcia et al. 2006; Zinn et al. 2007) and it continues to be the focus of this laboratory to identify novel DNA copy number variants and genes that contribute to congenital malformations or developmental diseases.

The entirety of my work has been to elucidate the genetic basis of different congenital birth defects and developmental disorders using a multitude of genetic techniques including array based genomic hybridization. The broad range of techniques has enabled the restriction of the critical region on chromosome 13q for hypospadias, imperforate anus and penoscrotal transposition phenotype seen in patients with chromosome 13q deletion syndrome. The refinement implicates ephrin B2 (*EFNB2*) as an important gene involved in normal genitourinary and anorectal development.

Next, I used microsatellite linkage to narrow the critical region for the genetic basis of XLPDR to a 4.9 Mb region, and sequencing allowed the elimination of many candidate genes in the region as the cause of this rare disease. Array CGH was utilized to show that patients with congenital heart disease frequently harbor cryptic copy number variants undetectable by traditional karyotyping, and chromosomal anomalies are more likely to be present if patient also presents with developmental delay. Finally, I identified a novel mitochondrial disorder caused by a 260 kb microdeletion on chromosome Xq24 that includes the adenine nucleotide translocase ANT2. This is the first mitochondrial disorder described that is associated with congenital anomalies and mitochondrial dysfunction.

CHAPTER TWO

Deletion mapping of chromosome 13 q-arm critical region for anorectal and urogenital malformations

BACKGROUND

Congenital urogenital and anorectal malformations

Urogenital and anorectal congenital birth defects occur frequently in the general population. Imperforate anus is a relatively common anorectal malformation, estimated to occur in 5 out of every 10,000 live births (Golalipour et al. 2007). Hypospadias, a urogenital malformation of the penis, is the second most common human birth defect, affecting 1 in 125 male births (Paulozzi 1999). It also appears that the incidence of hypospadias in the general population is increasing, possibly from environmental exposure to "endocrine disruptors"(Fisher 2004; Sharpe 2003). Despite excellent research attempts, the molecular mechanisms and factors that govern embryonic events such as penoscrotal positioning, urethral tubularization, cloacal septation, and closure of the perineum and how each contributes to congenital birth defects are not well understood. Furthermore, despite the commonality of these birth defects in the general population their etiology is mostly unknown. Understanding the genetic, molecular and developmental mechanisms that govern the proper formation of urogenital and anorectal morphology will undoubtedly be important as we endeavor to correct and prevent such birth defects.

Chromosome 13 q arm deletion syndrome

Chromosome 13q deletion syndrome is a chromosomal copy number variation syndrome which results in multiple congenital birth defects, including neurological, urogenital and anorectal, cardiovascular, auditory and dysmorphic anomalies. The syndrome was first described in 1969 (Allderdice et al. 1969), and as the name suggests, arises from the loss of one of the two copies of the long arm (q) of chromosome 13. Studies of 13q deletions by Bartsch and colleagues (Bartsch et al. 1996; Kuhnle et al. 2000) led to associations of penoscrotal inversion, hypospadias, reduced anogenital distance, imperforate anus, facial anomalies and developmental delay with 13q33.2- q terminus deletions. This suggested the presence of critical genes in 13q32.2-q34 that mediate genitourinary and anorectal malformations (Allderdice et al. 1969). Furthermore, ambiguous genitalia in males (Brown et al. 1995; Gutierrez et al. 2001; Luo et al. 2000), and absent or bicornuate uterus, imperforate anus with vaginal fistula or cloaca in females have all been associated with distal 13q deletions (Brown et al. 1993). It therefore seems likely that loss of one copy of one or more distal 13q genes results in these phenotypes.

Cytogenetic karyotyping is standard testing for children with multiple congenital birth defects, but accuracy and resolution is limited to chromosomal changes that are larger than 5 Mb, making associations with individual genes difficult. In this study, molecular markers were used to improve resolution in mapped distal 13q deletions and to refine the critical region for urogenital and anorectal malformations in an effort to identify candidate genes for these birth defects.

METHODOLOGY

Patient recruitment and phenotype analysis

Using University of Texas Southwestern Institutional Review Board-approved methods, patients were ascertained with karyotypes revealing haploinsufficiency for distal chromosome 13q (distal 13q deletion) via medical record review and search of cytogenetics databases. Patients and their family members were recruited through local sources and international collaborators. Detailed phenotypic data were collected from interviews with parents and physicians as well as from medical records. When available, local subjects were clinically evaluated by Dr. Linda Baker, an experienced pediatric urologist, documenting phenotype.

Genotype Mapping

Peripheral blood samples were collected from probands, their available parents, and any other affected family members. Epstein-Barr virus-immortalized lymphoblastoid cell lines were generated by standard methods from proband blood. Genomic DNA was extracted from all remaining family members' blood samples. 13q deletions were mapped to high resolution by testing for loss of heterozygosity (LOH) of 20 polymorphic microsatellite markers from the ABI PRISM® Linkage Mapping Set version 2.5 (Applied Biosystems, Foster City, CA, USA), supplemented by custom markers chosen from the genome database (www.gdb.org). One marker was specifically designed to amplify a polymorphic CA dinucleotide repeat within the ephrin-B2 (*EFNB2*) gene. For samples without parental DNAs or where key markers were not informative, fluorescence *in-situ* hybridization (FISH) was performed on proband lymphoblastoid metaphase preparations using probes from our panel of 35 BAC clones from the same chromosomal region (BACPAC Resource Center, Children's Hospital Oakland Research Institute, Oakland, CA, USA; (http://bacpac.chori.org/).

Determination of critical region by genotype-phenotype correlation

The data were synthesized and a deletion map defining the critical region was generated. Critical regions for urogenital and anorectal phenotypes were defined by the minimal overlap among deletions in patients with urogenital and/or anorectal phenotypes. With the possible exception of hypospadias, which is relatively common, 13q- patients with a genitourinary or anorectal anomaly should be deleted for the critical region for that phenotype. However, every patient who is deleted for the critical region will not necessarily have the associated phenotype, because haploinsufficiency of the culprit gene may show incomplete penetrance. Thus, we defined the critical region by comparing the deletions among only those patients with the phenotype in question.

Generation of the candidate gene list from annotated databases

A refined list of genes in the critical region was generated from the most current version of the UCSC Genome Browser. Functional genomic databases (e.g. GeneCards) and the PubMed literature database were searched to evaluate current knowledge about these genes regarding embryonic expression and known or suspected function in developmental signaling pathways.

RESULTS

Ten probands with known chromosome 13q32- qter and 24 related family members were recruited for this study (Table 2-1). Two patients whose deletions proved to be proximal to our region of interest were excluded and the remaining eight were analyzed. The phenotypic analysis of the eight probands is summarized in Table 2-2. Six of the eight probands were newly recruited for this study; the remaining two were obtained from Dr. Oliver Bartsch (sample #6) and the NIGMS Camden Repository (sample #7) (http://www.ccr.coriell.org/nigms). Three phenotypic groups are represented: 1) developmentally delayed male patients without anorectal malformations or genitourinary anomalies (#1-3), 2) four male patients with anorectal malformations, two with additional genitourinary anomalies (#4-7), and 3) one genetically male patient with normal anorectal anatomy but ambiguous genitalia, who was raised female (#8).

The 13q- deletions were mapped to high resolution using microsatellite markers to test for loss of heterozygosity in the probands. In cases where parental DNA was uninformative at key markers, FISH was performed using a set of chromosome 13 BAC clones for this cytogenetic region. The results were consistent in all cases where microsatellite markers and FISH were used.

Synthesis of cited literature to this point suggests a ~11Mb critical region for anorectal / genitourinary malformations distal to microsatellite marker D13S280. Different deletions suggest the following: genitourinary/anorectal malformation proximal of D13S280 (Figure 2-4). The refined deletions were compared to each other in an effort to narrow the critical region by narrowing overlapping deletions. Of the eight subjects, five have either anorectal or urogenital malformations, and three have both. The minimally overlapping deleted region for both phenotypes is bound proximally by D13S280 in cytogenetic band 13q33.1, refining the critical region boundaries to D13S280-D13S285 and including 9.5Mb. This assumption is based on the deletion present in patient #3, but the possibility of incomplete penetrance can not be excluded. If this is the case, then the critical region would be defined by D13S280- qtel which spans 11Mb.

Further refinement of the critical region for urogenital/ anorectal malformations is possible in patient #4, as markers D13S158 and D13S274 were uninformative, and additional genotyping markers or FISH studies have not been performed. Additionally, the breakpoint in patient #8 has already been mapped to a region between D13S280 and D13S158 spanning 400 kb.

The patients studied show that 13q deletions arising from both maternal and paternal chromosomes give rise to anorectal/ genitourinary malformations. This suggests that the combined phenotype does not involve an imprinted locus, although at present, all four of the patients with urogenital anomalies arose from paternal chromosomes. However, the small numbers of affected individuals in this study make it impossible to determine if this is the result of a maternally imprinted gene.

Finally, based on the deletion map boundaries, there are 20 annotated genes present between D13S280-D13S285 shown on the UC Santa Cruz Genome Browser annotation (May 2004 Freeze) and listed in Table 2-3.

DISCUSSION

Human chromosomal anomalies range in size from large deletions or duplications visible via karyotype to single nucleotide point mutations. This translates into a diverse range of phenotypic variability, especially when one considers the many and varied mechanisms of gene regulation. Previous studies based on cases of chromosomal or gene alterations have been extremely helpful in elucidating the genetic basis of many congenital birth defects.

Human chromosome 13 is depicted in Figure 2-5 with its associated Giemsa banding nomenclature. Chromosome 13 q deletion syndrome was first described in 1969 by Allderdice et al.(Allerdice et al. 1969). The complete list of symptoms associated with chromosome 13q deletion syndrome are listed in Table 2-4, and the exact phenotypes expressed are related to the chromosomal segment(s) deleted. Investigations into retinoblastoma or holoprosencephaly present in 13q deletion patients ultimately resulted in the positional cloning of two genes: the *RB* gene at 13q14 (Friend et al. 1986) which when disrupted results in retinoblastoma, and the *ZIC2* gene, located at 13q32, which causes holoprosencephaly when reduced in copy number (Smith 1988). After a review of 20 13q deletion patients, it was concluded that proximal deletions (q13-31) are associated with mental retardation without major deformities except for retinoblastoma, while deletions that include cytogenetic band 13q32 are usually associated with numerous major malformations. Additionally, it was reported that deletions from 13q33 to the telomere typically manifest with severe mental retardation and other more minor abnormalities, with the authors considering genitourinary or anorectal malformations as minor malformations (Brown et al. 1993).

One problem with traditional karyotype/phenotype correlations is correct interpretation of banding patterns in deleted chromosomes. Brown et al. concluded “it is particularly difficult to decide, in the case of distal 13q deletions involving loss of the Giemsa-dark band q33, whether a remaining Giemsa light band represents part of a q32 or q34 or both.” The authors concluded that the use of molecular markers was one of the only ways to conclusively define the exact deletions in the distal 13q region (Brown et al. 1993).

Two reports suggest a critical region on 13q33.2-q terminus mediating the clinical symptoms of penoscrotal inversion, hypospadias, reduced anogenital distance, imperforate anus, facial anomalies and developmental delay in distal chromosome 13 q deletions (Bartsch et al. 1996; Kuhnle et al. 2000). As seen in Figure 1-1 and Figure 1-2, there is variable severity of external genitalia abnormalities in male children with distal deletions of chromosome 13 q (Kuhnle et al. 2000; Walsh et al. 2001). Ambiguous genitalia in genetically male patients with chromosome 13 q deletions have been reported in some case reports, however, the criteria for this term is not well explained, leading to some confusion in the literature (Brown et al. 1995; Gutierrez et al. 2001; Luo et al. 2000). Regardless of the confusion, the male phenotype is severe enough for some probands to die in utero or shortly after birth. Females have been reported to have absent or bicornate uterus, imperforate anus with vaginal fistula, and cloaca (Bamforth and Lin 1997; Brown et al. 1993; Iafolla et al. 1991).

The focus in this study was on the male urogenital/anorectal malformations of the 13q deletion syndrome, specifically hypospadias, penoscrotal transposition and imperforate anus. Isolated hypospadias is a common human disorder with mild to severe phenotypic variability. Proximal hypospadias accounts for about 15% of these cases, and can be associated with additional malformations including penoscrotal transposition and anorectal malformations, with 2.5 -10.5% of male patients with anorectal malformations also presenting with hypospadias (Lerone et al. 1997; Metts et al. 1997).

Penoscrotal transposition is a severe anomaly where the scrotum is partially or completely situated above the penis (Figure 2-1 and Figure 2-2) and is most commonly associated with severe hypospadias, and strongly associated with deletions of chromosome 13q. Six of the 11 published reports of chromosomal anomalies and penoscrotal transposition had distal 13q deletions (Bartsch et al. 1996; Boduroglu et al. 1998; Chung et al. 2001; Fryns et al. 1980; Gershoni-Baruch and Zekaria 1996; Walsh et al. 2001).

Imperforate anus is associated with penoscrotal transposition in about one third of cases (Parida et al. 1995). Anorectal malformations affect both genders equally, with an incidence between 1 in 1500 to 1 in 5000 live births and also demonstrate great variability in their phenotype (Christensen et al. 1990; Kiesewetter and Chang 1977; Spouge and Baird 1986). Although male patients with these specific birth defects are rare, molecular based investigations of these patients may reveal pathways and developmental mechanisms not yet understood. It is possible that an alteration of human chromosome 13 could account for a significant proportion of patients with anorectal malformations and hypospadias/ penoscrotal transposition.

Genetic engineering or drug exposure can result in animal models of anorectal malformations or hypospadias. Mouse models mutant for SHH (Haraguchi et al. 2001; Perriton et al. 2002), BMP's and FGF's (Haraguchi et al. 2000), HOXA13 (de Santa Barbara and Roberts 2002; Morgan et al. 2003; Post and Innis 1999), HOXD13 (Warot et al. 1997) and retinoic acid treated animals all show pronounced hypospadias in males (Ogino et al. 2001; Suzuki et al. 2002). Additionally, several genes have been implicated in anorectal malformations in mouse models, namely SHH (Arsic et al. 2002; Kim et al. 2001; Mo et al. 2001; Ramalho-Santos et al. 2000), GLI (Bose et al. 2002; Kimmel et al. 2000) and EFNB2 (Dravis et al. 2004). EFNB2 null mice are embryonic lethal due in part to defects in angiogenesis (Wang et al. 1998). A partial loss of function mutation that interferes with signaling was generated in mice, revealing hypospadias in heterozygous males with 40% penetrance. Furthermore, the striking phenotype of male imperforate anus and female persistent cloaca was seen in homozygous mice at 100% penetrance (Figure 2-6, (Dravis et al. 2004)). The observations of this mutant mouse phenotype and cytogenetic location of human EFNB2 have prompted further investigation of the role of EFNB2 in human hypospadias and the 13q deletion syndrome.

Five patients have urogenital/anorectal malformations in this study of eight genetically male patients with distal 13q deletion syndrome, and three do not. The genotype mapping of their 13q deletions refines the minimum critical region for anorectal and urogenital malformations to 9.5 Mb and is delineated by microsatellite markers D13S280 and D13S285. Possible incomplete penetrance in patient #3 could expand this region to 11Mb, corresponding to 13q33.1-q34/tel. This is 3.5-5 Mb smaller than the previously described critical region defined cytogenetically (Bartsch et al. 1996). The new critical region contains 20 annotated genes, including EFNB2. Based on literature reviews, this gene appears to be the top candidate causal gene for anorectal or urogenital malformations. Both phenotypes are seen with either maternal or paternal deletions, suggesting that imprinting is not a factor in this chromosome 13q copy number variation syndrome. There does appear to be incomplete penetrance in one of our patients, and a larger sampling of male 13q deletion patients will be needed to further refine the region as well as confirm or refute EFNB2's role in the urogenital/anorectal phenotype of 13q-deletion syndrome. Furthermore, the introduction of molecular karyotyping such as microarray comparative genomic hybridization may further validate this work with greater resolution.

FIGURE 2-1

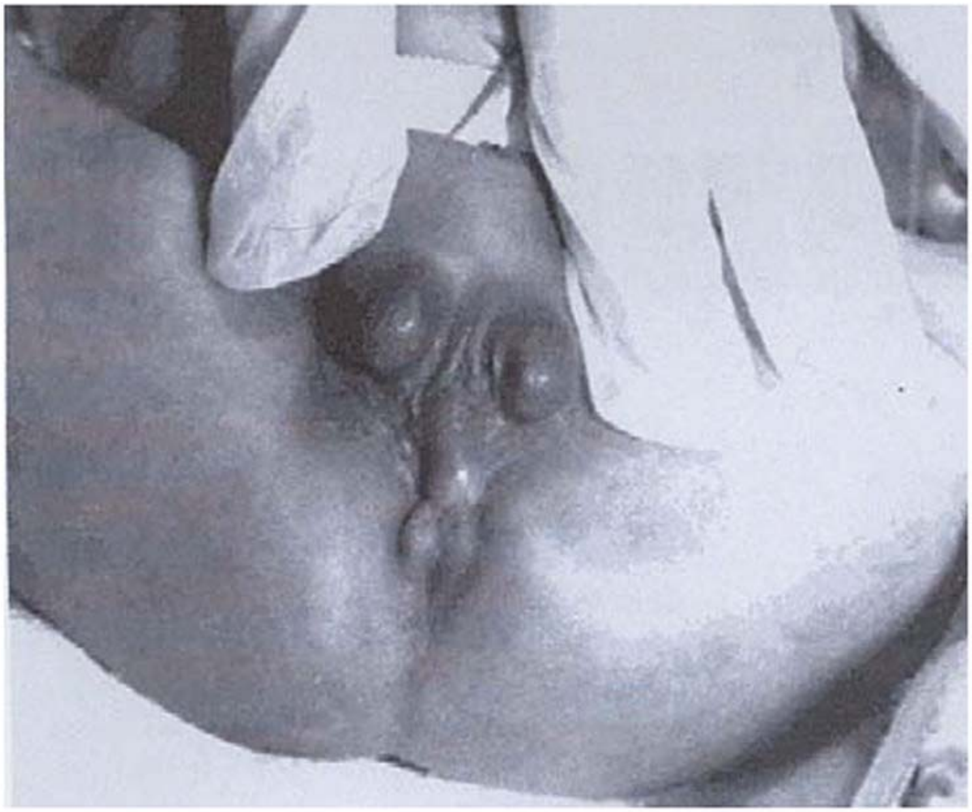

FIGURE 2-1

The perineum of a 46, XY, del (13) (q31.1) male with complete penoscrotal transposition, perineal hypospadias and imperforate anus (Walsh et al. 2001).

FIGURE 2-2

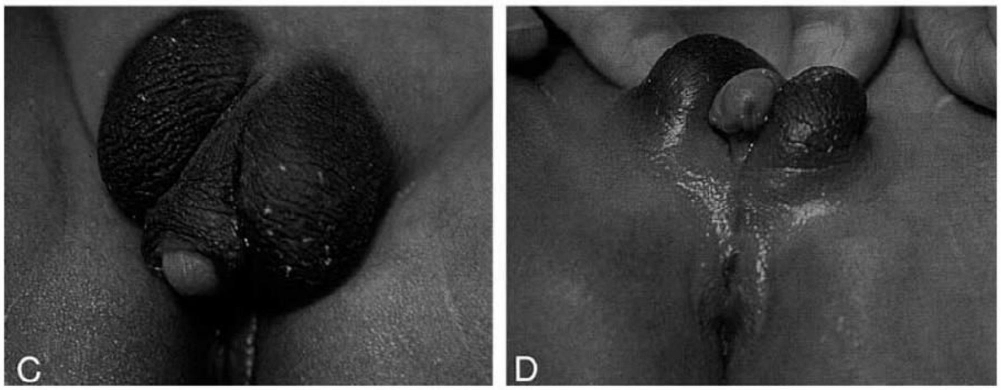

FIGURE 2-2

The external genitalia and the perineum of a male with mosaicism of ring chromosome 13 and monosomy 13q del q33.2-qter (Kuhnle et al. 2000).

FIGURE 2-3

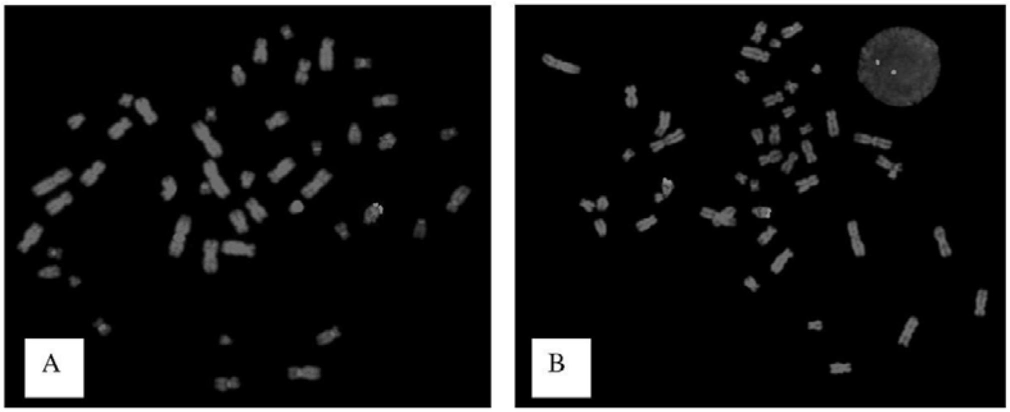

FIGURE 2-3

FISH on lymphoblastoid metaphase preps. Green probe is BAC AL138689.21, containing the ephrin-B2 gene (EFNB2). Red probe is retinoblastoma gene (RB) control. (A) Proband #7-EFNB2 is deleted. (B) Proband #3-EFNB2 is not deleted.

FIGURE 2-4

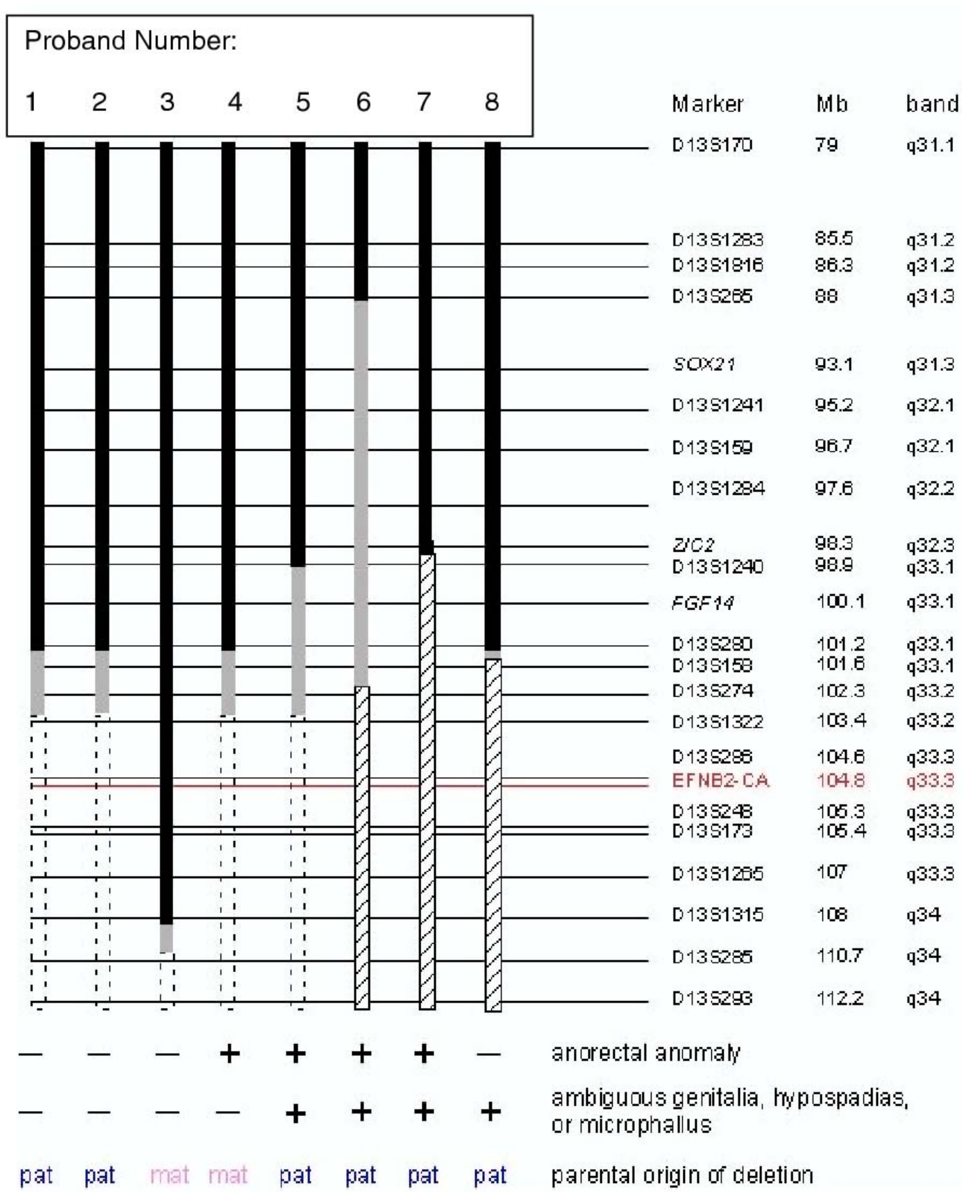
Proband Number:
1 2 3 4 5 6 7 8
Marker Mb band
D13S170 79 q31.1
D13S1283 85.5 q31.2
D13S1816 86.3 q31.2
D13S265 88 q31.3
SOX21 93.1 q31.3
D13S1241 95.2 q32.1
D13S159 96.7 q32.1
D13S1284 97.6 q32.2
ZIC2 98.3 q32.3
D13S1240 98.9 q33.1
FGF14 100.1 q33.1
D13S280 101.2 q33.1
D13S158 101.6 q33.1
D13S274 102.3 q33.2
D13S1322 103.4 q33.2
D13S286 104.6 q33.3
EFNB2-CA 104.8 q33.3
D13S248 105.3 q33.3
D13S173 105.4 q33.3
D13S1265 107 q33.3
D13S1315 108 q34
D13S285 110.7 q34
D13S293 112.2 q34
— — — + + + + — anorectal anomaly
— — — — + + + + ambiguous genitalia, hypospadias, or microphallus
pat pat mat mat pat pat pat pat parental origin of deletion

FIGURE 2-4

Deletion mapping of 13q-patients. Solid black bars indicate 13q sequences that are not deleted; dashed open boxes denote deletions; gray bars indicate regions of uncertainty; hatched bars indicate deletions due to unbalanced translocations. Loci names and physical and cytogenetic map locations of microsatellite markers and selected FISH probes (italics) according to the UC Santa Cruz Genome Browser (genome.ucsc.edu, July 2003 assembly) are indicated. EFNB2- CA marker is indicated in red. Presence (+) or absence (-) of phenotypes and parental origin (pat = paternal; mat = maternal) of deletions are listed.

FIGURE 2-5

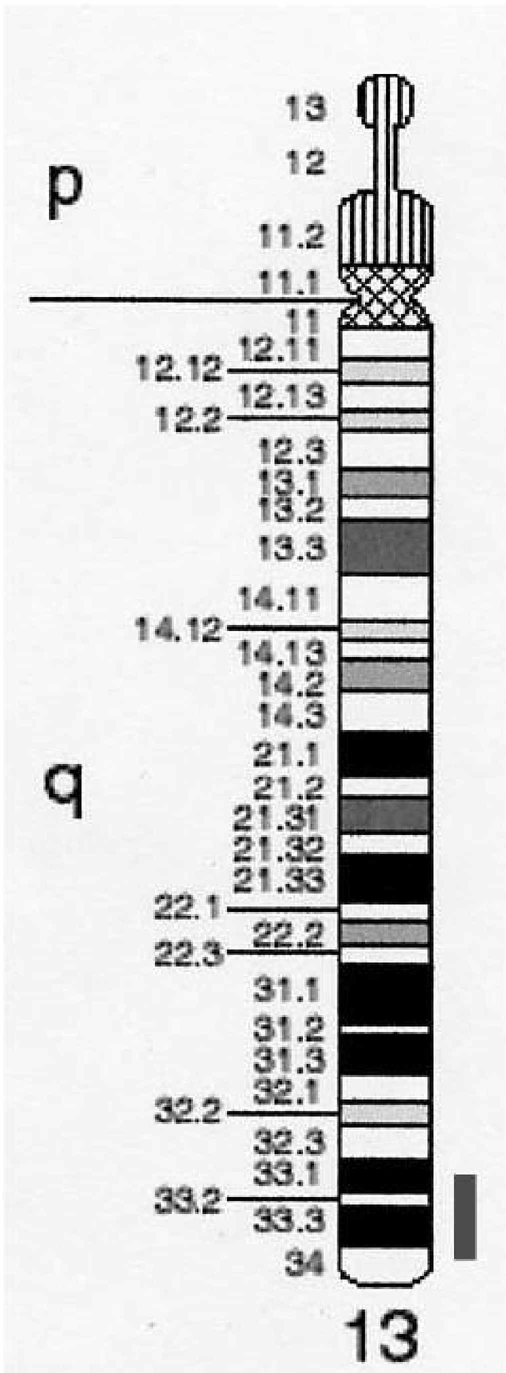
p
q
13
12
11.2
11.1
11
12.11
12.12
12.13
12.2
12.3
13.1
13.2
13.3
14.11
14.12
14.13
14.2
14.3
21.1
21.2
21.31
21.32
21.33
22.1
22.2
22.3
31.1
31.2
31.3
32.1
32.2
32.3
33.1
33.2
33.3
34
13

FIGURE 2-5

Ideogram of chromosome 13. Red bar indicates critical region.

FIGURE 2-6

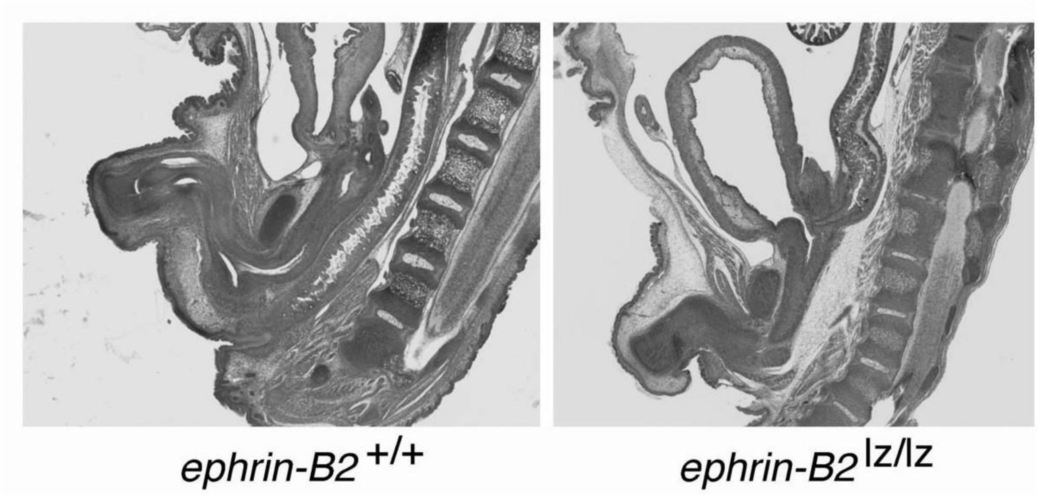

FIGURE 2-6

Left panel reveals a sagittal H&E-stained section of an embryonic day 18 wild-type male mouse with normal genitourinary and anorectal development. Right panel contrasts the embryonic day 18 ephrin-B2 lacZ/lacZ male littermate with malformed urethra, high imperforate anus and abnormal colonic connection to the base of the bladder (rectovesical fistula). From (Dravis et al. 2004).

TABLE 2-1

Ethnicity (Gender)	**13q Deletion probands**	**13q Family members**	**TOTAL**
Caucasian (MALE)	3	5	8
(FEMALE)	1	8	9
African-American (MALE)			
(FEMALE)			
Hispanic (MALE)	5	4	9
(FEMALE)		7	7
Asian (MALE)			
(FEMALE)			
Other (MALE)			
(FEMALE)			
Unknown	1		1
TOTAL	10	24	34

TABLE 2-1

Sex and racial distribution of the 13q-deletion study participants.

TABLE 2-2

Patient no.	Group	Sex	Karyotype	Phenotype
1	11	M	ring 13q	Bilateral VUR, dysplastic upper tracts, meningomyelocoele, microcephaly and developmental delay
2	1	M	46,XY del 13q33.2	No genitourinary anomalies, microcephaly
3	1	M	46,XY del 13q33.2	Right ureteral duplication, no genital or anal anomalies
4	2	M	46,XY del 13q33.2	Anorectal malformation
5	2	M	46,XY del13q33	Bilateral cleft lip and palate, anteriorly displaced anus, hypospadias
6	2	M	45,XY,-13,-22,+der(13:22)(q32.2;p11)	Perineal hypospadias, penoscrotal transposition, bifid scrotum, bilaterally descended testes, low anteriorly displaced imperforate anus
7	2	M	46,XY,-13,+der(13)t(6;13)(13pter>13q32::6q27>6qter)mat	Bifid scrotum, displaced anus, micropenis
8	3	Intersex, raised female	46,XY,der(13)t(6;13)(p25;q33)	Ambiguous genitalia (Male pseudohermaphrodite), no anal anomaly

TABLE 2-2

Phenotypic characterization of eight XY patients with known 13q32-34 deletions.

TABLE 2-3

Candidate gene name	Description	Comment
SLC10A2	Ileal sodium/bile acid cotransporter	Mutations cause 1° bile acid malabsorption
DAOA	D-amino acid oxidase activator	
EFNB2	Ephrin B2	Cell-cell signaling; neural and vascular development; hypospadias and anorectal malformation in mice46
FLJ10154	Hypothetical protein	Unknown function
LIG4	DNA ligase 4	Functions in immunoglobulin gene rearrangement
C13orf6	Novel protein	Esterase motif
TNFSF13B	TNF ligand superfamily	B cell cytokine
KIAA0865	Novel protein	Expressed in brain
IRS2	Insulin receptor substrate 2	Implicated in type II diabetes
COL4A1	alpha 1 type IV collagen preproprotein	Structural component of kidney glomerulus basement Membrane
COL4A2	alpha 2 type IV collagen preproprotein	Structural component of kidney glomerulus basement Membrane
RAB20	RAS oncogene family member	Plays a role in apical endocytosis/recycling
FLJ10769	Hypothetical protein	Unknown function
FLJ12118	Hypothetical protein	cysteinyl-tRNA synthase motif
ING1	Inhibitor of growth family member 1	Tumor suppressor; interacts with p53
LOC283487	Hypothetical protein	Unknown function
ANKRD10	Ankryn repeat domain 10	
ARHGEF7	Rho guanine nucleotide exchange factor 7 isoform	Induces cellular membrane ruffling
MGC35169	Hypothetical protein	Actin crosslinking domain
SOX1	SRY-box 1 gene	Transcription factor; mouse mutation causes epilepsy and abnormal brain development

TABLE 2-3

The 20 annotated genes in the interval D13S280-13qter, based on the UC Santa Cruz Genome Browser annotation (May 2004 Freeze).

TABLE 2-4

Phenotype	**Frequency**
Psychomotor retardation	94%
Hypertelorism, microcephaly	94%
Holoprosencephaly - ZIC2 gene at 13q32	
Agenesis of the corpus callosum	
Prominent nasofrontal bones	66%
Ear abnormalities	79%
Microphthalmia/coloboma of the iris	25%
Retinoblastoma - RB1 gene at 13q14.1-q14.2	18%
High arched or cleft palate	
Congenital heart disease (atrial septal defect, ventricular septal defect, tetralogy of Fallot, patent ductus arteriosus, aortic coarctation)	55%
Factor VII and X clotting deficiency	
Hypoplasia or aplasia of the thumbs/toes, syndactyly, brachydactyly	27%
Duodenal atresia, intestinal malrotation, Hirschsprung's disease	
Renal hypoplasia, hydronephrosis	
Biseptate or absent uterus, cloaca	
Imperforate or anteriorly displaced anus*	16%
Genital ambiguity*	
Hypospadias, penoscrotal transposition, bifid scrotum*	38%
Neural tube defects	

* Genitourinary/anorectal phenotypes.
When known, causal genes, their chromosomal location, and the frequency of the anomaly are noted

TABLE 2-4

Common phenotypes observed in the human chromosome 13q-deletion syndrome.

CHAPTER THREE

X-linked Reticulate Pigmentary Disorder

BACKGROUND

X-Linked Reticulate Pigmentary Disorder

X-linked reticulate pigmentary disorder with systemic manifestations in males (XLPDR, OMIM 301220) is an exceedingly rare genetic disease. Thus far, only four families with the disorder, three multiplex with affected relative pairs and one singleton, have been reported (Ades et al. 1993; Anderson et al. 2005; Megarbane et al. 2005; Partington et al. 1981). The disorder is X-linked dominant with variable expressivity, with males much more severely affected than females. Affected males in the first family described, a large Canadian kindred, showed diffuse reticulate hyper- and hypopigmentation beginning in infancy, recurrent pneumonia, corneal opacification, gastrointestinal inflammation, urethral stricture, failure to thrive, and characteristic upswept hair and flared eyebrows (Partington and Prentice 1989). Female carriers showed only patchy pigmentary skin lesions along the lines of Blaschko, with incomplete penetrance.

Incontinentia Pigmenti

Incontinentia Pigmenti (IP) is an uncommon X-linked dominant disorder, which is lethal in males and variably expressed in females. The main clinical manifestation is skin abnormalities, but IP is also associated with hair, nail and dental abnormalities, as well as ophthalmologic and neurological defects. IP has four cutaneous stages that begin only a few weeks after birth. The first stage begins with erythema and inflammatory vesicles, and is also known as the vesicular stage (Figure 3-1A, B). The second stage is also known as the verrucous stage, so named for the hyperkeratotic, linearly arranged verrucous papules and plaques which begin to appear (Figure 3-2). Wart-like lesions and irregular whorl-like slate gray hyperpigmentation appear in stage 3 and finally become atrophic, hypovascular, hairless streaks in stage four (Figure 3-3A, B and 3-4) (Berlin et al. 2002).

A susceptibility locus for IP was mapped to Xq28 (Sefiani et al. 1989; Smahi et al. 1994) and later mutations in the nuclear factor κB essential modulator (NEMO) (aka γ-subunit of the inhibitor κB kinase (IKKγ)) were discovered in IP patients. A single mutation resulting in the deletion of exons 4-10 was found to account for more than 80% of all IP cases (Smahi et al. 2000). NEMO functions as an essential modulator of the NFκB, which is a transcription factor that is broadly involved in many pathways, including immune and inflammatory responses (Hayden and Ghosh 2004).

NFκB activation and skin disease

NFκB activation has been shown to initiate transcription of a variety of genes participating in immune and inflammatory response, cell adhesion, growth control and protection against apoptosis (Hayden and Ghosh 2004; Karin and Ben-Neriah 2000). Interestingly, of the 6 known mutations in genes in the NFκB activation pathway, 3 result in skin disorders: cylindromatosis, ectodermal dysplasia and incontinentia pigmenti (Courtois and Smahi 2006). Cylindromatosis is characterized by the development of numerous benign tumors that appear on the hairy areas of the body, but can also involve hair follicle tumors (Bignell et al. 2000; Poblete Gutierrez et al. 2002). Ectodermal dysplasia results from the abnormal development of hair follicles, skin and teeth, and often is seen in conjunction with immunodeficiency (Abinun et al. 1996; Frix and Bronson 1986; Schweizer et al. 1999; Sitton and Reimund 1992). Finally, Incontinentia Pigmenti, as described previously, has the most severe skin phenotype involving multiple stages of pathologic skin lesions. The diverse but consistently present skin phenotypes in disorders of NFκB regulation clearly point to a role in skin homeostasis for NFκB, and this transcription factor also has been recommended as an ideal candidate pathway for involved genes when investigating a disease with skin pathology but no known genetic etiology (Courtois and Smahi 2006).

Inflammation and XLPDR

Based on the above recommendation to investigate NFκB when presented with a disease with skin pathology of unknown genetic etiology, XLPDR was scrutinized for possible links to NFκB and its many diverse roles. When taken from this point of view, multiple symptoms of XLPDR can be explained by either direct NFκB involvement or processes that are controlled by NFκB, like inflammation. Two of the most striking symptoms of XLPDR are reticulate pigmentation and chronic Cystic Fibrosis-like bronchitis. The reticulate pattern of skin hyperpigmentation is strikingly similar to IP (Figure 3-5) and strongly implicates NFκB. The continuous lung infections found in XLPDR patients mirror those in Cystic Fibrosis patients, which is a chronic inflammatory lung disease where high levels of NFκB cytokines are present due to constant infection, resulting in further lung damage and perpetuation of the disease (Nichols et al. 2008). Other symptoms include colitis and adult onset amyloidosis, both of which have been shown to be induced by NFκB activation (Yan et al. 2000; Yan et al. 2008). Taken together, it seems likely that NFκB activation could play a role in a number of the pathologies seen in XLPDR patients.

Genetic studies of XLPDR

Gedeon et al. (1994) mapped the XLPDR gene by linkage analysis of the Canadian pedigree to a greater than 40 cM interval of Xp22–p21 bounded by DXS999 distally and DXS228 proximally. Three other unrelated families in whom one or more individuals were diagnosed with XLPDR have since been reported (Ades et al. 1993; Anderson et al. 2005; Megarbane et al. 2005). My hypothesis is that an unknown genetic anomaly is present in XLPDR probands, resulting in chronic systemic inflammation via NFκB activation.

METHODOLOGY

DNA Collection

DNAs were obtained previously from members of the Canadian family (Gedeon et al. 1994). Informed consent and blood or DNA samples were obtained from additional members of this family and members of other reported XLPDR families. Lymphoblasts were immortalized from one or more affected males from each of the Canadian, Texas, and Australian XLPDR families. DNA was extracted from blood or lymphoblastoid cells using standard techniques.

Genotyping

ABI Linkage V2.5 microsatellite markers for the short arm of the X chromosome and additional custom markers DXS365, DXS443, DXS1052, DXS989, DXS8099, DXS1202, and DXS8192 selected from GDB (http://www.gdb.org) were analyzed using an ABI 3100 capillary electrophoresis instrument and ABI GeneMapper software version 3.7.

Linkage Analysis

XLPDR exhibited a dominant mode of inheritance, and the underlying gene was highly penetrant, particularly in males; therefore we performed multipoint model-based linkage analysis by fitting a liability model with penetrance equal to 0.99 and 0.90 for males and females, respectively. Both disease allele frequency and sporadic rate were set to be 0.0001. To evaluate the significance level of the result, we simulated 10,000 replicates under the null hypothesis of no linkage conditional on pedigree structure and marker informativity. We constructed the most likely haplotype to infer the location of the XLPDR susceptibility gene by comparing haplotype similarity between affected individuals and dissimilarity between discordant individuals in each family. To confirm the linkage signal irrespective of genetic models, we also performed model-free linkage analysis. All analyses were conducted by using the MINX module of the software MERLIN (Abecasis et al. 2002).

Candidate Gene Sequencing

Primers were designed flanking the splice sites and boundaries of coding exons for all annotated protein-coding genes in the linked region (UCSC Genome Browser, hg36 assembly) and several genes beyond the boundaries. Standard PCR amplification was performed and amplified products were sequenced using ABI Big Dye terminator chemistry. Sequences were examined using SeqMan II version 5.05 (DNASTAR, Madison, WI). Variations from the reference sequence were checked against dbSNP. Unannotated nonsynonymous SNPs were evaluated for potential effect on protein structure and function using PolyPhen (Sunyaev et al. 2001).

Expression Studies

Total RNA was extracted from lymphoblastoid cell lines using Trizol reagent (Invitrogen, Carlsbad, CA). RT-PCR primers spanning introns were designed for *ACOT9*, *SAT1*, *GRPR* and *PRDX4*. Primers flanking the entire coding region were included if transcript size allowed, otherwise the product was separated into amplifiable sizes. *ACOT9* was amplified both as the entire coding region and as two separate products using the primer pairs ACOT9.FL GTTGGCTCATTGCTCTTTCTTT, TTCTTTCTCCCCTCAGCCCCATCC; ACOT9.1 GGCTCCCGGGCTGTCCTCA, ATGCCGGCCCTTTATTTTC; ACOT9.2 AGCTTGGGAGTTCTTATTTGTTAC, AGGGAGGCCACTTCACTG. The full *SAT1* coding region was amplified as well as an alternate transcript of *SAT1* including an alternate exon 3 and 3_UTR using the primer pairs SAT1.FL GACTGGTGTTTATCCGTACTC, AGAATCAAACAGAAACTCTAAGTACCA; SAT1AE3 TGGTGTTTATCCGTCAC TCG, CGGGTCTCCACAGCACTTAT. *PRDX4* was amplified into two segments using primer pairs PRDX4.1 GCGCCAAGGGACGTGTTTCTG, TTGTCTTCGAGGGGGTA TTA; PRDX4.2 GTTGATTCACAGTTTACCCATTTG, AACCGTGAACTTTATTGAGAACTT. *GRPR* was amplified in four segments using primer pairs GRPR.1 TCTGTTAAGCTAGGTAGGAACTGC, GCACTGTGACTGGAGATGTTG; GRPR.2 GACTGTTTCCTTCTGAACTTGGA, GGATTCAATCTGCTTCTTGAC; GRPR.3 ATTCCACTGTCGATCATCTCTG, CACATCAGAAGAAACGTTCACAA; GRPR.4 TTGAAAGAAGCCATCAAGTCTTA, AAAGGATTGCTCTTCTATGGTG.

GRPR RFLP Analysis

Primers CAAAGAGCCCGGCATAGAT and GTGAGTGTGAAGACAGACACCC were used to generate a 500 bp PCR product from genomic DNA. This product is cleaved at three sites by restriction enzyme HpyCH4III (New England Biolabs) to give products of 194, 128, 121 and 57 bp. The c.17G→C SNP eliminates one of these sites, resulting in products of 194, 178 and 128 bp. Restriction fragments were resolved by electrophoresis using 4% agarose gels.

RESULTS

All XLPDR families in this study have been previously reported (Ades et al. 1993; Anderson et al. 2005; Megarbane et al. 2005; Partington et al. 1981). Stored DNA samples from previously studied members of the Canadian family (Figure 3-6) were obtained and linkage analysis using newer microsatellite markers for the short arm of the X chromosome was repeated. The pedigree was expanded after obtaining samples from IV-13, IV-14, IV-15 and IV-16, who were born since the original report. The additional family members were then genotyped with the same microsatellite markers and the combined results analyzed for linkage. Based on the results, selected family members were genotyped for additional microsatellite markers DXS365, DXS443, DXS1052, DXS989, DXS8099, DXS1202, and DXS8192 to narrow the location of meiotic recombination events. The refined XLPDR linkage interval of ~4.9 Mb was bounded distally by DXS1052 and proximally by DXS1061 (Figure 3-7). The proximal boundary was determined by an observed recombination in IV-13 between DXS1202 and DXS1061. The distal boundary was determined by an inferred recombination in II-6 between DXS1052 or DXS1226 and DXS989. Since DXS1052 and DXS1226 are ~0.5 Mb apart, and do not contain any annotated genes in between, there were no further attempts taken to refine the distal boundary of the XLPDR linkage interval.

Based on these results, the other multiplex families were genotyped for selected Xp markers. Within each family, all affected members shared common haplotypes, although the mutations in the different families arose independently on different haplotypes, as expected for a highly penetrant deleterious gene (Figure 3-8). Australian family member II-2 showed a recombination between DXS1061 and DXS8102, and Texas family member II-1 showed a recombination between DXS1214 and DXS8102, but both recombinations were proximal to the XLPDR interval defined by the recombination in Canadian family member IV-13 (Figure 3-8).

The peak LOD score with model-based linkage is 5.279 in the interval between DXS1226 and DXS1061. DXS1061 is slightly more informative than DXS1052 and was therefore used. With model-free linkage analysis, the peak LOD score was 4.41, but the interval is larger, with a proximal boundary of DXS8090. To be conservative, a multipoint model-based LOD score of 5.279 corresponds to a P value of 5.3 x 10^{6} (Xing et al. 2007), and none of the 10,000 replicates generated a greater LOD score.

Annotated coding exons and surrounding splice sequences in the DXS1052–DXS1061 interval were then sequenced in one proband from each of the four reported XLPDR families with a summary of the results found in Table 3-1. Only one variation was identified, a c.934G→C mutation in the *ACOT9* gene in the proband from the Australian family. This variation, which was not present in dbSNP, alters the first nucleotide of *ACOT9* exon 12, changing glutamic acid 312 to glutamine. Polyphen predicted that this substitution is benign. Although G is the preferred base at this exon position, it is not invariant among spliced mRNAs (Zhang 1998). To test whether the mutation abrogated efficient *ACOT9* splicing, RT-PCR was performed, using RNA from EBV-immortalized lymphoblasts and primers from flanking exons. An RT-PCR product of the expected size that was not abundantly or qualitatively different from controls in the Australian proband suggested that the mutation did not prevent efficient splicing (data not shown). Quantitative RT-PCR also showed no systematic difference in *ACOT9* mRNA abundance in immortalized lymphoblasts from any of the XLPDR probands compared to controls (data not shown). Given that there were no *ACOT9* coding mutations in the other three unrelated XLPDR probands and no evidence of abnormal *ACOT9* expression in any proband tested, it was concluded that the *ACOT9* c.934G→C mutation in exon 12 is a rare variation unrelated to XLPDR.

Several biologically plausible candidate genes outside of the reduced linked interval were also sequenced in some or all of the probands before results from the analysis of the expanded pedigree were obtained (Table 3-2). One of these was the spermine synthase gene *SMS*. *SMS* is in the same polyamine synthetic pathway as spermine acyl transferase, encoded by *SAT1*, one of the candidate genes in the critical region. An Xp duplication that includes *SAT1* has been associated with keratosis follicularis spinulosa decalvans (KFSD) (Gimelli et al. 2002), a disease with skin and cornea involvement, like XLPDR. Furthermore, transgenic overexpression of *SAT1* in the skin of mice resulted in permanent hair loss and dermal cysts (Pietila et al. 2005). While loss of function mutations in *SMS* cause X-linked mental retardation (XLMR)(Cason et al. 2003), it seemed reasonable that a gain of function mutation could result in a disease phenotype similar to KFSD and might cause XLPDR. However, no *SMS* coding mutations were identified, and quantitative RT-PCR studies did not show any increase in *SAT1* expression in lymphoblastoid cells of XLPDR probands compared to controls (data not shown).

Having failed to identify a causal mutation for XLPDR, advantage was taken of the International Genetics Of Learning Disability (IGOLD) study (carried out at the Wellcome Trust Sanger Institute, Hinxton, UK) (Raymond and Tarpey 2006; Tarpey et al. 2006) to resequence 737 X-chromosome genes annotated by VEGA (Vertebrate Genome Annotation Database; http://vega.sanger.ac.uk/index.html) in probands from all three families. This large scale re-sequencing identified a nonsynonymous substitution in the Australian proband in the first exon of the *GRPR* (gastrin-releasing peptide receptor) gene, c.17G→C, that changes conserved cysteine residue seven to serine in the extracellular portion of the protein. This mutation was confirmed by independent sequencing, but sequencing of *GRPR* in the other XLPDR probands did not reveal this or other coding mutations. *GRPR* was a plausible biological candidate for XLPDR, as it encodes a G-protein coupled receptor that is highly expressed in lung epithelium. The C7S mutation was not present in any of ~250 predominantly Caucasians with XLMR also sequenced by the Sanger Center. The Australian XLPDR family was of Maltese ancestry (Ades et al. 1993). To determine whether the *GRPR* C7S mutation is a polymorphism in the Maltese population, cord blood DNA samples from 191 Maltese subjects of unknown sex were assayed. The c.17G→C mutation eliminates an HpyCH4III restriction site. PCR/RFLP analysis demonstrated that 14 of the Maltese samples (7.3%) carried at least one mutant allele, 9 heterozygous and 5 either homozygous or hemizygous, demonstrating that it is present at polymorphic frequency in this population and therefore ruling it out as the cause of XLPDR.

Since traditional methods for disease gene mapping failed to result in the discovery of a single gene mutation, the possibility of X chromosome copy number variation (CNV) was considered. If a portion of the X-chromosome was duplicated, resulting in increased copy number for a given gene, traditional sequencing and microsatellite mapping would be blind to this difference. . Similarly, deletions of regulatory sequences outside of coding exons would not be detected by exonic sequencing. High resolution oligonucleotide array comparative genomic hybridization using a X chromosome specific tiling array was performed on male probands from each XLPDR family to detect copy number variants of the X chromosome. Despite excellent resolution, (169bp average probe spacing) no CNV in the XLPDR critical region and no CNV of any known functional sequences elsewhere on the X chromosome was found in any XLPDR proband.

DISCUSSION

Linkage mapping narrowed the location of the gene causing XLPDR to a ~4.9 Mb interval containing approximately 18 genes. Two of these genes were plausible candidates, based upon the likely inflammatory pathogenesis of the disorder. The first, *PRDX4,* encodes a thioredoxin peroxidase that has been shown to regulate NFκB activation in cultured cells (Jin et al. 1997). The second*, SAT1*, encodes spermine synthase, overexpression of which may be responsible for keratosis follicularis spinulosa decalvans, another disorder affecting skin and cornea (Gimelli et al. 2002). Unfortunately, comprehensive sequencing of the coding exons of these 18 genes revealed no mutations in XLPDR kindreds, nor was there any evidence of aberrant expression in lymphoblastoid cells from affected males. Systematic resequencing of other other functionally annotated sequences in the critical region also failed to reveal the genetic cause of XLPDR. There are several possible explanations for this inconclusive result. First, the linkage interval could be erroneous. The distal boundary is based on an inferred meiotic recombination and the proximal boundary is based on an observed recombination, assuming complete penetrance. XLPDR clearly shows incomplete penetrance in females, but the literature suggests that the disorder is fully penetrant in males. Sex-specific penetrance is consistent with X-linked inheritance. Linkage analysis could also be erroneous if there is variation in marker order in the Canadian family, e.g., due to a cryptic chromosomal inversion. Finally, there is a small but not zero (<0.0001) probability that a LOD score of greater than 5 could occur by chance. However, comprehensive resequencing of VEGA-annotated X chromosome coding sequences also failed to reveal a causal XLPDR mutation.

A more likely explanation for the failure to identify the cause of XLPDR is that the disorder is due to mutation(s) outside of the exons that were sequenced. There could be a mutation in an unannotated gene, a noncoding region, or an alternative transcript of one of the annotated genes in the interval. It is also possible that a mutation of a noncoding RNA gene in the interval causes XLPDR. One annotated noncoding small nucleolar RNA, *ACA12*, encoded by the *SCARNA23* gene within an intron of POLA was sequenced. The *ACA12* RNA is predicted to guide the pseudouridylation of residue U40 of the spliceosomal U6 snRNA (Kiss et al. 2004). This RNA gene was considered to be a plausible XLPDR candidate because mutations in dyskerin (*DKC1*), a component of the telomerase complex that associates with H/ACA small nucleolar RNAs (Tollervey and Kiss 1997), cause dyskeratosis congenita, a skin disorder with some similarity to XLPDR (Mitchell et al. 1999). However, no *SCARNA23* mutations were identified in any XLPDR proband.

The possibility that XLPDR could result from copy number variation, such as duplication, that could be missed by PCR and sequencing was next considered. Incontinentia pigmenti presents in females with a reticular pigmentary abnormality reminiscent of that seen in males with XLPDR (Partington et al. 1981). Identification of *IKKγ* (NEMO) mutations as the cause of incontinentia pigmenti was hindered by the presence of a nearby pseudogene, which frequently caused recombinations that gave rise to *IKKγ* deletions (Smahi et al. 2000). Interestingly, an Xp duplication including *SAT1* has been associated with keratosis follicularis spinulosa decalvans, a disorder also affecting skin and cornea (Gimelli et al. 2002). High resolution array comparative genomic hybridization on an affected male from each of the five XLPDR families using a custom X chromosome tiling array with average probe spacing of ~169 bp (Nimblegen), was performed, but failed to detect copy number variations anywhere on the X chromosome (data not shown). The molecular basis of XLPDR remains unknown. Large scale genomic resequencing of the XLPDR linkage interval, or if necessary, the entire X chromosome of affected XLPDR family members, should ultimately reveal the genetic basis of this enigmatic disorder.

FIGURE 3-1

FIGURE 3-1

Vesicular stage of incontinentia pigmenti with typical findings of erythema and inflammatory vesicles. A, Early stage. B, Late stage with crusting and early verrucous changes (Taken from Berlin et al. 2002).

FIGURE 3-2

FIGURE 3-2

Vesicular stage of incontinentia pigmenti involving the scalp, presenting with vesicles and crusting. (Taken from Berlin et al. 2002).

FIGURE 3-3

FIGURE 3-3

Verrucous stage of incontinentia pigmenti presenting with linear wart-like lesions on extremities and plantar hyperkeratosis. (Taken from Berlin et al. 2002).

FIGURE 3-4

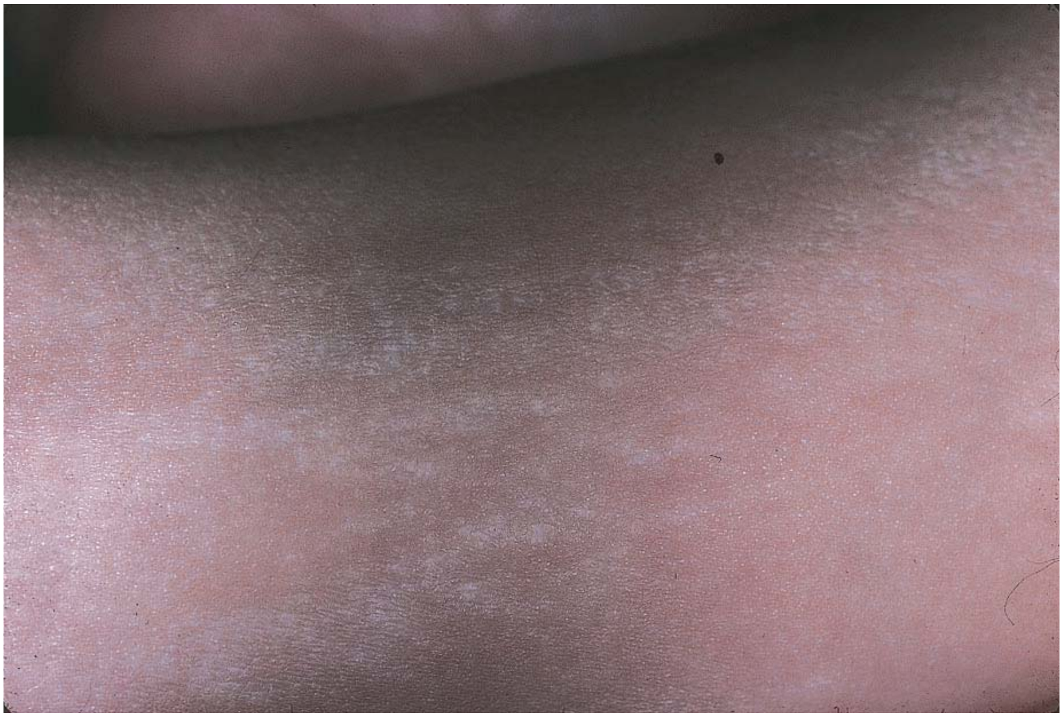

FIGURE 3-4

Typical atrophic, hypovascular, hairless streaks associated with stage 4 of incontinentia pigmenti. (Taken from Berlin et al. 2002).

FIGURE 3-5

FIGURE 3-5

Left: Irregular, whorl-like, slate-gray hyperpigmentation of stage 3 of incontinentia pigmenti affecting the torso. (Taken from Berlin et al. 2002).

Right: X-linked Reticulate Pigmentary Disorder male proband, showing reticulate pigmentation of the arm. (Taken from (Anderson et al. 2005)

FIGURE 3-6

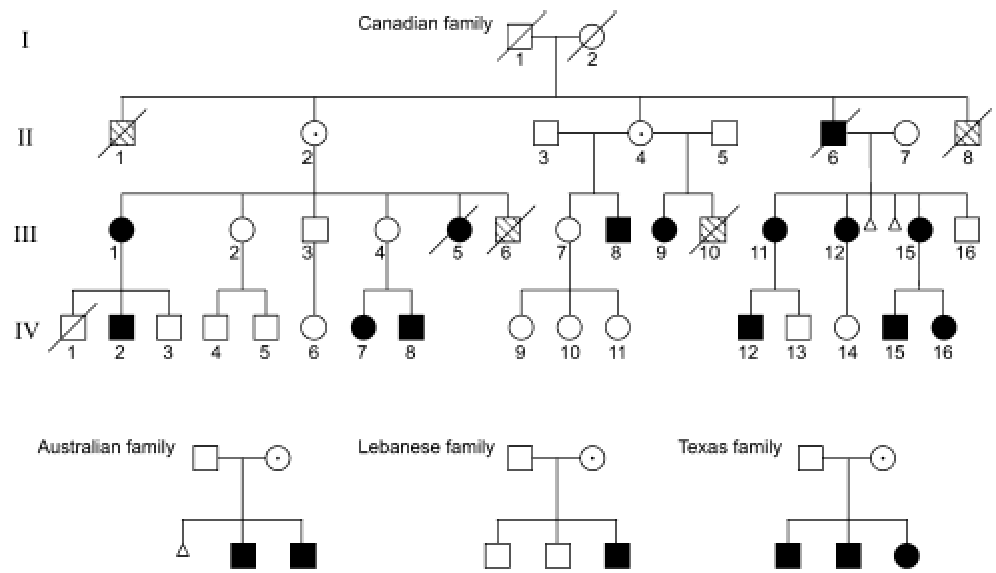
Canadian family
I
II
III
IV
1
2
3
4
5
6
7
8
9
10
11
12
13
14
15
16
Australian family
Lebanese family
Texas family

FIGURE 3-6

XLPDR pedigrees in this study. Canadian family members are numbered according to previous reports (Gedeon et al. 1994; Partington et al. 1981)

FIGURE 3-7

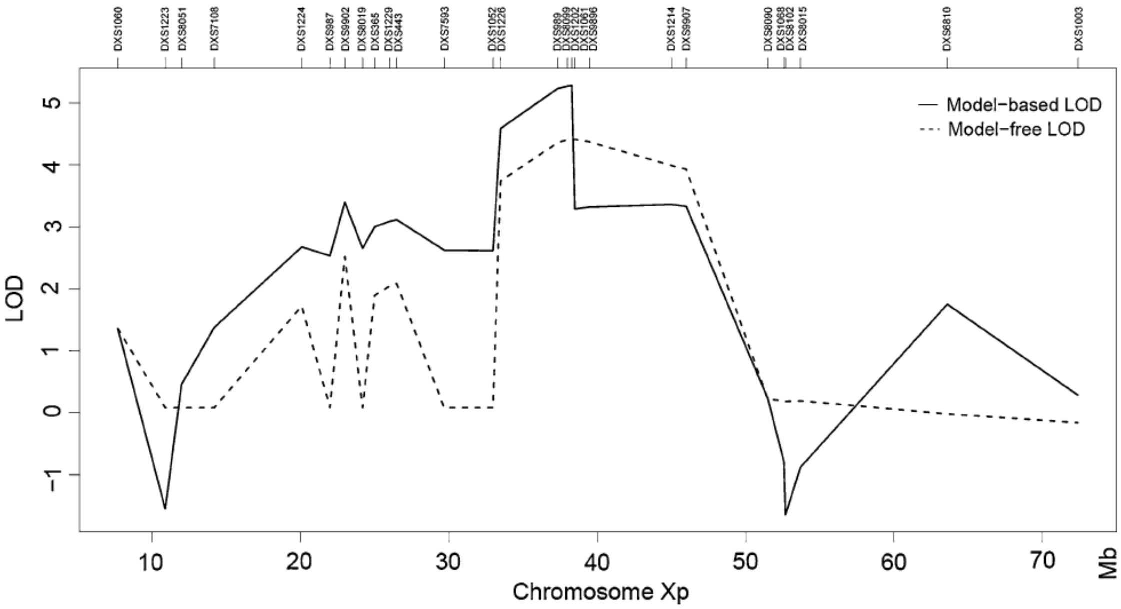
DXS1060
DXS1223
DXS8051
DXS7108
DXS1224
DXS987
DXS9902
DXS8019
DXS365
DXS1229
DXS443
DXS7593
DXS1052
DXS1226
DXS989
DXS8099
DXS1202
DXS1061
DXS9896
DXS1214
DXS9907
DXS8090
DXS1068
DXS8102
DXS8015
DXS6810
DXS1003
Model−based LOD
Model−free LOD
LOD
5
4
3
2
1
0
−1
10
20
30
40
50
60
70
Mb
Chromosome Xp

FIGURE 3-7

Model-based and model free LOD score plots for Xp markers genotyped in XLPDR families.

FIGURE 3-8

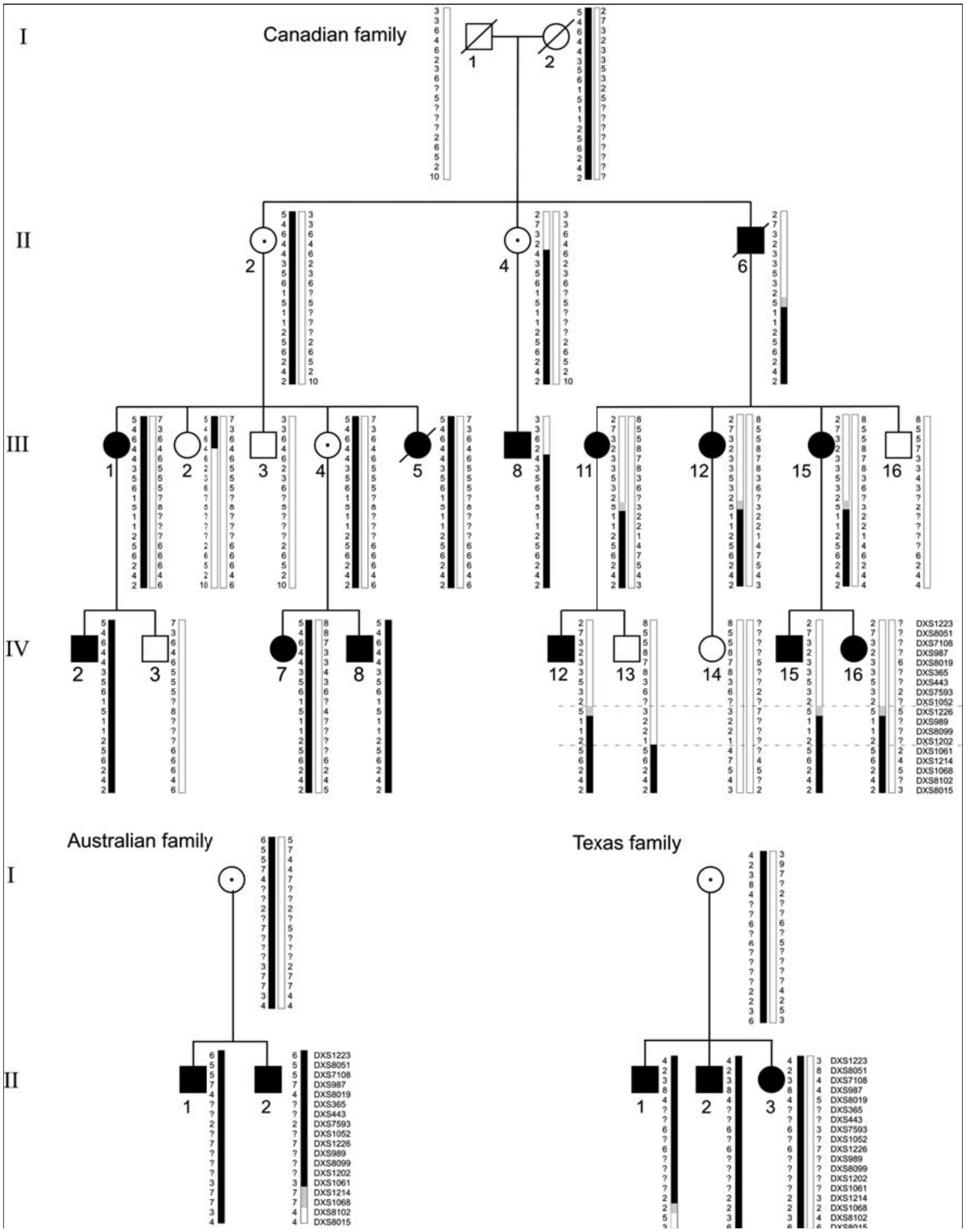
Canadian family
Australian family
Texas family
I
II
III
IV
DXS1223
DXS8051
DXS7108
DXS987
DXS8019
DXS365
DXS443
DXS7593
DXS1052
DXS1226
DXS989
DXS8099
DXS1202
DXS1061
DXS1214
DXS1068
DXS8102
DXS8015

FIGURE 3-8

Partial pedigrees showing haplotypes defining XLPDR interval. *Black bars* denote chromosomes or regions carrying disease allele. *Grey bars* denote regions of uncertainty. *Dashed lines* indicate minimal linkage interval for XLPDR gene.

TABLE 3-1

Gene name	RefSeq or ENSEMBL identifier	No. of coding exons	Variation detected	Comment (see also text)
DDX53	NM_182699	1		
FLJ11556	ENST00000356867	1		
PTCHD1	NM_173495	3		
Predicted gene	ENST00000352495	1		
PRDX4	NM_006406	7, ae1		Regulates NFκB
ACOT9	NM_001033583	15, ae1, ae3	c.934G → C (E312Q)	
SAT1	NM_002970	6, ae4		Overexpression may cause keratosis follicularis spinulosa decalvans
APOO	NM_024122	9		
RPL9-like	ENST00000329019	1		Retrotransposed pseudogene?
CXorf58	NM_152761	9		
KLHL15	NM_030624	2		
EIF2S3	NM_001415	12		
ZFX	NM_003410	9		
FAM48B1	ENST00000327866	1		
PDK3	NM_005391	11		
PCYT1B	NM_004845	8, ae1		
POLA	NM_016937	37		
SCARNA23	ENSG00000212474	0		snoRNA ACA12
LOC644820	NM_001089876	1		
ARX	NM_139058	5		
Predicted gene	ENST00000351630	0		Noncoding RNA
Predicted gene	ENST00000366348	8		
RANBP1-like	ENST00000304245	1		Retrotransposed pseudogene?
MAGEB18	NM_173699	3		
MAGEB6	NM_173523	2		
MAGEB5	ENST00000379029	1		

ae Alternate exon

TABLE 3-1

Sequencing results for annotated genes in XLPDR linkage interval.

TABLE 3-2

Gene name	RefSeq or other identifier	No. of coding exons	Variation detected	Comment (see also text)
GRPR	NM_005314	3	c.17G → C (C6S)	Gastrin-releasing peptide receptor
PPEF1	NM_006240	16		
SH3KBP1	NM_031892	18		Enhances TNF-mediated apoptosis
EIF1AX	NM_001412	7		
CNKSR2	NM_014927	22		
MBTPS2	NM_015884	11		
SMS	NM_004595	11		Encodes enzyme in same pathway as *SAT1*
FLJ32742	AK057304	2		
IL1RAPL1	NM_014271	11		
MAP3K7IP3	NM_152787	11		Upstream activator of NFκB

TABLE 3-2

Sequencing results for selected candidate genes outside XLPDR linkage interval.

CHAPTER FOUR
Chromosomal copy number variation and congenital heart defects

BACKGROUND

Congenital Cardiovascular Disease

Congenital cardiovascular defects are the most common type of birth defect and cause the most fatalities in the first year of life. Most cardiovascular malformations have an estimated incidence of eight per 1000 live births and affect 10% of spontaneous miscarriages (Hoffman and Kaplan 2002). Congenital heart defects (CHD) occur when the normal process of heart formation is perturbed, resulting in abnormal heart structure(s) which then affects cardiovascular function. Recent advances in medical and surgical management have allowed nearly 85% of affected children to survive to adulthood; as a result, there are an estimated 1,000,000 adults living with congenital heart disease in the United States and similar numbers in Europe (Gatzoulis 2004; Warnes et al. 2001). The proposed causes for CHD are multifactorial, including viral infections, chemical teratogens, maternal disease and genetics, with the reported incidence of CHD stable for several decades.

Genetic etiology of congenital heart disease

Genetics have long been suspected of playing a role in the development of some congenital heart diseases. Common cardiac malformations are seen in multiple birth defect syndromes which arise from chromosomal aberrations. Children born with Down syndrome arising from an extra chromosome 21, or with Turner syndrome resulting from the loss of the X chromosome have increased risk for developing CHD. Early epidemiological studies reported that less than 8% of CHD was due to chromosomal or single gene defects and the remaining 92% was thought to be multifactorial in nature (Nora 1993). Most CHD is termed “nonsyndromic” despite 20-40% of patients presenting with additional birth anomalies (Bernstein 2004). However, despite these scientific advances, most children with CHD, including those with additional birth anomalies, have no obvious genetic abnormalities.

Genetic Screening Techniques

Karyotyping chromosomal analysis has been the standard method used in the genetic evaluation of children with multiple birth defects since its introduction in the late 1950s (Trask 2002). However, the most striking limitation to conventional cytogenetic evaluation is the threshold of detection. Chromosomal changes smaller than 5-10 Mb cannot be detected using karyotype analysis. Fluorescence in situ hybridization (FISH) can detect such changes (deletions, duplications or rearrangements) but is impractical for a genome wide approach. Array Comparative Genomic Hybridization (aCGH) is a new methodology for concurrently identifying submicroscopic and larger chromosomal copy number changes (CNV) in the entire genome (du Manoir et al. 1993; Kallioniemi et al. 1992; Pollex and Hegele 2007). This method has evolved into a powerful and practical means to screen an entire genome for subtle and cryptic chromosomal abnormalities. As a result, it has led to the discovery of a number of pathological small copy number changes in patients with specific birth defects or neurological diseases like autism and learning disabilities (Menten et al. 2006; Sebat et al. 2007; Shaw-Smith et al. 2004). It was therefore the purpose of this study to determine if such subtle or cryptic chromosomal anomalies existed in children with CHD but had failed to be previously detected. Furthermore, as chromosomal anomalies typically involve multiple genes with disparate functions, the underlying hypothesis of this study is that children with CHD and additional birth defects are more likely to harbor such chromosomal anomalies than children with isolated CHD.

METHODOLOGY

Subjects

The subject population was comprised of 40 unrelated individuals (21 males, 19 females) with CHD. From January to December 2006, subjects were prospectively recruited for genetic testing and informed consent obtained according to protocol as approved by the Institutional Review Board at the University of Texas Southwestern Medical Center. Twenty subjects with CHD had additional diagnoses and are listed in Table 4-1 (population A). The types of CHD varied and included: 4 subjects with tetralogy of Fallot; 4 with ostium secundum atrial septal defects; 1 with a sinus venosus atrial septal defect; 2 with atrioventricular septal defect; 1 with a perimembranous ventricular septal defect; 2 with pulmonic valve stenosis; 2 with hypoplastic left heart syndrome; 1 with aortic coarctation and bicuspid aortic valve; 1 with dysplastic mitral valve; 1 with patent ductus arteriosus; and 1 with double outlet right ventricle. The individuals included 10 male and 10 females and were of variable ethnicity specifically 12 European-Americans, 7 Hispanics, and 1 Asian. A control population (population B, Appendix B) was randomly selected from our database of individuals enrolled in an ongoing program at Children's Medical Center Dallas. These subjects were matched to population A according to the type of heart defect, but had no other known anomalies. This control population was comprised of 11 males and 9 females and included 11 European Americans, 8 Hispanics, and 1 Asian. All subjects with CHD and additional anomalies had previous genetic testing including a karyotype that was interpreted as normal by conventional cytogenetic G-banding methodology. All subjects underwent complete cardiac evaluation at Children's Medical Center Dallas and echocardiogram, cardiac catheterization and operative reports were reviewed when available. In addition, the entire medical record was retrospectively reviewed to identify the presence of additional diagnoses. Because the clinical assessment of additional anomalies was performed in a retrospective manner, all patients were neither examined by the same geneticist/neurologist nor had medical testing that was not part of routine medical care. Developmental assessments were used only if evaluation was performed in subjects after 18 mo of age.

DNA Collections

Venous blood samples were collected and genomic DNA isolated using the PUREGENE kit (Gentra Systems) from recruited subjects.

Array Comparative Genomic Hybridization

Genomic DNA was submitted to Nimblegen Systems (Madison, WI) for high-resolution whole genome CGH analysis. Each array contained 385,000 isothermal 50- to 75-bp oligonucleotide probes spanning the entire nonrepetitive human genome with a median spacing of 6270 bp. Pooled normal male DNA (Promega G1471) was used as a reference sample for hybridizations. Array data were analyzed for copy number changes by Nimblegen using a circular binary segmentation algorithm with unaveraged probe signal intensities as well as probes averaged over 60 kb, 120 kb, and 300 kb windows (Venkatraman and Olshen 2007). Relative intensity of the sample *versus* reference signals was reported on a log2 scale, so that a normal copy number (relative intensity =1) should give a value of log2 (1) =0. Heterozygous duplications theoretically should give a value of $\log_2$ (3/2) =0.58 and heterozygous deletions a ratio of log2 (1/2) =1.0, but the actual magnitude of the ratio observed is somewhat less due to background hybridization. Inspection of array data from other studies revealed that the vast majority of signals with log2 ratios in the range of > +0.3 to <- 0.3 are either technical artifacts or represent genomic regions that show variable copy numbers among normal individuals (Database of Genomic Variants); therefore, only signals with log2 ratio > +0.3 or <-0.3 were considered to denote potential causal variations.

FISH and quantitative PCR

Chromosomal copy number abnormalities detected by array CGH were confirmed by FISH. Peripheral blood samples were collected from probands and their available parents and FISH was performed on lymphocyte metaphase preparations using probes specific for the reported abnormalities. These included commercially available 1q, 7q, 15q, 16q, 17q, and 19p subtelomeric probes (Vysis, Inc.), a commercially available 22q11.2 probe (TUPLE1, Vysis, Inc.), and custom 2q BAC clone probes, RP11-91M5 and RP11-81P3 (BACPAC Resources, Inc.). For six putative copy number changes too small to detect by FISH, real-time quantitative polymerase chain reaction (RT qPCR) was performed using custom Taqman probes and a reference RNAseP genomic probe (sequences available upon request). RT qPCR was performed using an ABI instrument and Taqman Universal PCR Master Mix kit (Applied Biosystems, Foster City, CA) using DNA from probands, parent(s) (if available), and unrelated ethnically-matched control individuals. 10–30 ng of genomic DNA was used for each RT PCR reaction. Experiments were performed in triplicate and mean ratios of regions of interest, normalized to RNAseP, were calculated for probands, parent(s) (if available), and unrelated normal controls. Proband/control ratios <1.3 or >0.7 were considered evidence of duplication or deletion, respectively.

Statistical analysis

Bivariate analysis was performed using Fisher's Exact test (two- tailed) for associations between categorical variables and *t* test to compare means of continuous variables in the analysis of copy number variations (CNV) between populations. p Values of ≤ 0.05 were considered statistically significant.

RESULTS

High resolution oligonucleotide array CGH was used to screen twenty subjects with CHD and additional birth anomalies (population A) and twenty subjects with isolated CHD (population B). Combining both populations, a total of 296 CNV were identified. Both populations had similar numbers of CNV per subject, with no significant difference in their values. Population A had 161 CNV for an average of 8.1 ± 3.2 CNV/ subject while population B had 135 CNV with an average of 6.8 ± 2.9 CNV/ subject.

In an effort to screen out CNV known to be present in the general population at large, we compared our list to the Database of Genomic Variants (http://projects.tcag.ca/variation). Doing so revealed that 254 of the 296 (86%) were commonly occurring and were excluded from further study, on the basis that they are likely common copy number polymorphisms. Additionally, we scrutinized the chromosomal regions of the remaining CNV to determine if any resided in known chromosomal segmental duplications or in regions with no known or hypothetical genes. CNV found in segmental duplications or found to be intergenic were excluded from further study as potentially associated with congenital heart disease and are summarized in Appendix A.

The remaining CNV were analyzed to determine their likelihood of being associated with congenital heart defects. Of the thirteen, seven large CNV were identified in five patients. Five of the seven were the result of cryptic unbalanced translocations, creating both partial duplication of one chromosome and partial deletion of a second. The summary of these translocations in patients A9, A10 and A20 can be found in Figure 4-1

B, C and E, and also summarized in Table 4-2. FISH studies confirmed the presence of six of the seven large CNV, with the small 75kb 7q36.3 deletion in patient A20 too small for adequate resolution by this method using commercial probes (Figure 4-2).

Further genetic testing using FISH was performed on the parents of patients A10 and A20. The unbalanced translocation in patient A10 was found to have been transmitted paternally after initially arising from a balanced translocation of chromosomes 15q26.2 and 1q43. Patient A20's unbalanced translocation was determined to have been transmitted maternally arising from a balanced translocation of chromosomes 7q36.3 and 17q24.3. Analysis of the inheritance of patient A9's unbalanced translocation was not performed because parental evaluation was declined.

The two remaining patients with large CNV, A8 and A11, were found to have an interstitial chromosomal deletion and duplication respectively (Figure 4-1A and D). Paternal testing of patient A8 was unavailable, but maternal testing proved normal and devoid of 2q33 duplication. Both parents of patient A11 showed normal karyotypes with no evidence of 22q11.2 deletion. It should be noted that FISH was able discern the inheritance patterns of an unbalanced translocation in both A10 and A20 as well as a *de novo* deletion in A11.

The remaining six CNV were too small to be resolved using FISH, and a Real Time quantitative PCR method was employed for confirmation. The approximately 120,000bp and 180,000bp microdeletions on chromosome 7 and 13 were verified, as well as the 60,000bp microduplication of chromosome 3. The remaining three CNV could not be corroborated, suggesting false positives and are summarized in appendix C.

The microdeletions of chromosomes 7 and 13 were not detected in 200 ethnically matched controls, however, both were found to be inherited from an unaffected parent who had a normal transthoracic echocardiogram (appendix C). DNA was unable to be obtained from the parents of the subject carrying the chromosome 3 microduplication, and therefore inheritance cannot be studied. However, a similar duplication was found in 1/200 ethnically matched controls using quantitative PCR methods and is therefore assumed to be a copy number polymorphism (appendix C).

Statistical analysis of our data clearly shows a higher risk for chromosomal anomalies in patients with CHD and additional birth defects compared to isolated CHD (5/20 versus 0/20, $p<0.05$, Table 3-3). Additionally, the presence of a neurological anomaly, which was defined here as either developmental delay or a neurological structural abnormality, in conjunction with CHD had the highest correlation with CNV compared with the other types of birth defects or isolated CHD (5/11 versus 0/9, p value <0.04; 5/11 versus 0/20, p value <0.005). There was a higher incidence of chromosomal abnormalities in children with cardiac and neurological birth defects than has been seen by current cytogenetic banding methodology in our study population.

DISSCUSSION

Twenty-five percent of children with congenital heart defects and additional birth defects had chromosomal copy number changes in this study. Significantly, none of the abnormalities were visible by traditional G-banded karyotyping, but all were resolved by whole genome array CGH. The incidence of chromosomal copy number changes like translocations, small deletions or duplications increased to nearly 50% in children with congenital heart disease and additional neurological defects such as developmental delay (Table 4-3). No chromosomal copy number changes were seen in the control population of isolated congenital heart disease, although it is possible that CNV exist but were smaller than the threshold of detection for array CGH. Additionally, mosaic abnormalities, which would result in signals below the agreed upon level for CNV ($\log_2$ ratio >0.3 or <-0.3) cannot be excluded. Despite the small size and heterogeneous nature of the study population, the results suggest that there is a substantial subset of patients with CHD, especially in conjunction with developmental delay, that harbor chromosomal anomalies which would be missed by traditional karyotyping methods.

All of the chromosomal copy number changes discovered in this study are large and affect large regions of DNA including multiple genes. Additionally, three of the five cases have been demonstrated to be *de novo* mutations. The likely explanation for the disease phenotype in patients A9, A10 and A20 are the presence of the unbalanced translocations, which result in the deletion and duplication of numerous genes (Ravnan et al. 2006). Unfortunately in our study, these unbalanced translocations prevent identification of candidate genes for CHD in the translocated regions, given the multitude of affected genes and range in the number of their copies. Deletions of 22q11.2 and duplications of chromosome 2q33 have both been reported in the literature to be associated with congenital malformations (Bird and Mascarello 2001; Ryan et al. 1997; Sebold et al. 2005). While standard manifestations of the 22q deletion syndrome in humans or the equivalent mouse model do not include myelomeningocele, case reports of tetralogy of Fallot and neural tube defects have been described (Baldini 2002; Maclean et al. 2004). Small CNV were identified in 7.5% (3/40) with CHD, and since they were also present in unaffected parents or normal control individuals, it is likely that they are not responsible for the development of CHD with complete penetrance. However, it is also equally possible that these CNV function as susceptibility loci for CHD. Furthermore, the presence of 21 novel CNV in regions that contain no known or predicted genes illustrates both the uncertainty of their function and also the need for larger public databases for reporting normal CNV.

Single gene defects and chromosomal abnormalities have been determined to be responsible for only 10-15% of CHD, with the vast majority believed due from a complex interaction of environmental and genetic factors (Ferencz et al. 1989). The data presented in this study, as well as other recent reports, suggests that increased clinical use of array CGH will result in the identification of increasing numbers of CNV associated with CHD and additional birth defects (Thienpont et al. 2007). In this study, children with CHD and neurological defects were at the highest risk for such CNV. The small control population of isolated CHD suggests that these children are less likely to harbor chromosomal anomalies that are detectable by array CGH, but as new technologies arise, it is possible that smaller- disease causing CNV will be identified. This study shows that cryptic and subtle chromosomal anomalies are being missed by routine genetic testing in current clinical practice.

The majority of the CNV identified in this study were localized to the telomeric chromosomal regions. Sub-telomeric FISH would have identified 60% (3/5) of the cryptic abnormalities but a single test, array CGH, detected all CNV while additionally defining the breakpoint boundaries. Additionally, high resolution oligonucleotide array CGH can identify complex sub-telomeric arrangements, like the 75kb deletion of chromosome 7 in patient A20. Due to the smaller size, this deletion is likely to have been missed by standard sub-telomeric FISH panels which rely on large single clones to the most distal unique sequences (Ballif et al. 2007).

The importance of identifying the genetic etiologies of CHD is underscored in the genetic counseling arena, where accurate counseling to parents helps them to determine the likelihood of having additional affected children, which can greatly influence future reproductive plans. Most CHD has a variable recurrent risk of 2-6%, but this can be greatly increased when parents harbor balanced translocations or chromosomal deletions or duplications. This was the case in some of the participating families, and is of great importance for patients with CHD to be properly informed as they grow older and begin starting families. Additionally, increased knowledge of the underlying genetic condition improves medical treatment as well as parental understanding about future expectations of their children. Finally, the use of sensitive methods such as array CGH could prove important when looking at long-term outcome in patients with or without genetic abnormalities.

Array CGH has already been used to discover several disease causing genes. In the case of CHD, the most commonly employed methodology is linkage analysis, which requires large pedigrees spanning multiple generations and with numerous affected family members. Currently known genetic causes of CHD involved less severe cardiac malformations like septal defects and valvular disease which can segregate in multiple generation pedigrees (Garg 2006). Use of array CGH when studying the genetic causes of CHD will become especially useful when evaluating more severe forms of heart disease which were until recently neonatally lethal, thus eliminating the prospect of extended pedigrees for linkage. Increases in the discovery of CNV associated with CHD will no doubt further the need to have large and extensive databases of phenotypically well characterized populations to aid in determining significance (Lee et al. 2007). In keeping with this vein, all results generated from this study have been deposited in DECIPHER (DatabasE of Chromosomal Imbalance and Phenotype in Humans using Ensembl Resources, http://decipher.sanger.ac.uk)

This study demonstrates that children with congenital heart defects frequently harbor cryptic chromosomal anomalies that are not detectable using standard karyotyping techniques. This is also especially true in children with congenital heart defects and additional neurological defects. Based on the results of this study, it is logical to advocate for genetic testing in patients with CHD, especially when neurological defects such as developmental delay are present. Additionally, this study also proves the validity and advantage of using an array based technique when searching for such genetic copy number changes, in addition to standard genetic techniques, such as sub-telomeric FISH and G-banding methods. As this technique becomes more widely utilized in clinical settings, it will unquestionably serve as an important tool in the genetic evaluation of children with multiple birth defects.

TABLE 4-1

Subject	Cardiac diagnosis	Other diagnoses
A1	Pulmonary valve stenosis	Duplicated renal collecting system, DD, DF
A2	Hypoplastic left heart syndrome	Congenital hip dysplasia, DF
A3	Atrioventricular septal defect	Triphalangeal thumb
A4	Double outlet right ventricle	Omphalocele, absent diaphragm
A5	Dysplastic mitral valve	Chiari I malformation, DD, DF
A6	Hypoplastic left heart syndrome	Congenital hydrocephalus, horseshoe kidney, DF
A7	Sinus venosus atrial septal defect	DD, DF
A8	Aortic coarctation	DD, DF, hypoplastic fingernails
A9	Atrial septal defect	DD
A10	Atrioventricular septal defect, LV noncompaction	Hypoplastic corpus callosum, DF, duplicated left renal collecting system, intestinal malrotation
A11	Tetralogy of Fallot	Myelomeningocele, Arnold-Chiari Type II malformation
A12	Atrial septal defect	Absent radii and thrombocytopenia
A13	Atrial septal defect	Absent left depressor anguli oris muscle
A14	Tetralogy of Fallot	DD, DF, right cryptorchidism, ear anomalies
A15	Patent ductus arteriosus	DF
A16	Atrial and ventricular septal defects	DF
A17	Tetralogy of Fallot	Cleft lip, speech delay, pre-auricular tag
A18	Atrial septal defect, patent ductus arteriosus	Talipes equinovarus, small eye
A19	Pulmonary valve stenosis	DD, extrapupillary membrane, partial aniridia
A20	Tetralogy of Fallot	DD, hearing loss

DD, developmental delay; DF, dysmorphic facies; LV, left ventricle.

TABLE 4-1

Population with congenital heart disease and associated birth anomalies.

FIGURE 4-1

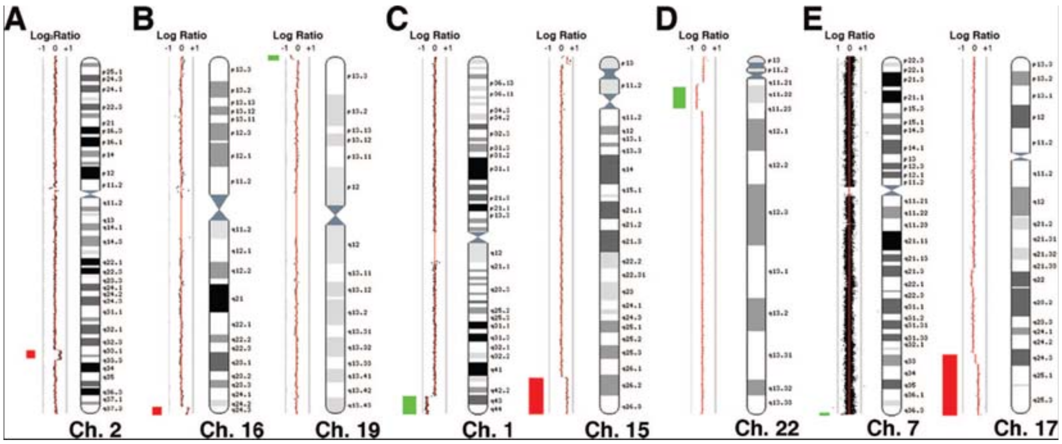

FIGURE 4-1

Copy number variations discovered by array CGH. *A*, In subject A8, a 6.6 Mb duplication of chromosome (ch) 2q.33 was found. *B*, A 2 Mb duplication of ch16q and 600 kb deletion of ch19p was identified in subject A9. *C*, A 12.3 Mb deletion of ch1q and 8.1 Mb duplication of ch15q was discovered in subject A10. *D*, In subject A11, a 3Mb deletion of chromosome 22q11 is identified. *E*, In subject A20, a 75 kb deletion of ch7q and 14.1 Mb duplication of ch17q was identified. The respective chromosomes are shown and labeled. Signal intensity is plotted on a log2 scale, so that a normal copy number gives a value of 0. Chromosome deletions are denoted by leftward segments (*green*) whereas duplicated segments are rightward (*red*).

TABLE 4-2

Subject	Genetic abnormality (gain/loss) ISCN karyotype and FISH results	Parental findings
A8	*Duplication of 2q33.1–q33.3*	Mat: NL
	46,XY,dup(2)(q33.1q33.3).ish dup(2)(q33.1q33.3)(RP11-91M5++,RP11-81P3++)	Pat: UNK*
A9	*Unbalanced 16q24.2;19p13.3 translocation (duplication of 16q;deletion of 19p)*	Mat: UNK*
	46,XY.ish der(19)t(16;19)(q24;p13.3)(16QTEL013+,129F16/SP6−)	Pat: UNK*
A10	*Unbalanced 1q43;15q26.2 translocation (duplication of 15q;deletion of 1q)*	Mat: NL
	46,XY.ish der(1)t(1;15)(q43;q26.2)(D1S3738−,D15S396+)pat	Pat: BAL†
A11	*Deletion of 22q11.2-q11.2*	Mat: NL
	46,XX.ish del(22) (q11.2q11.2)([TUPLE1,D22S553, D22S609,D22S942]−)	Pat: NL
A20	*Unbalanced 7q36.3:17q24.3 translocation (duplication of 17q;presumptive partial deletion of 7q subtelomere)*	Mat: BAL‡
	46,XX,der(7)t(7;17)(q36.3;q24.3).ish der(7)t(7;17)(q36.3;q24.3)(VYJyRM2000+, D17S928+)mat	Pat: NL

* Parents declined cytogenetic evaluation.
† ISCN karyotype: 46,XY.ish t(1;15)(q43;q26.2)(D1S3738−, D15S396+; D1S3738+, D15S396−).
‡ ISCN karyotype: 46,XX,t(7;17)(q36.3;q24.3).
ISCN, International System for Human Cytogenetic Nomenclature; Mat, maternal; Pat, paternal; NL, normal; UNK, unknown; BAL, balanced carrier.

TABLE 4-2

Cryptic chromosomal abnormalities uncovered by array CGH.

FIGURE 4-2

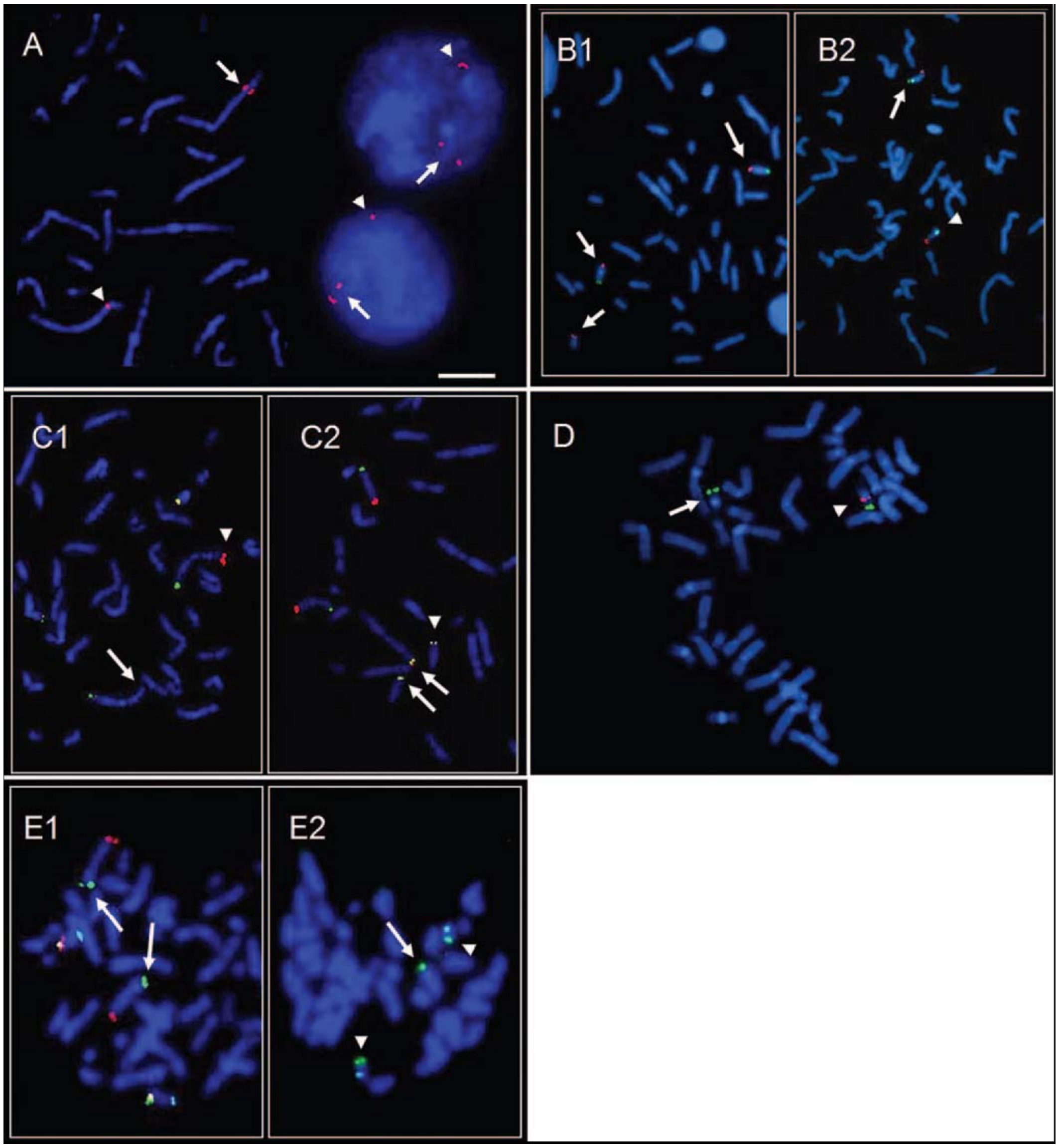

FIGURE 4-2

FISH demonstrates chromosomal abnormalities in five subjects with CHD and additional anomalies. *A*, Interstitial duplication of long arm of chromosome (ch) 2. FISH using custom BAC clones shows normal hybridization signals to the normal homologue of ch2 (*arrowhead*) and duplicated hybridization signals to the abnormal homologue of ch2 (*arrow*). Hybridization signals are also seen in interphase cells (*right*) with *long arrows* showing two signals (duplication) and *arrowhead* showing a single signal (normal). *B*, Unbalanced translocation involving the long arm of chromosome 16 and short arm of ch19. *B1*, FISH using subtelomeric probes to the short arm (*green signal*) and long arm of ch16 (*red signal*) indicate trisomy for the terminal region of ch16. *B2*, FISH using probes for the subtelomeres of the short arm (*green*), long arm (*red*), and centromere (*aqua*) of ch19. Absence of the green signal (*arrowhead*) indicative of deletion of the distal segment of the short arm of ch19 when compared with normal ch19 (*arrow*). *C*, Unbalanced translocation involving the long arm of ch1 and the long arm of ch15. *C1*, FISH using subtelomeric sequences for the short arm (*green*) and the long arm (*red*) of chromosome 1. *Arrow* identifies the distal long arm of the abnormal chromosome 1 (signal missing), *arrowhead* identifies the distal long arm of the normal chromosome 1. Additional signals (*yellow*) in C1 identify Xp/Yp subtelomeric regions used as reporter sequences. C2, *Arrows* identify hybridization signals for the subtelomeric sequences of ch15. *Arrowhead* indicates a ch15q hybridization signal on the long arm of ch1. Additional signals in C2 indicate short arm of ch10 (*green*) and long arm of 10 (*red*) as reporter sequences. *D*, FISH showing normal hybridization to the DiGeorge/velo-cardio-facial syndrome critical region at chromosome 22q11.2 using a TUPLE1 probe.

Arrowhead identifies normal hybridization pattern (*red*), arrow points to the deleted region. *Green* signal identifies distal ch22q, a reporter sequence encoding the arylsulfatase A gene. *E*, Unbalanced translocation involving the long arm of ch7 and the long arm of ch17. *E1*, FISH showing hybridization of subtelomeric sequences to the short arm (*red*) and the long arm (*green*) of ch7. *Arrows* indicate hybridization to the long arms of both the normal and abnormal homologues of ch7 indicating that the subtelomeric sequences on the abnormal chromosome are intact. The second set of signals is a reporter and identifies ch14. *E2*, *Arrowhead* identifies hybridization to the telomeres of the long arms of the normal homologues of ch17. *Arrow* identifies a ch17 hybridization signal on the distal long arm of ch7. The scale bar in A represents 5 μm and the same magnification of 600x is used in all images.

TABLE 4-3

Population	Chromosomal abnormality	*p*
CHD + birth defects	5/20 (25%)	<0.05*
CHD + neurologic defects	5/11 (45%)	<0.04†
CHD + non-neurologic defects	0/9 (0%)	
CHD (isolated)	0/20 (0%)	<0.005‡

* CHD + birth defects compared with isolated CHD.
† CHD + neurologic defects compared with CHD + non-neurologic defects.
‡ CHD + neurologic defects compared with CHD + isolated CHD.

TABLE 4-3

Frequency of genetic abnormalities in congenital heart disease populations.

CHAPTER FIVE

A novel mitochondrial disorder resulting from an *ANT2* null human

BACKGROUND

Congenital Malformations

Congenital birth anomalies are morphologic defects that are present at birth. These congenital malformations are the leading cause of mortality in the first year of life and are responsible for the deaths of an estimated 747 infants for every 100,000 live births. Congenital heart defects are the most common kind of congenital birth anomalies but all organs systems can be affected (Martin et al. 2005; Nussbaum Robert L. 2007).

Causes of Congenital Malformations

Genetics and environmental teratogens have both been found to cause congenital malformations. One quarter of congenital malformations are caused by chromosomal imbalances, with single gene mutations accounting for an additional 20%. However, half of all major birth defects have no identifiable cause but recur more frequently than expected in families with affected children. The cause of these defects is thought to be multifactorial and may involve many genes (Nussbaum Robert L. 2007). With the prevalence of so many clinical malformations and clinical cases assigned an unknown etiology, it becomes all the more crucial to discover the identity of genes that govern embryonic development. Moreover, it is critical to understand how gross or subtle perturbation of these complex pathways affect normal embryonic development.

Genetic analysis by karyotype is standard when a patient presents with problems of early growth and development, including developmental delay, dysmorphic facies, and multiple malformations or mental retardation. G-banding karyotype is a well established method and has been used for many years to discern changes in chromosomal number or size (Nussbaum Robert L. 2007). However, the resolution of G-banding is 5Mb, which is often not sensitive enough to identify smaller pathogenic deletions or duplications (de Ravel et al. 2007). Array comparative genomic hybridization (aCGH) has revolutionized clinical cytogenetics by enabling the detection of genome-wide DNA copy number alterations as small as 100 kb (Edelmann and Hirschhorn 2009). When aCGH is used in conjunction with traditional karyotyping methods, it has proven very effective in revealing the presence of cryptic microdeletions or duplications that would otherwise have been missed, and thus has been instrumental in identifying and characterizing new genetic syndromes (Selzer et al. 2005; Urban et al. 2006).

Mitochondrial disease

Mitochondrial diseases are a collection of inherited disorders that are associated with a extensive range of presentations, symptoms, severity and outcomes (Debray et al. 2008) and are perhaps some of the most challenging to diagnose and manage. On the whole, they form one of the most common groups of inherited metabolic diseases, with a minimum prevalence estimated at 1 per 5000 live births (Calvo et al. 2006; Mancuso et al. 2007). Since oxidative phosphorylation is necessary for nearly all cells of the body, any organ can be affected in mitochondrial diseases. Symptoms of mitochondrial dysfunction range from relatively mild aspects like muscle weakness, pigment or hair anomalies to more severe phenotypes such as ophthalmoplegia, seizures, neuropathy, deafness, pancreatic insufficiency and cardiomyopathy (Dimauro and Davidzon 2005; von Kleist-Retzow et al. 2003). In some forms of mitochondrial disease symptoms will appear in the first week of life. Other symptoms are adult onset and require decades to fully manifest.

Contributing to the general complexity of this disease family is its genetic nature. Mitochondrial disease can be caused by mutations in genes encoding any of the numerous proteins involved in oxidative phosphorylation (OXPHOS) and related mitochondrial transporters as well as genes that function in mitochondrial biogenesis. Only 13 mitochondrial proteins are encoded by the mitochondrial genome, a 16.5 kb circular plasmid DNA present in great number in cells. The remainder are encoded in over 1,000 nuclear genes (Mancuso et al. 2007; von Kleist-Retzow et al. 2003). If a mitochondrial disease is suspected, clinically-available mutational studies focus on well-characterized, common disease causing mutations and do not detect mutations in other genes. As a result, many suspected mitochondrial disorders do not have a confirmed genetic etiology and less is known about the relative contribution of specific complexes and subunits to overall mitochondrial function in humans.

In the present study, a novel microdeletion of Xq24 is detected by array CGH. The deletion encompasses a mitochondrial transporter gene previously unassociated with mitochondrial disease. The unusual constellation of congenital anomalies seen in the patient suggests new roles for mitochondrial dysfunction in the development of congenital malformations.

METHODS AND MATERIALS

Array Comparative Genomic Hybridization

Genomic DNA was purified from cultured cells or peripheral blood lymphocytes by standard methods. Array Comparative Genomic Hybridization (aCGH) was performed by Nimblegen Systems Inc. (Madison, Wisconsin) using a whole genome array containing ~385,000 isothermal 50 – 75mer oligonucleotide probes. The aCGH performed on lymphocyte genomic DNA from S016P had a mean probe density of one probe per 6270 bp for the whole genome array. Pooled human reference DNA from phenotypically normal males was obtained from Promega (Madison, Wisconsin).

Refinement of deletion breakpoints

Eleven sets of PCR primers were designed using Primer3 software (Rozen and Skaletsky 2000) that tiled the deletion and surrounding genes. All PCR products are ~500 base pairs in length and amplify with a 60 °C annealing temperature.

Sequence	Description	Amplified Region	Length
ccataactctcactggtgtagcc cagaaaggtcatcgtactcatcc	PGRMC1	118257917- 118258401	485
tcaatcactgatctagctgcaaa accatgcctggactagttgagta	~20 kb downstream of PGRMC1	118281451- 118281867	417
ccaaaccaatgttcatcctacat aattcccactcagtgatctttca	Midpoint between PGRMC1 and SLC25A43	118335103- 118335586	484
acgaggtcgagagatcgaga tgatcttggctcactgcaac	SLC25A43	118469319- 118469725	407
gaacccagttttggctctacttt	SLC25A5	118487857- 118488363	507

ctgggaataggaaagagatgctt			
actcatcaattcattcagccagt tgtttgcccttgaagtctacatt	Midpoint between SLC25A5 and CXorf56	118521115- 118521543	429
gcttttgtccccactctctttat agggtgtagcagaagagtgtcag	CXorf56	118574285- 118574851	567
aagggtttctgagagggactatg gaggaaaggccaggtaagaaata	UBE2A	118598911- 118599379	469
aggcaaggacaatgactttgtaa ttgttggctctgttgtaaggttt	Midpoint between UBE2A and NKRF	118603564- 118604039	476
caagctgcattgttggtacg ggctttgtaactgcctctgc	NKRF intron 2	118609388- 118609772	385
tacctctcatcttcaggtgggta ataaacctcgagcaacaaatcaa	NKRF intron 1	118620980- 118621468	489

Family linkage

Transmission of the chromosome harboring the deletion was traced using X chromosome microsatellite markers. A genotype consisting of 4 microsatellite markers that spanned 2,563 kb of the X chromosome including the deleted region was created using three commercially available markers (DXS064, 1,260kb proximal from the deletion, DXS8067, 827kb distal to the deletion and DXS1001, 476 kb distal from DXS8067). The fourth marker was custom designed to measure a CA repeat found in the deleted region using the following primers: tccgtattcctatgagacctgaa, aagtgatgcaaacagccatagac, which amplify the repeat found at chrX: 118382948-118382982 (hg 18 assembly).

Fluorescence in Situ Hybridization

Metaphase chromosomes from immortalized lymphoblasts were used for fluorescence in situ hybridization (FISH). Bacterial artificial chromosome (BAC) clones (BACPAC Resources, Oakland, CA) were cultured, and BAC DNA was isolated using the BACMAX DNA isolation kit (Epicentre, Madison, WI). DNA was labeled with Spectrum Orange (Vysis, Downers Grove, IL) according to the manufacturer's instructions, precipitated, resuspended in hybridization buffer (Vysis) and visualized with an Olympus BX-61 fluorescent microscope equipped with a charge coupled device camera and Cytovision digital image acquisition system (Applied Imaging, San Jose, CA). For determination of maternal X-inactivation, metaphase chromosomes from PHA-stimulated whole blood lymphocytes were cultured in the presence of Bromodeoxyuridine (BrdU), and underwent the FISH protocol as described above. Determination of X-inactivation was performed using FISH to identify the deleted X chromosome and immunofluorescent detection of Bromodeoxyuridine incorporation to identify the active X chromosome as described previously (Wei et al. 2001). The percentage of inactivated X chromosomes was determined by analyzing 100 metaphases.

Flow Cytometry

Cells were analyzed with a Becton Dickinson FACS Calibur Flow Cytometer (Becton Dickinson, San Jose, CA) in the University of Texas Southwestern Flow Cytometry Core facility. The standard emission filters for the FL1 (JC-1 monomers and NAO), FL2 (JC-1 aggregates), and FL3 (PI and DHE) photomultipliers were used on the FACS Calibur. All cells were initially gated based on forward and side scatter to exclude dead cells and debris, and further gated to include ≥ 20,000 G1/S/G2 cells, unless specified otherwise. Flow Cytometry data was analyzed using Becton Dickinson CellPro Software.

Mitochondrial Membrane Potential

Each sample was suspended in 1ml warm PBS at 1x 10^6 cells/mL. For a control tube, 1 µL of 50mM CCCP (Sigma, St. Louis, MO) was added and incubated at 37 °C for 5 minutes (50µM final concentration). JC-1(Invitrogen, Grand Island, NY) was added to each sample to a final concentration of 2µM and the cells were incubated at 37 °C, 5% CO_2 for 15 to 30 minutes. The cells were washed with warm PBS and pelleted by centrifugation. Samples were resuspended in 500mL of PBS and promptly analyzed on a flow cytometer. Membrane potential was estimated using the ratio of red fluorescence (FL2) to green fluorescence (FL1).

Mitochondrial inner membrane content

1 x 10^6 cells were incubated for 30 minutes at 37°C in RPMI media with 5µM Nonyl Acridine Orange (NAO) (Sigma, St. Louis, MO). The cells were incubated for 30 minutes at 37°C, 5% CO_2, washed in PBS without Ca^{2+} and Mg^{2+} and resuspended in PBS at a final concentration of 1 x 10^6 cells/ml. Cells were then fixed for 30 minutes at 4°C in 1mL of a 70% ethanol solution. After washing in PBS, the cells were incubated for 30 minutes at 37°C with RNAse A (Sigma, St. Louis, MO) solution (50 pg/ml) prepared in PBS without Ca^{2+} and Mg^{2+}. After washing in PBS, the cells were resuspended in 1 ml of propidium iodide solution (Roche, Mannheim, Germany). Cells were then analyzed using flow cytometry. The DNA content, proportional to the

propidium iodide fluorescence, was evaluated on a linear scale using FL3 and the NAO green fluorescence on a logarithmic scale using FL2. For each parameter, a total of 20,000 cells were analyzed. Mitochondrial inner membrane content was normalized to nuclear DNA.

Mitochondrial superoxide production

Dihydroethidium (DHE)(Invitrogen, Grand Island, NY) was used to detect intracellular superoxide. The dye is mitochondrial specific and when oxidized, emits a red fluorescence. Cell lines were collected and washed twice with PBS and incubated ($0.5x10^6$/200µl) for 120 minutes at 37°C in buffer containing PBS, 20mM glucose and 2µM DHE. Fluorescence was recorded immediately after adding DHE (time zero) and after 120 minute incubation in ≥20,000 non-apoptotic cells using flow cytometry standard filter FL3. Superoxide production was expressed as mean fluorescence per cell.

Viability Index

Approximately 1x 10^6 cells were collected and centrifuged. 200 × g centrifuged cell pellet was gently resuspended in 1.5 ml hypotonic fluorochrome solution (PI 50 µg/ml in 0.1% sodium citrate plus 0.1% Triton X-100, Sigma), and placed at 4° C in the dark overnight. The tubes containing the cells were covered in aluminum foil to prevent photobleaching and flow cytometry analysis was preformed the following day. All cells were recorded after initially gating out dead cells and debris (based on size and cell complexity) and ≥20,000 cells were counted to determine percentage of non-viable or viable (non-apoptotic) cells. The protocol is adapted from (Nicoletti et al. 1991).

Cell culturing protocol

All cells are cultured in RPMI Advanced 1640 Medium (Invitrogen, Grand Island, NY) supplemented with 15% FBS, glutamine, 1x antimycotic/antibiotic, and 2mM uridine. For antioxidant experiments, the standard medium was supplemented with antioxidants, 60µM Ascorbic Acid, 3.75mM N-acetyl cysteine (Sigma, St. Louis, MO), or both.

Quantitative PCR assay for mitochondrial deletions

Applied Biosystems Taqman probes for NADH Dehydrogenase subunit 1 (ND1) and NADH Dehydrogenase subunit 4 (ND4) were used to estimate mitochondrial genome deletions (Krishnan et al. 2007). Total genomic DNA was used for this assay at a concentration of 20ng per well with a total volume of 20 µl. All samples were run in triplicate on an Applied Biosystems 7900HT Sequence Detection System and analyzed using SDS.2.2.2 software.

Oximetry

Cellular respiration was measured in nonpermeabilized lymphoblasts. 1x 10^6 viable cells (based on trypan blue staining) were resuspended in 200 µL respiration buffer (0.3M Mannitol, 5mM $MgCl_2$, 10mM KCl, 10mM K_2P0_4, pH 7.4) augmented with 20ug/mL succinate. Cells were loaded into a Strathkelvin Mitocell MT100, and total oxygen concentration was recorded every 30 seconds. After 5 minutes, 1µM final concentration of the mitochondrial uncoupler carbonyl cyanide m-chlorophenylhydrazone (CCCP)(Sigma, St. Louis, MO) was added to depolarize the membrane. Rate of oxygen consumption before and after addition of uncoupler was calculated using Linear Anaysis and Graph Pad Prism 5 Software.

Statistical Analysis

Statistical significance between the two groups was determined using Student's T-Test, two tailed distribution assuming equal variance between samples, and calculated using GraphPad Prism 5 software.

RESULTS

Case Report

The proband, S016P, was seen clinically by a collaborating pediatric urologist, Dr. Linda Baker, for cryptorchidism, and congenital kidney stones. The male proband also presented with multiple additional birth anomalies including congenital cataracts, sensorineural deafness, bilateral duplicated kidneys, and multiple heart defects (Table 5-1). The full spectrum of phenotypes suggested potential involvement of two separate conditions, a chromosomal anomaly and a possible mitochondrial disorder. According to genetics textbooks, screening for chromosomal anomalies is clinically indicated for problems of early growth and development, including developmental delay, dysmorphic facies, and multiple malformations or mental retardation. While these symptoms are not exclusive to chromosomal anomalies, they are still very commonly associated (Nussbaum Robert L. 2007). The presence of at least four indicating symptoms in this patient strongly pointed to chromosomal perturbation. However, a conventional G-banded karyotype was normal 46, XY. Moreover, many of the phenotypes involve seemingly unrelated organs or tissues, which are a hallmark of mitochondrial disorders. Mitochondrial disease can affect any organ at any age and can exhibit great variability in clinical presentation, but commonly is associated with renal, neuromuscular, hepatic, endocrine, cardiac, ophthalmologic, developmental delay, sensorineural hearing loss and hematological anomalies (Munnich and Rustin 2001). Based on these dual indications of a unifying explanation for the patient's phenotype, genetic analysis using high resolution oligonucleotide array comparative genomic hybridization (aCGH) was performed.

Chromosome Xq24 Microdeletion

The results of the aCGH suggested a ~240 kb microdeletion on Xq24, encompassing 2 genes, ANT2 and SLC25a43, both mitochondrial solute carriers. The deletion was confirmed and its endpoints refined by PCR amplification of eleven sequences in and around the putative deletion. The results showed that the deletion encompassed two additional genes, UBE2A and CXorf56, and part of a third gene, NKRF (Figure 5-1). To determine if the deletion was transmitted or was de novo, the proband's mother was tested using fluorescent in situ hybridization (FISH). FISH using bacterial artificial chromosomes that spanned ~66% of the deleted region (RP11-54K19 and RP3-404F18) showed that the deletion was present in the mother, who was clinically unaffected. The pattern of X inactivation was then assayed to determine if she was protected by preferential inactivation of the deleted X chromosome (skewed inactivation). She was homozygous for the androgen receptor CAG repeat, and therefore the androgen receptor methylation assay could not be used to measure X-inactivation (Allen et al. 1992). As an alternative, we estimated the degree of inactivation of the deleted chromosome using a BrDU-based late replication assay (Wei et al. 2001). The mother's deleted X chromosome was inactivated in 90% of peripheral blood lymphocytes, consistent with her lack of phenotypic sequelae (Figure 5-2).

Familial Transmission

S016P is part of a large family with multiple members affected with adult onset cataracts, calcium oxalate kidney stones or both. In order to determine if the microdeletion seen in the patient was also present in extended family members, genetic linkage was done to both trace the origination of the affected chromosome and to determine its prevalence in the family (Figure 5-3). Microsatellite markers that flanked the deleted region by ~1200 kb both proximally and distally, as well as a new microsatellite marker custom-designed to measure a CA repeat found within the deleted region were used for genotyping. Linkage analysis revealed that the affected chromosome was transmitted by the unaffected maternal grandmother, and therefore excluded this microdeletion from contributing to adult-onset kidney stones or cataracts in the extended family, since all affected members were related through the proband's maternal grandfather.

Analysis of Deleted Genes

The microdeletion found in the patient represents a contiguous gene deletion of 5 genes: *ANT2, SLC25A43, UBE2A*, *CXorf56* and *NKRF. NKRF* is a repressing factor for the transcription factor NFκB, and works to silence certain NFκB responsive genes involved in immune and inflammatory response, cell adhesion, growth control and protection against apoptosis. *UBE2A* is an ubiquitin conjugating enzyme and involved in proteolytic degradation. *ANT2* and *SLC25A43* are both inner membrane mitochondrial solute carriers. The solute for *SLC25A43* is unknown, and is expressed very weakly but predominantly in the brain and kidney in the rat (Haitina et al. 2006). *ANT2*, also known as *SLC25A5*, is a mitochondrial ADP/ATP translocase which catalyzes the exchange of cytosolic ADP for ATP synthesized in the mitochondrial matrix. As a result, *ANT2* plays an important role in maintaining the cytosolic phosphorylation potential crucial for cell growth (Klingenberg 2008; Luciakova et al. 2003).

Studies of Mitochondrial Function

The broad range of clinical symptoms and affected organ systems and loss of a genes directly involved in mitochondrial function suggest mitochondrial disease. Having established the presence of a chromosomal microdeletion in the patient encompassing known mitochondrial genes, the possibility of mitochondrial dysfunction was next investigated biochemically. Analyses included assays of mitochondrial membrane mass, mtDNA integrity, reactive oxygen species production, mitochondrial membrane potential and cellular respiration rate.

Mitochondrial diseases commonly involve deletions, depletion and or point mutations in mtDNA. A highly sensitive quantitative PCR approach was used to assess the stability of the mitochondrial DNA in the proband. The most common mitochondrial DNA deletion (ΔmtDNA4977) seen in patients deletes 4,977 bp and arises from a 13 nucleotide repeat found at position 8,470 and 13,447. As a result, 99% of mitochondrial deletions result in the loss of this span, which includes the NADH dehydrogenase subunit 4 gene, ND4. The remaining portion is kept and includes the NADH dehydrogenase subunit 1 gene, ND1 (Krishnan et al. 2007). Quantitative Taqman PCRs for ND1 and ND4 were used to assay relative amounts of the two genes in isolated genomic DNA of the patient and several normal controls (Figure 5-4). The ratio of ND4 to ND1 was used to calculate the relative amount of mitochondrial DNA deletions present in the proband, and it was determined that 36.4 % of the mitochondrial DNA in the proband harbored a deletion of ND4 sequences. By contrast, controls showed a loss of less than 4% of ND4 sequences.

Next, several measures of cellular and mitochondrial function were assessed in immortalized lymphoblasts using fluorescent dyes and flow cytometry. To determine if the patient's cells had an abnormal amount of mitochondria, the fluorescent dye nonyl acridine orange was used to stain the mitochondrial inner membrane, and normalized to the amount of nuclear DNA present using propidium iodide as a counter-stain (Lizard et al. 1990). As seen in Figure 5-5, there is no appreciable difference between the relative amount of mitochondrial inner membrane (and by inference number of mitochondria) as compared to normal male controls. Next, the mitochondrial inner membrane potential was measured using the fluorescent probe JC-1 (5,5',6,6'-tetrachloro-1,1',3,3'-tetraethylbenzimidazolylcarbocyanine iodide). JC-1 is a cationic dye that accumulates in mitochondria and exists as a green fluorescing monomer at low concentrations, but at higher concentrations forms aggregates and fluoresces red (Reers et al. 1995). The ratio of red to green fluorescence is then used to estimate membrane potential in live cells. All cells were gated based on forward and side scatter to exclude apoptotic cells, in which the membrane potential is lower. Mitochondrial membrane potential was found to be significantly elevated in the proband's non-apoptotic cells (Figure 5-6). This is both significant and expected since the adenine nucleotide transporter is critical in helping to maintain membrane potential (McMillin and Pauly 1988).

Another common symptom found in patients with mitochondrial disease is high levels of superoxide which damage proteins and nucleic acids and are responsible for unusually high levels of oxidative stress (Hoye et al. 2008). Intracellular superoxide was measured using dihydroethidium, which oxidizes in the presence of superoxide radicals and fluoresces red (Peshavariya et al. 2007). The patient's cells showed an almost three fold increase in the levels of superoxide compared with controls (Figure 5-7).

The high levels of superoxide, coupled with frequent mitochondrial DNA damage likely creates an environment conducive to cell death. Additionally, since one of the deleted genes, ANT2, is directly involved in apoptotic regulation (Halestrap and Brennerb 2003), the endogenous rate of cellular death was investigated in immortalized lympoblasts. The viability index, or percentage of viable cells found in the whole population of cells was measured using a modified protocol (Nicoletti et al. 1991). Briefly, cells were fixed in a hypotonic propidium iodide (PI) solution overnight and then measured by flow cytometry the next morning. All cells excepting for obviously dead or cellular debris were included in the analysis, unlike in previous flow cytometry experiments, where only healthy cells in the G1, S or G2 phase of the cell cycle were used. The propidium iodide is excluded from live cells and stains nuclear DNA in dead cells. In an unfixed population, it can therefore be used to differentiate live from dead/apoptotic or necrotic cells. In a healthy actively cycling cell, this signal is above a threshold of ~17 on the filter for PI. Since apoptosis results in fragmented, small sized DNA, cells registering below the threshold are considered non-viable. The percentage of non-viable and cycling cells can then estimated, and allows for a complete picture of the proportion of dying and healthy, cycling cells. After fixation and analysis of the lymphoblasts, it was found that more than 95% of the patient's cells were apoptotic, compared with a range of 60-70 % in controls (Figure 5-8). A diminished viability index is common in artificially immortalized cell lines and B cell lines (Kessel et al. 2006; Satoh et al. 2003). Nevertheless, the very low viability index in the proband's lymphoblasts points to a larger problem of uncontrolled cell death and a diseased intracellular environment.

Because the high rate of apoptosis/necrosis coupled with high levels of oxidative stress, it was hypothesized that mitigating superoxide production would stem the tide of apoptotic cell death. To test this hypothesis, antioxidants were introduced into the cell culture medium. N-acetyl cysteine, ascorbic acid (vitamin C) or both were administered for differing amounts of time to the patient's cells (Figure 5-9). The cells improved their rate of survival 5 to 15 fold with the addition of antioxidants. Moreover, the endogenous viability index in the presence of both n-acetyl cysteine and ascorbic acid improved to the same index as the control cells without treatment.

Finally, cellular respiration was measured in the patient's cells to assess if oxidative phosphorylation (OXPHOS) was perturbed as the result of the microdeletion and loss of ANT2. A well established method for studying cellular respiration is to record oxygen consumption in the presence of a substrate like succinate, and then add a mitochondrial membrane uncoupler, such as CCCP or FCCP (Barrientos 2002). Addition of the uncoupler causes a massive increase in the use of oxygen due to the mitochondria attempting to reestablish the membrane potential by magnifying oxidative phosphorylation.

When the rate of oxygen consumption was measured in the presence of succinate, the patient's cells consumed oxygen at almost half the rate of controls (14.324 $\pm$ 2.865 versus 8.017 $\pm$ 0.825, $p \leq 0.05$) (Figure 4-10, Table 5-2). Most significantly, when a mitochondrial inner membrane uncoupler was added, (1 μM CCCP) there was no increase in oxygen consumption, illustrating global OXPHOS dysfunction in the patient's cells. This same concentration of uncoupler is effectively doubled the rate of oxygen consumption by normal cells (Figure 5-10).

DISCUSSION

Microdeletion analysis

In this study, a patient with a novel Xq24 microdeletion was identified using array CGH. Traditional karyotyping was unable to detect the microdeletion due to the limits of g-banding, which is not sensitive enough to distinguish anomalies smaller than 5 Mb. Array CGH is a more powerful method which can easily detect genome-wide changes in DNA copy number as small as 100kb with great accuracy (de Ravel et al. 2007; Edelmann and Hirschhorn 2009). The patient had a clinical constellation of findings both indicative of a chromosomal anomaly, as well as symptoms suggestive of a mitochondrial disorder. Both appear to be consistent with the genetic analysis of the patient- a chromosomal microdeletion was identified, and also encompasses genes critical for proper mitochondrial function. Several of the deleted genes are plausible candidates for some of the patient's multiple phenotypes.

Two of the deleted genes are *SLC25A43* and *CXorf56*. *CXorf56* is a hypothetical protein with possible expression in lymphoblast cells (Gurkan et al. 2005), and does not have any identifiable protein motifs. While it is possible that this hypothetical protein is in fact a real gene, lack of recognizable function, coupled with lack of conservation makes it, unlikely to be causative for a multiple organ system disorder.

The second, *SLC25A43,* is also a mitochondrial solute carrier, although its substrate is not known, and its classification is based on conserved SOLCAR repeats which are found in mitochondrial proteins that act as carriers or transporters (Haitina et al. 2006). Mitochondrial involvement initially made *SLC25A43* an attractive candidate gene, but expression studies show it to be so weakly expressed that ≥ 40 RT-PCR cycles are needed to show any appreciable expression in multiple human tissue RNA panels. Even with the large cycle numbers, only whole brain and kidney show weak expression. The extremely low expression levels of *SLC25A43* RNA and the limited spatial expression combine to make loss of *SLC25A43* unlikely to be causative for the multiple organ system disorder seen in our patient.

NFκB repressing factor (*NKRF*) is directly involved in the NFκB signaling pathway and acts as a repressing factor to certain NFκB responsive genes. NFκB is broadly involved in many cellular pathways including immune and inflammatory response, cell adhesion, growth control and protection against apoptosis (Hayden and Ghosh 2004; Karin and Ben-Neriah 2000). Given the diverse pathways involved and also the importance of the regulation of these pathways, *NKRF* seemed a plausible candidate gene. However, *NKRF* null mice have been generated and are indistinguishable from wildtype- even after pathogenic challenge (Froese et al. 2006). It seems highly unlikely that a severe phenotype involving multiple organ systems would have no discernable difference in a murine knock out model, even considering species differences. The possibility that subtle developmental defects existed in the *NKRF* null mice that could be easily missed, such as hearing loss or kidney stones, was considered. *NKRF* null mice were examined for hearing deficiencies or kidney anomalies, but were found to be phenotypically normal, leaving loss of *NKRF* an unlikely cause of the symptoms seen in our patient.

UBE2A is also deleted in the patient, and is an ubiquitin conjugating enzyme, involved in the addition of ubiquitin molecules to proteins fated for degradation.

Nonsense mutations in *UBE2A* have been shown to be a cause of nonsyndromic X-linked Mental Retardation in a family from Brazil. Therefore, it is plausible that the developmental delay seen in the patient is the result of loss of *UBE2A* expression. To help ascertain if *UBE2A* may play a role in the myriad of other symptoms seen in the patient, the senior author of the paper describing the Brazilian family was contacted. Although there are many clinical anomalies associated with this family, including multiple facial dysmorphisms, marked general hirsutism, and seizures, none match the constellation seen in S016P. Moreover, affected members of the Brazilian family are phenotypically normal with regards to hearing, vision and heart septation (Morgante, AV. personal communication). The mutation seen in exon 5 of the Brazilian family, Q128X, is a nonsense mutation that prematurely terminates the catalytic domain of the E2 conjugating enzyme. One possible explanation is that the Q128X mutation functions as a dominant negative mutation, allowing *UBE2A* to bind to the E1 ubiquitin activating enzyme, but is unable to catalyze the exchange of ubiquitin. While functional analysis of the mutation is needed for confirmation, it may account for the discrepancy in phenotypes between S016P and the Brazilian family previously described.

ANT2, also known as *SLC25A5*, is a nuclear encoded mitochondrial protein. This gene codes for the adenine nucleotide translocase, which transports ATP out of the mitochondrial matrix in exchange for cytosolic ADP. As a result, both intracellular ATP concentrations and intramitochondrial adenine nucleotide concentrations are maintained and the production of ATP from ADP continues. ANT proteins are also components of the mitochondrial permeability transition pore, and as such are involved in the regulation of apoptosis signaling and cytochrome c release (Klingenberg 2008). In humans, there are four ANT isoforms which differ largely based on tissue expression. *ANT1* is expressed in cardiac and skeletal muscle, as well as the brain. *ANT2* is expressed in rapidly dividing tissues and thought to be inducible. *ANT3* is constitutively expressed in all tissue but at low levels. *ANT4* is expressed only in testis and involved in spermatogenesis (Lunardi et al. 1992; Stepien et al. 1992).

Expression of ANT in mice is somewhat different. *ANT1* is largely the same, with expression limited to cardiac and skeletal muscle, as well as brain. However, mice lack the *ANT3* isoform, and its role is thought to be combined with *ANT2*, expressed through the remainder of the body (Ceci 1994; Ellison et al. 1996; Levy et al. 2000).

Mutations in human *ANT1* result in Chronic Progressive External Ophthalmoplegia (CPEO), a mitochondrial disorder broadly characterized by pathology involving the eyes, skeletal muscle, and central nervous system, and accumulation of multiple deletions of mtDNA in postmitotic patient's tissues (Sharer 2005). Patients with CPEO also sometimes present with cataracts and sensorineural deafness. Given that mutations in *ANT1* result in a common mitochondrial disease, it is plausible that loss of a tissue specific ANT isoform could also be involved in the pathogenesis seen in our patient. Moreover, *ANT2* null mice have been generated and exhibit a surprising phenotype: embryonic lethality at day e14.5 due to massive cardiac septal defects (Douglas C. Wallace 2002). The patient in this study is a functional null for *ANT2* and presented with multiple congenital heart defects, including a patent ductus artereosus, multiple ventricular septal defects and an arterial septal defect. While these cardiac defects did not result in embryonic lethality in our proband, this is likely due to species differences of isoforms. In mice, there are only two ANT isoforms, and the role of *ANT2* is expanded to encompass that of *ANT3*. One explanation for the difference in severity of cardiac defects is that the presence of *ANT3* blunts some of the impact of the loss of *ANT2*. Patients with isolated ASD/VSD have been screened for mutations in *ANT2,* but no obvious disease causing mutations have been identified. The total number of patients screened are low (n =61, data not shown), and *ANT2* remains a promising candidate gene for cardiac septal defects.

One way to determine the relative contribution of specific genes in a contiguous gene deletion syndrome to associated phenotypes is to identify individuals with sporadic or familial birth defects harboring point mutations in individual genes. Dr.Burdon and colleagues have mapped a locus for X-linked congenital cataract to Xq24, including the deleted region in S016P (Craig et al. 2008). Based on the results of this study, Dr. Burdon sequenced all five candidate genes in an affected family member but did not identify any mutations. Alternatively, point mutations could be identified if larger patient cohorts were tested. Since S016P represents a unique case, it is formally possible (but unlikely) that the proband's clinical findings are unrelated to his deletion. It is also possible that concomitant deletion of more than one gene is required to cause congenital heart disease, cataracts, or other phenotypes seen in the proband.

The male proband in this study harbors a 260 kb deletion on the X chromosome. This chromosome, as well as the deletion, was inherited from his mother. Genotyping of the deleted chromosome revealed that the chromosome on which the deletion arose was transmitted from the maternal grandmother. Despite a family history of cataracts and calcium oxalate kidney stones, it appears that this deletion and the chromosome on which it arose are unrelated to the adult onset cataracts and calcium oxalate kidney stones seen in other family members, since all extended family members who were affected with cataracts or kidney stones were related through the proband's maternal grandfather. DNA is not available from the grandmother so it is currently unclear at which point the deletion arose. Additionally, the mother of the proband shows strong skewing in her expression of the deleted chromosome, as measured in whole blood. The deleted X was inactivated 90% of the time and this high rate of inactivation may account for her relatively mild phenotype, which appears to solely include adult onset calcium oxalate kidney stones. The incidence of kidney stones in the general population is estimated to be 17 per 1,000, and over 70% of kidney stones are composed of calcium oxalate. As a result, it is quite likely that the presence of adult onset calcium oxalate kidney stones in the mother is unrelated to the microdeletion. The mother of the proband also has a sister although her DNA has not been collected. The range of individuals in this family who harbor the microdeletion is possibly much larger than initially expected, and may include the maternal grandmother, maternal aunt and possibly sister (Appendix D). Additional patient recruitment is clearly needed to determine the prevalence of this microdeletion in the family, as well as refine the phenotype of carrier females.

In this study, the overall function of a patient with ANT2 null mitochondria was measured using a variety of methods to show that 1. There is mitochondrial dysfunction, 2. The dysfunction is largely similar with to a previously described analysis of ANT2 null cells, 3. The effect is consistent with the loss of a mitochondrial nucleotide carrier and 4. The mitochondrial dysfunction can be partially helped with antioxidant therapy. The ANT2 null cells exhibit a lower basal rate of oxygen consumption, insensitivity to mitochondrial membrane uncouplers, higher mitochondrial membrane potential, overproduction of reactive oxygen species, large amounts of mitochondrial DNA deletions and an extremely high rate of apoptosis, which taken together demonstrate broad mitochondrial dysfunction.

A previous account of ANT2 null mice (Douglas C. Wallace 2002) described lack of ANT contributing to a high mitochondrial membrane potential, and an increased rate of oxygen consumption in hepatocytes. The mitochondrial membrane potential was significantly higher in the patient's cell line and perfectly mirrored that seen in the null mouse. However, in lymphoblasts the basal oxygen consumption was approximately half that of controls. This discrepancy is likely caused by species differences and tissue differences. The null mouse described was null for all ANT protein in hepatocytes, while the patient described in this study is missing only one isoform and presumably still expresses low but ubiquitous levels of ANT3. Additionally, lymphoblasts are not a very metabolically active tissue, and have relatively few mitochondria. It is entirely possible that were a more energy demanding tissue assayed, like muscle or liver, the basal rate would be elevated.

In mitochondrial disorders where nucleotide carriers are affected, high rates of oxidative stress and nucleotide imbalances lead to mitochondrial DNA deletions and mutations (Copeland 2008). When assayed in the patient, more than one third of mitochondrial DNA harbored the common ΔmtDNA4977 deletion, and the amount of superoxide per cell was nearly three fold that of controls, consistent with a nucleotide imbalance.

Finally, the patient cell line exhibited extremely high rates of apoptotic/necrotic cell death. Combined with high levels of reactive oxygen species, it seemed plausible that superoxide was contributing to the rate of cell death. Administration of antioxidants n-acetyl cysteine and ascorbic acid increased the viability of the patient's cells to nearly normal levels seen in immortalized lymphoblasts, but the rate of cell death was still excessively high (~70% apoptotic/necrotic cells). It is true that B lymphoblasts exhibit high rates of apoptosis (Kessel et al. 2006), however, even with this condition at play, the patient cells underwent cell death easily. The fact that antioxidant therapy had such a robust effect on what was almost an entirely dying population lends some support for traditional mitochondrial disease therapy- which includes supplementation with large concentrations of antioxidants. This is an important step since high levels of oxidative stress damage many tissue and may be responsible for the cataracts frequently seen in patients with mitochondrial disease (Williams 2008).

Mitochondrial diseases are a heterogeneous group of disorders that broadly affect mitochondrial function. One reason for the diversity of symptoms is that disease can arise from mutations in any of the genes of the oxidative phosphorylation pathway. Components of oxidative phosphorylation are encoded by numerous mitochondrial DNA and by nuclear genes. Given that mitochondria are present in practically all tissues of the body, a single gene mutation can affect multiple seemingly unrelated organ systems. Depending on which tissues are affected symptoms can include peripheral neuropathy, muscle weakness, ophthalmoplegia, cataracts, cardiomyopathy, and sensorineural deafness to name a few (Dimauro and Davidzon 2005; von Kleist-Retzow et al. 2003).

Perhaps the most interesting aspect of the present study is the presence of congenital birth defects that are associated with ANT2 deficiency and mitochondrial disease. Many and varied symptoms exist as a consequence of mitochondrial dysfunction, but congenital structural anomalies have never been described. While the presence of mild ventricular and atrial septal defects in our patient could possibly be unrelated to the observed microdeletion, the fact that ANT2 null mice die from massive cardiac septal defects lends strength to the argument that ANT2 plays an important role in cardiac septation. ANT2 deficiency also results in the first mitochondrial disease that includes congenital cardiac anomalies as a symptom and opens the door to the possibility of mitochondrial dysfunction as a cause of congenital birth defects.

In this study, a novel mitochondrial disorder is presented, which is caused by a 260 kb microdeletion on chromosome Xq24 that includes the adenine nucleotide translocase, ANT2. Studies of mitochondrial function show high rates of oxidative stress and apoptosis, which are consistent with loss of ANT2. To the knowledge of the author, this is the first mitochondrial disorder described associated with congenital structural anomalies in addition to mitochondrial dysfunction.

TABLE 5-1

Characteristic	Associated with chromosomal anomalies	Associated with mitochondrial disease
Neurological		
Hypoplastic Cerebellum	Yes	
Developmental Delay	Yes	Yes
Sensorineural deafness		Yes- hallmark
Hypotonia	Yes	Yes
Cardiac		
Ventricular Septal Defect	Yes- multiple malformations	
Patent Ductus Arteriosus	Yes- multiple malformations	
Genitourinary		
Bilateral cryptorchidism	Yes	
Bilateral duplicated kidneys	Yes- multiple malformations	
Hydronephrosis		
Kidney Stones*		
Congenital Cataracts		Yes
Dysmorphic Facies	Yes	Yes

TABLE 5-1 Clinical characteristics of S016P. Symptoms associated with either chromosomal anomalies or mitochondrial diseases are indicated. * unknown stone type

FIGURE 5-1

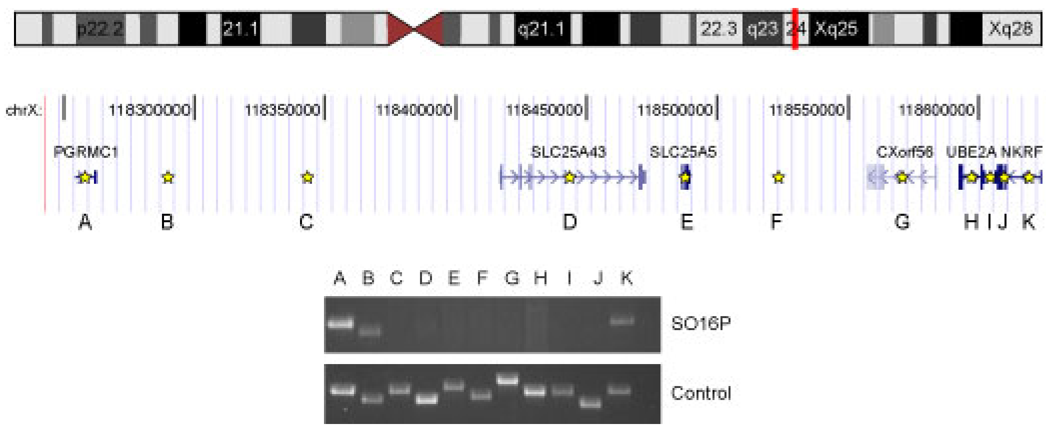
p22.2
21.1
q21.1
22.3
q23
24
Xq25
Xq28
chrX:
118300000
118350000
118400000
118450000
118500000
118550000
118600000
PGRMC1
SLC25A43
SLC25A5
CXorf56
UBE2A
NKRF
A
B
C
D
E
F
G
H
I
J
K
SO16P
Control

FIGURE 5-1

Deleted region and refinement of deletion breakpoints by PCR. The eleven PCRs that tile the region are labeled A-K, and their corresponding PCR products are shown below.

FIGURE 5-2

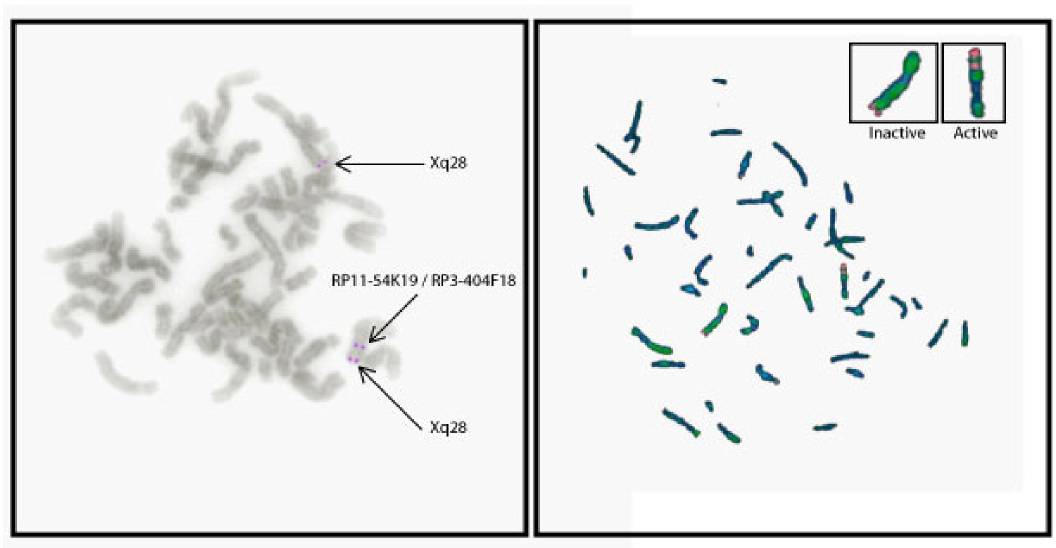

FIGURE 5-2

Left: Fluorescence in situ hybridization of maternal chromosomes for RP11-54K19/ RP3-404F18 and Xq28.

Right: Fluorescence in situ hybridization of maternal chromosomes for RP11-54K19/ RP3-404F18 and Xq28 with Bromodeoxyuridine incorporation. Inactive regions of the X chromosome stained green, active regions stain blue.

FIGURE 5-3


I - 4
DXS8064 216 216
XqCA 353 361
DXS8067 101 101
DXS1001 198 200
II - 8
II - 9
DXS8064 216
XqCA 353
DXS8067 101
DXS1001 198
III - 8
DXS8064 216 214
XqCA 353 ----
DXS8067 101 91
DXS1001 198 196
IV - 5
DXS8064 214
XqCA ----
DXS8067 91
DXS1001 196

FIGURE 5-3

Linkage map of S016P and family. The proband, S016P, is represented as IV-5. XqCA is a newly designed genotyping marker with variable CA repeats located in the deleted region. The linked chromosome was transmitted to the mother of the proband from the maternal grandmother.

FIGURE 5-4

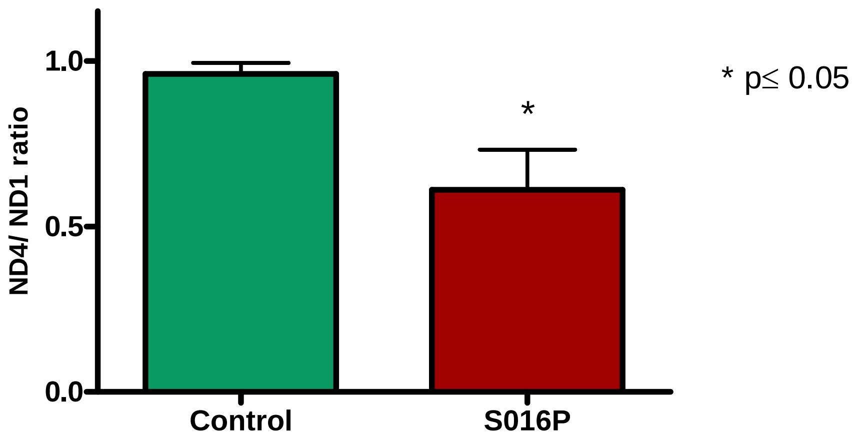

FIGURE 5-4

Mitochondrial DNA stability. Stability was estimated based on ND4/ND1 gene copy number from control and patient isolated total genomic DNA.

FIGURE 5-5

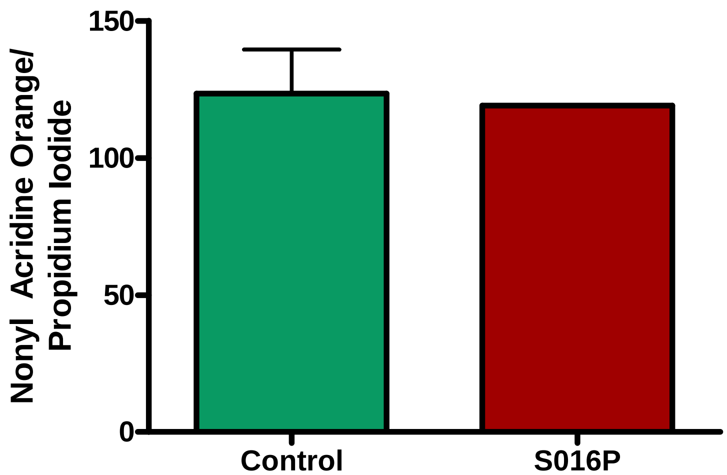
150
100
50
0
Nonyl Acridine Orange/
Propidium Iodide
Control
S016P

FIGURE 5-5

Mitochondrial inner membrane content. Mitochondrial inner membrane content was estimated by nonyl acridine orange staining and normalized to nuclear DNA staining (PI) in control and patient cells.

FIGURE 5-6

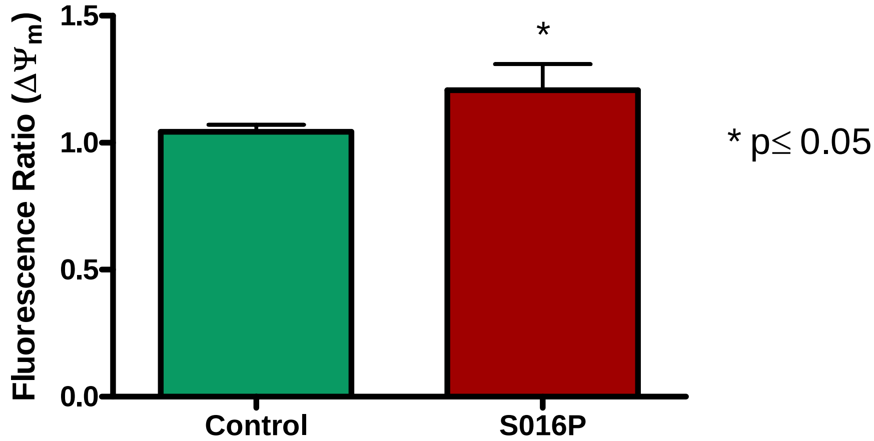

FIGURE 5-6

Mitochondrial membrane potential, as estimated using the fluorescent dye JC-1 in control and patient cells.

FIGURE 5-7

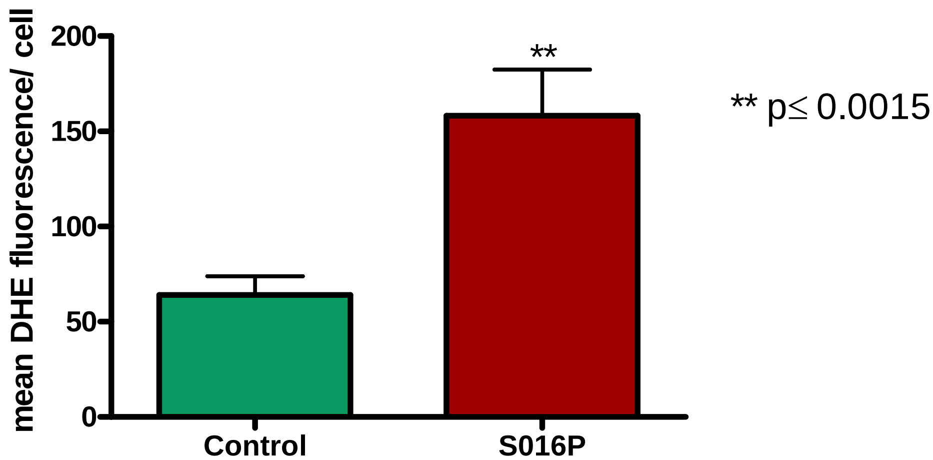
mean DHE fluorescence/ cell
200
150
100
50
0
**
Control
S016P
** p≤ 0.0015

FIGURE 5-7

Reactive Oxygen Species (ROS) production as estimated by Dihydroethidium (DHE) in control and lymphoblast cells. ROS production and is represented as mean DHE fluorescence per cell.

FIGURE 5-8

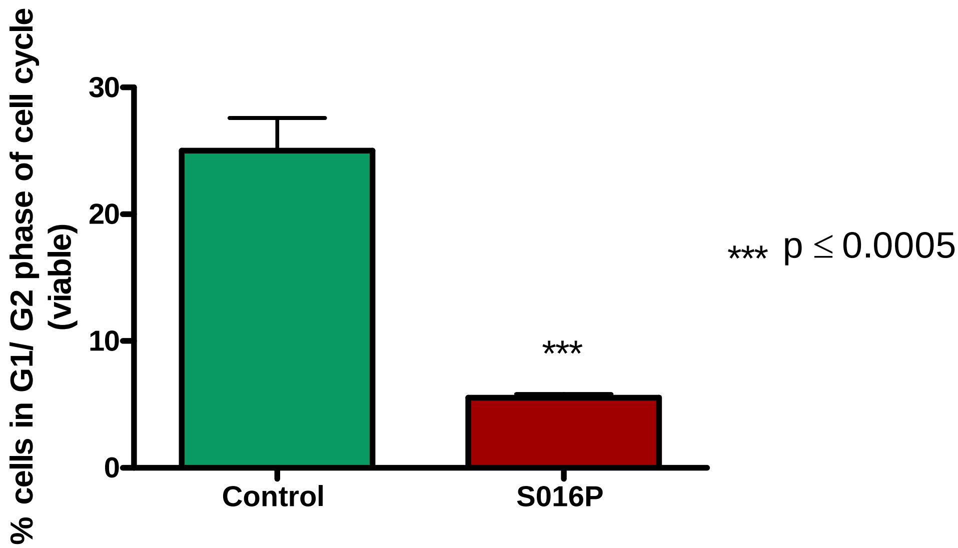
30
20
10
0
% cells in G1/ G2 phase of cell cycle (viable)
***
Control
S016P
*** p ≤ 0.0005

FIGURE 5-8

Basal Viability Index (VI) in control and patient cells.

FIGURE 5-9

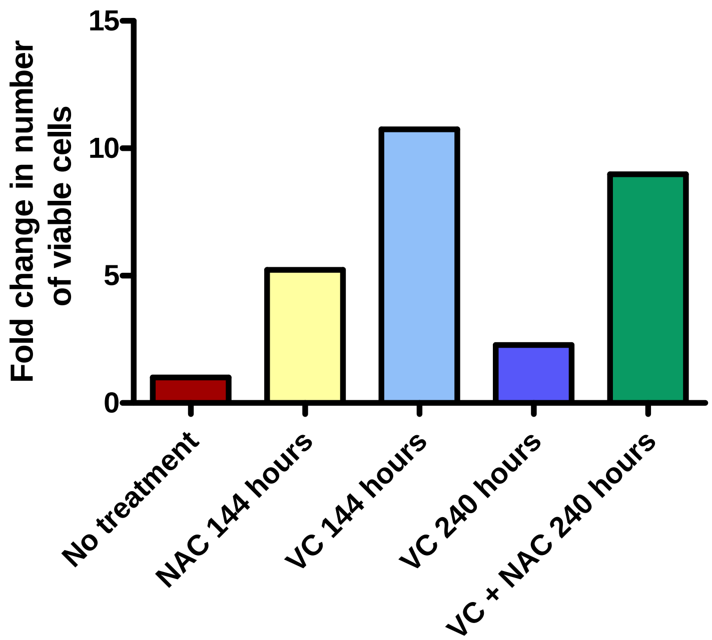
Fold change in number of viable cells
15
10
5
0
No treatment
NAC 144 hours
VC 144 hours
VC 240 hours
VC + NAC 240 hours

FIGURE 5-9

Viability Index after antioxidant treatment in cell culture medium of patient cells. NAC= n-acetyl cysteine, VC= vitamin C, ascorbic acid.

FIGURE 5-10

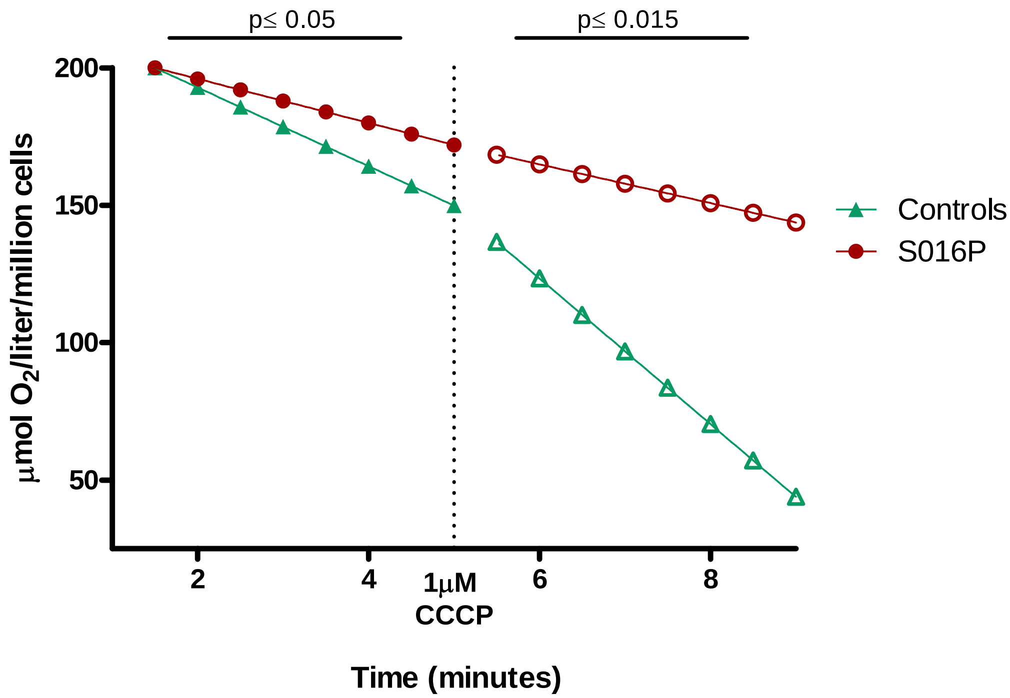
p≤ 0.05
p≤ 0.015
200
150
100
50
μmol O2/liter/million cells
2
4
1μM
CCCP
6
8
Time (minutes)
Controls
S016P

FIGURE 5-10

Oxygen consumption rates in whole lymphoblasts before and after membrane uncoupling. Respiration rate before and after addition of 1μM CCCP uncoupler in controls and patient lymphoblasts.

TABLE 5-2

Oxygen consumption in whole lymphoblasts			
substrate	*controls*	*patient*	*p value*
succinate	14.324 ± 2.865 μmol O_2	8.017 ± 0.825 μmol O_2	≤0.05
succinate + CCCP	26.5 ± 6.265 μmol O_2	7.05 ± 1.096 μmol O_2	≤0.015

TABLE 5-2

Oxygen consumption in whole lymphoblasts. Oxygen consumption rates in control and patient lymphoblasts as measured by polarographic oximetry in the presence of substrate and uncoupler.

CHAPTER SIX
Concluding Remarks

Chromosome 13q deletions and anorectal/genitourinary malformations

After narrowing the critical region on chromosome 13 necessary for imperforate anus, penoscrotal transposition and hypospadias in 13q deletion patients, it became clear that ephrin B2 (EFNB2) was an important gene for normal genitourinary and anorectal development in mice, and loss of copy number was likely the cause of malformations in humans. When a transgenic mouse model of EFNB2 was created that generates a partial loss of function mutation that interferes with EFNB2 signaling, hypospadias was observed in heterozygous males with 40% penetrance. It seems plausible that small perturbations in EFNB2 signaling or expression are the cause of common human defects such as hypospadias or imperforate anus. Sequencing of promoter and enhancer regions of the EFNB2 genes may prove to be more useful than traditional exon sequencing and is the direction I would pursue to resolve the role of EFNB2 in congenital urogenital and anorectal defects. Finally, increased numbers of patients with 13q deletions need to be recruited for study and examined using a high resolution technique like array Comparative Genomic Hybridization to precisely map the deletions.

X-Linked Reticulate Pigmentary Disorder

Future directions for the study of XLPDR are less straightforward than other studies in detailed in this thesis. Chiefly responsible for the difficulty in identifying a genetic cause is that all traditional avenues for isolating the gene responsible for XLPDR have already been taken. The only advisable plan is to wait for more families to surface and recruit additional family members as they become available in order to further narrow the gene location. Even still, the genetic cause will likely be revealed only as a result of sequencing the entire linkage interval, not just coding regions of known genes, unless new affected probands demonstrate an obvious genetic lesion detectable by karyotyping or aCGH. It might be possible to uncover a cellular phenotype and clone the gene by complementation; preliminary attempts to do so were not fruitful.

Cryptic chromosomal copy number variants and congenital heart disease

Future directions for the identification of novel chromosomal copy number variants include narrowing the scope of patients studied to pursue only one kind of congenital heart defect, such as left heart hypoplasia. Assessing chromosomal copy number variants in patients with the same heart defect who also present with neurological defects, like developmental delay, will greatly increase the likelihood of identifying new copy number variants that are specific to those defects. With the increasing addition of array CGH into clinical practice, databases that consolidate the results of clinical findings such as Genoplyphix (Signature Genomics) can be mined for useful CNV that are associated with congenital heart disease.

Novel mitochondrial disorder resulting from an ANT2 null human

Studies of S016P, out patient with a microdeletion including ANT2, are important for several reasons. First, I have described a new form mitochondrial disease, based on absolute lack of ANT2, and this definition may be useful for diagnostic purposes. Second and more importantly, is the presence of congenital defects that are associated with loss of a mitochondrial gene. This is the first mitochondrial disease that presents with congenital heart defects, both in mice and man, and raises the possibility of mitochondrial dysfunction as a major player in the formation of congenital malformations. Future directions include the continued screening of patients with ASD/VSD or congenital cataract formation for mutations in ANT2. Studies of the role that ANT2 plays in embryonic cardiac remodeling are also needed to understand how congenital heart malformations take place. Tissue and organ specific knock out of ANT2 in mice also is recommended to try and determine which of the clinical constellation of symptoms seen in the proband are the result of loss of ANT2 and which are unrelated. While local mouse studies at this point seem unlikely, given difficulties with procurement of animals and professional collaboration with the creator of the ANT2 transgenic mouse, they are still directions which I hope will ultimately be undertaken.

APPENDIX A
Summary of total CNV found in both populations

Supplementary Table 2

Subjects with Isolated Congenital Heart Disease

Summary of Total CNV in Control Population

Classification		
1	Database of genomic variants	116
2	Gene desert	10
3	UCSC region of genomic duplication	6
4	Putative but unconfirmed by qPCR	1
5	Real and confirmed by FISH/qPCR	2
	Total CNV in Control Population	135

Chromosome Deletion	Start	End	Value	Patient	Classification
chr01	16950000	17010000	-0.609	B13	1
chr01	16950000	17010000	-0.3885	B16	1
chr01	16950000	17010000	-0.69	B5	1
chr01	103950000	104010000	-0.3014	B15	1
chr01	120750000	141450000	-0.3624	B18	2
chr01	121140000	141540000	-0.3461	B6	2
chr02	88950000	89910000	-0.3203	B20	1
chr02	89670000	89910000	-0.4234	B15	1
chr02	242550000	242663761	-0.4292	B7	1
chr02	242550000	242663761	-0.3517	B8	1
chr03	162930000	163050000	-0.3197	B8	1
chr03	164010000	164070000	-0.5514	B14	1
chr03	164010000	164070000	-0.6432	B4	1
chr03	164010000	164070000	-0.4824	B5	1
chr04	48810000	49230000	-0.5217	B18	1
chr04	69030000	69150000	-0.5487	B1	1
chr04	69150000	69450000	-0.3641	B13	1
chr04	70170000	70290000	-0.479	B16	1
chr04	145050000	145110000	-0.5476	B4	1
chr04	179310000	179550000	-0.3705	B16	2
chr05	70350000	70650000	-0.3059	B6	1
chr06	26940000	27060000	-0.4369	B18	1
chr06	26970000	27030000	-0.32	B8	1
chr06	26970000	27090000	-0.4355	B2	1
chr06	32610000	32730000	-0.3109	B15	1
chr06	32610000	32730000	-0.4916	B16	1
chr06	32610000	32790000	-0.3074	B7	1
chr06	61950000	62010000	-0.3088	B16	2
chr07	61260000	61620000	-0.3534	B18	1
chr07	80250000	80370000	-0.489	B3	5
chr08	39390000	39450000	-0.9714	B3	1
chr08	39390000	39450000	-0.9774	B17	1
chr08	39390000	39450000	-0.7278	B8	1
chr08	39390000	39450000	-0.7742	B5	1
chr08	39390000	39510000	-0.5531	B19	1
chr08	39390000	39510000	-0.5342	B12	1
chr08	137790000	137910000	-0.4367	B19	2
chr09	42300000	43260000	-0.3095	B6	1
chr09	42330000	43590000	-0.3342	B14	1
chr10	38700000	39180000	-0.4452	B18	1
chr10	38790000	39210000	-0.3631	B20	1
chr10	38790000	39210000	-0.3297	B19	1
chr10	38790000	42030000	-0.3748	B10	1
chr10	39150000	39210000	-0.5756	B12	1
chr10	39150000	39210000	-0.3476	B8	1
chr10	39150000	41790000	-0.408	B13	1
chr14	18510000	19470000	-0.3345	B5	1
chr14	18870000	19470000	-0.3157	B7	1
chr14	19260000	19500000	-0.3201	B20	1
chr14	19260000	19500000	-0.3588	B12	1
chr14	19290000	19470000	-0.3369	B15	1
chr14	19350000	19470000	-0.4282	B13	1
chr14	105510000	105630000	-0.3226	B2	1
chr15	18300000	19860000	-0.3875	B2	1
chr15	18900000	20100000	-0.3919	B17	1
chr15	18900000	20100000	-0.3796	B19	1
chr16	35100000	45060000	-0.3401	B2	2

Subjects with Congenital Heart Disease and Additional Anomalies

Summary of Total CNV in Multiple Defects Population

Classification		
1	Database of genomic variants	138
2	Gene desert	11
3	UCSC region of genomic duplication	2
4	Putative but unconfirmed by qPCR	2
5	Real and confirmed by FISH/qPCR	8
	Total CNV in Multiple Defects Population	161

Chromosome Deletion	Start	End	Value	Patient	Classification
chr01	12810000	13110000	-0.4895	A18	1
chr01	12900000	13140000	-0.3655	A9	1
chr01	12900000	13140000	-0.381	A15	1
chr01	16650000	16710000	-0.5101	A1	1
chr01	16830000	17250000	-0.306	A12	1
chr01	103830000	103950000	-0.4551	A2	1
chr01	121050000	121170000	-0.4825	A14	2,3
chr01	141990000	144450000	-0.4285	A12	1
chr01	193470000	193530000	-0.5755	A2	1
chr01	234510000	247163852	-0.575	A10	5
chr02	89250000	89850000	-0.3385	A8	1
chr02	89700000	89940000	-0.3128	A20	1
chr02	90990000	91170000	-0.3518	A12	1
chr03	163980000	164100000	-0.4274	A2	1
chr03	163980000	164100000	-0.4142	A16	1
chr03	163980000	164100000	-0.3126	A19	1
chr04	48900000	49260000	-0.6006	A12	1
chr04	69210000	69330000	-0.5718	A7	1
chr04	70140000	70260000	-0.3604	A13	1
chr05	69780000	69900000	-0.4356	A20	1
chr05	70290000	70470000	-0.343	A2	1
chr06	26850000	27030000	-0.4045	A18	1
chr06	32550000	32610000	-0.3811	A20	1
chr06	32610000	32730000	-0.3292	A2	1
chr06	32610000	32730000	-0.414	A14	1
chr06	32610000	32730000	-0.3934	A19	1
chr06	95670000	95910000	-0.4066	A13	1
chr08	7020000	7740000	-0.3554	A3	1
chr08	12270000	12330000	-0.4015	A12	1
chr08	12330000	12510000	-0.3875	A9	1
chr08	39390000	39450000	-0.7466	A9	1
chr08	39390000	39450000	-0.8916	A11	1
chr08	39390000	39450000	-0.6054	A17	1
chr09	7350000	7470000	-0.3463	A4	1
chr09	41850000	43650000	-0.3357	A8	1
chr09	41850000	43650000	-0.49	A13	1
chr09	68310000	69150000	-0.3518	A8	1
chr10	38790000	38910000	-0.4015	A8	1
chr10	38790000	39210000	-0.3244	A15	1
chr10	38790000	41730000	-0.3745	A13	1
chr10	39150000	39210000	-0.3987	A10	1
chr11	4230000	4350000	-0.3256	A8	1
chr11	37650000	37770000	-0.4292	A17	2
chr12	9450000	9570000	-0.4598	A10	1
chr12	9510000	9570000	-0.641	A8	1
chr13	95910000	95970000	-0.4741	A13	5
chr14	18450000	19470000	-0.3067	A2	1
chr14	18750000	19350000	-0.3531	A16	1
chr14	19260000	19500000	-0.5574	A9	1
chr14	19350000	19470000	-0.4679	A11	1
chr15	18810000	20070000	-0.3346	A15	1
chr15	18900000	20100000	-0.4102	A9	1
chr15	18900000	20100000	-0.3099	A17	1
chr15	26700000	26940000	-0.3467	A12	1
chr16	14970000	15030000	-0.5219	A12	1
chr16	21390000	21450000	-0.5194	A1	1
chr16	32070000	32190000	-0.844	A12	1

chr16	[illegible]	[illegible]	[illegible]	B13	2
chr16	75090000	75210000	-0.4889	B6	1
chr17	41490000	41670000	-0.3942	B18	1
chr17	41550000	41670000	-0.3273	B1	1
chr17	41550000	41670000	-0.4504	B12	1
chr17	41550000	41670000	-0.3847	B5	1
chr17	41580000	41700000	-0.3853	B8	1
chr18	1710000	1830000	-0.347	B19	1
chr18	14550000	14670000	-0.391	B12	1
chr19	59970000	60030000	-0.593	B3	1
chr20	28290000	29250000	-0.5432	B10	1
chr20	28290000	29310000	-0.3057	B17	1
chr21	9750000	9870000	-0.3655	B20	3
chr21	9750000	9990000	-0.3745	B13	3
chr22	19860000	19980000	-0.5365	B14	3
Duplication					
chr01	1470000	1590000	0.3656	B14	1
chr01	16740000	17100000	0.33	B12	1
chr01	16770000	16890000	0.451	B19	1
chr01	16770000	16890000	0.4961	B11	1
chr01	16770000	17010000	0.3694	B4	1
chr01	17070000	17130000	0.3892	B15	1
chr01	142050000	142350000	0.5608	B2	1
chr01	142050000	142350000	0.6455	B11	1
chr02	18810000	19410000	0.3189	B13	1
chr02	87450000	87990000	0.491	B13	1
chr02	87450000	87990000	0.3055	B1	1
chr02	113910000	114090000	0.3147	B13	1
chr02	113970000	114090000	0.321	B17	1
chr02	113970000	114090000	0.361	B16	1
chr02	113970000	114090000	0.718	B11	1
chr02	113970000	114090000	0.3265	B1	1
chr02	113970000	114090000	0.594	B12	1
chr02	132090000	132210000	0.4432	B11	1
chr03	50220000	50580000	0.3399	B10	1
chr03	101850000	101910000	0.5958	B14	5
chr03	114750000	114870000	0.313	B11	4
chr04	3660000	4020000	0.3096	B12	1
chr04	49230000	49290000	0.7352	B11	1
chr04	153090000	153210000	0.3089	B18	1
chr05	750000	930000	0.6102	B19	1
chr06	26790000	26850000	0.4562	B6	1
chr06	168090000	168330000	0.448	B17	1
chr07	61020000	61140000	0.3024	B8	1
chr07	62700000	62820000	0.3084	B1	2
chr07	73950000	74250000	0.3105	B15	1
chr08	7050000	7650000	0.3224	B13	1
chr08	11820000	12540000	0.3001	B2	1
chr08	12030000	12270000	0.486	B20	1
chr08	39390000	39450000	0.3752	B14	1
chr08	39390000	39450000	0.3655	B4	1
chr08	39390000	39450000	0.4622	B11	1
chr08	39390000	39450000	0.3445	B1	1
chr08	47130000	47250000	0.3609	B12	2
chr08	47190000	47250000	0.3297	B13	2
chr09	60000	180000	0.3017	B5	1
chr09	90000	150000	0.4795	B11	1
chr09	44250000	45450000	0.3126	B12	1
chr09	66630000	66750000	0.723	B2	1
chr09	68220000	68340000	0.338	B13	1
chr09	68220000	68460000	0.3683	B4	1
chr10	46350000	46650000	0.3138	B13	1
chr14	18270000	19470000	0.3039	B6	1
chr15	18270000	19410000	0.3221	B11	1
chr15	82710000	82770000	0.6122	B2	1
chr15	82710000	82770000	0.5065	B19	1
chr15	82710000	82770000	0.3758	B16	1
chr16	14850000	16350000	0.3295	B17	1
chr16	31890000	32190000	0.5716	B11	1
chr16	31950000	32190000	0.5013	B7	1
chr16	31980000	32340000	0.3452	B20	1
chr16	31980000	32340000	0.3559	B15	1
chr16	32100000	32340000	0.5081	B2	1

Nucleotide positions for subjects B1-B20 refer to human genome build hg18, NCBI 36.

chr16	[illegible]	[illegible]	[illegible]	A11	1
chr16	32220000	33300000	-0.3484	A1	1
chr16	33270000	33390000	-0.3468	A6	1
chr16	33270000	33450000	-0.3747	A8	1
chr16	35250000	44850000	-0.4238	A13	2
chr17	41550000	41670000	-0.3681	A17	1
chr17	41610000	41730000	-0.4689	A9	1
chr17	41610000	41730000	-0.5477	A19	1
chr17	41820000	42060000	-0.3749	A3	1
chr17	63570000	63630000	-0.7235	A8	2,3
chr18	14550000	14790000	-0.3514	A13	1
chr18	15210000	15390000	-0.3948	A9	1
chr18	15210000	16770000	-0.32	A17	2
chr18	15420000	16740000	-0.426	A15	2
chr19	150000	750000	-0.3173	A9	5
chr19	48060000	48180000	-0.3104	A11	1
chr19	48390000	48450000	-0.4554	A13	1
chr20	28020000	29220000	-0.3113	A12	1
chr20	28050000	28110000	-0.3308	A5	1
chr20	29220000	29340000	-0.3328	A17	1
chr22	14430000	14790000	-0.3115	A2	1
chr22	17070000	17250000	-0.442	A7	1
chr22	17250000	19890000	-0.432	A11	5
chr22	18930000	18990000	-0.8774	A7	1
chr22	19830000	20010000	-0.4111	A7	3
chr22	32250000	32370000	-0.4916	A14	2
Duplication					
chr01	30000	150000	0.362	A1	1
chr01	16710000	17070000	0.3146	A4	1
chr01	142020000	143460000	0.4038	A18	1
chr01	159810000	159870000	0.3652	A13	3
chr02	87450000	87990000	0.3395	A11	1
chr02	87450000	87990000	0.484	A19	1
chr02	87930000	87990000	0.3326	A5	1
chr02	91260000	91380000	0.467	A9	1
chr02	91410000	91470000	0.626	A15	1
chr02	110220000	110340000	0.3994	A19	1
chr02	111810000	112350000	0.3026	A18	1
chr02	113970000	114090000	0.6645	A16	1
chr02	113970000	114090000	0.313	A19	1
chr02	113970000	114090000	0.4105	A18	1
chr02	199620000	206220000	0.3627	A8	5
chr03	9690000	9870000	0.3148	A16	4
chr03	46350000	46470000	0.3056	A11	1
chr03	50220000	50580000	0.3485	A18	1
chr03	164010000	164070000	0.5307	A8	1
chr03	164010000	164070000	0.5142	A10	1
chr03	164010000	164070000	0.3076	A13	1
chr03	196710000	197010000	0.3049	A20	1
chr04	9030000	9090000	0.522	A5	1
chr04	69030000	69150000	0.3136	A8	1
chr04	69180000	69300000	0.3618	A3	1
chr05	149700939	149771556	0.4225	A4	4
chr06	168210000	168390000	0.3942	A20	1
chr06	168210000	168570000	0.3431	A7	1
chr07	56790000	56850000	0.5234	A13	2,3
chr07	64170000	64650000	0.3084	A14	1
chr07	74550000	74670000	0.5449	A4	1
chr07	101790000	101850000	1.0218	A4	1
chr07	149220000	149460000	0.395	A19	1
chr07	153150000	153330000	0.6507	A19	1
chr08	7230000	7770000	0.369	A12	1
chr08	12270000	12330000	0.6245	A8	1
chr08	12270000	12330000	0.6205	A13	1
chr08	12270000	12450000	0.3453	A6	1
chr08	12300000	12540000	0.3197	A15	1
chr08	39390000	39450000	0.6127	A10	1
chr08	39390000	39510000	0.4088	A12	1
chr08	47070000	47550000	0.4159	A4	2
chr08	86790000	86850000	0.4878	A7	1
chr09	90000	150000	0.3925	A18	1
chr09	68190000	68310000	0.5255	A14	1
chr09	68220000	68460000	0.3533	A16	1

Nucleotide positions for subjects A1-A5, A7 and A20 refer to human genome build hg17, NCBI 35 and subjects A6 and A8-19 refer to build hg18, NCBI 36.

APPENDIX B
Population with Isolated Congenital Heart Disease

Subject	Cardiac diagnosis
B1	Pulmonary valve stenosis
B2	Hypoplastic left heart syndrome
B3	Atrioventricular septal defect
B4	Double outlet right ventricle, hypoplastic left ventricle
B5	Dysplastic mitral valve
B6	Hypoplastic left heart syndrome
B7	Sinus venosus atrial septal defect
B8	Aortic coarctation, bicuspid aortic valve
B9	Atrial septal defect
B10	Atrioventricular septal defect
B11	Tetralogy of Fallot
B12	Atrial septal defect
B13	Atrial septal defect
B14	Tetralogy of Fallot
B15	Patent ductus arteriosus
B16	Atrial and ventricular septal defect
B17	Tetralogy of Fallot
B18	Atrial septal defect
B19	Pulmonary valve stenosis
B20	Tetralogy of Fallot

APPENDIX C
Confirmation of copy number variations by real time quantitative PCR (RT qPCR).

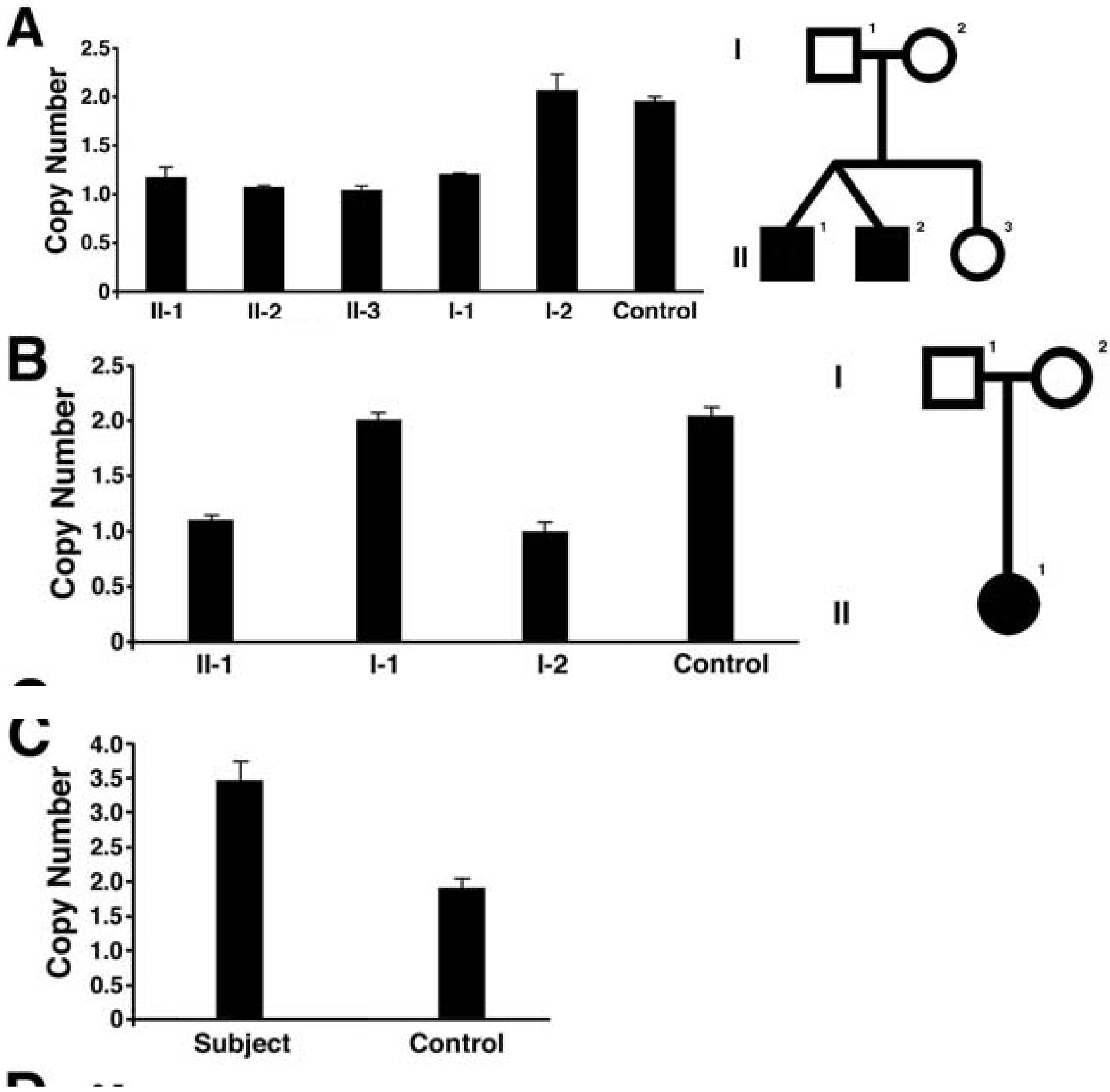

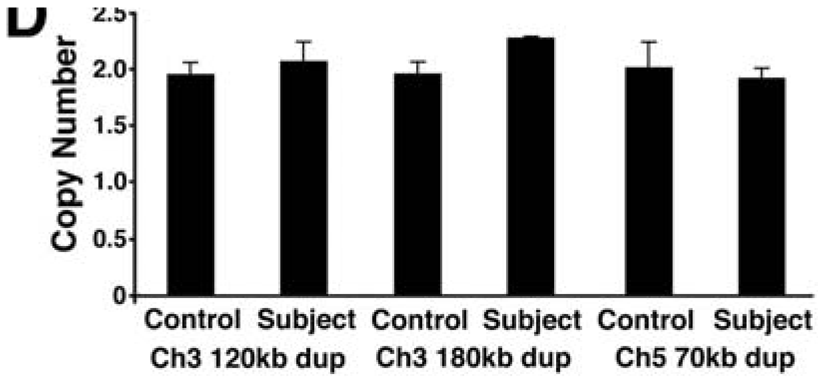

Suppl. Figure 1

A, ~120 kilobase (kb) microdeletion on chromosome (ch) 7 was identified in II-1 (twin A, subject B3) with an endocardial cushion defect and confirmed by RT qPCR. A similar microdeletion was detected in the affected twin B(II-2), unaffected sister (II-3) and unaffected father (I-1) but not in the mother (I-2) or 800 control chromosomes. B, ~60kb microdeletion on ch13 was confirmed by RT qPCR in a child with an atrial septal defect (II-1, Subject A13) and inherited from an unaffected mother (I-2). The father and 200 control chromosomes had no evidence of deletion by RT qPCR. C, ~120kb microduplication on ch3 was confirmed in a child with tetralogy of Fallot (Subject B14). Two copies were detected in all 200 control alleles except one which demonstrated a similar duplication. D, Two putative microduplications of ch3 and one of ch5 were not confirmed by RT qPCR. They were identified in subjects B11, A16 and A4, respectively. All RT qPCR experiments were performed in triplicate and representative controls are shown. In A and B, kindreds with two generations (indicated by Roman numerals) are shown and participating members are designated numerically. Affected family members are shaded black.

APPENDIX D
S016P Family Pedigree

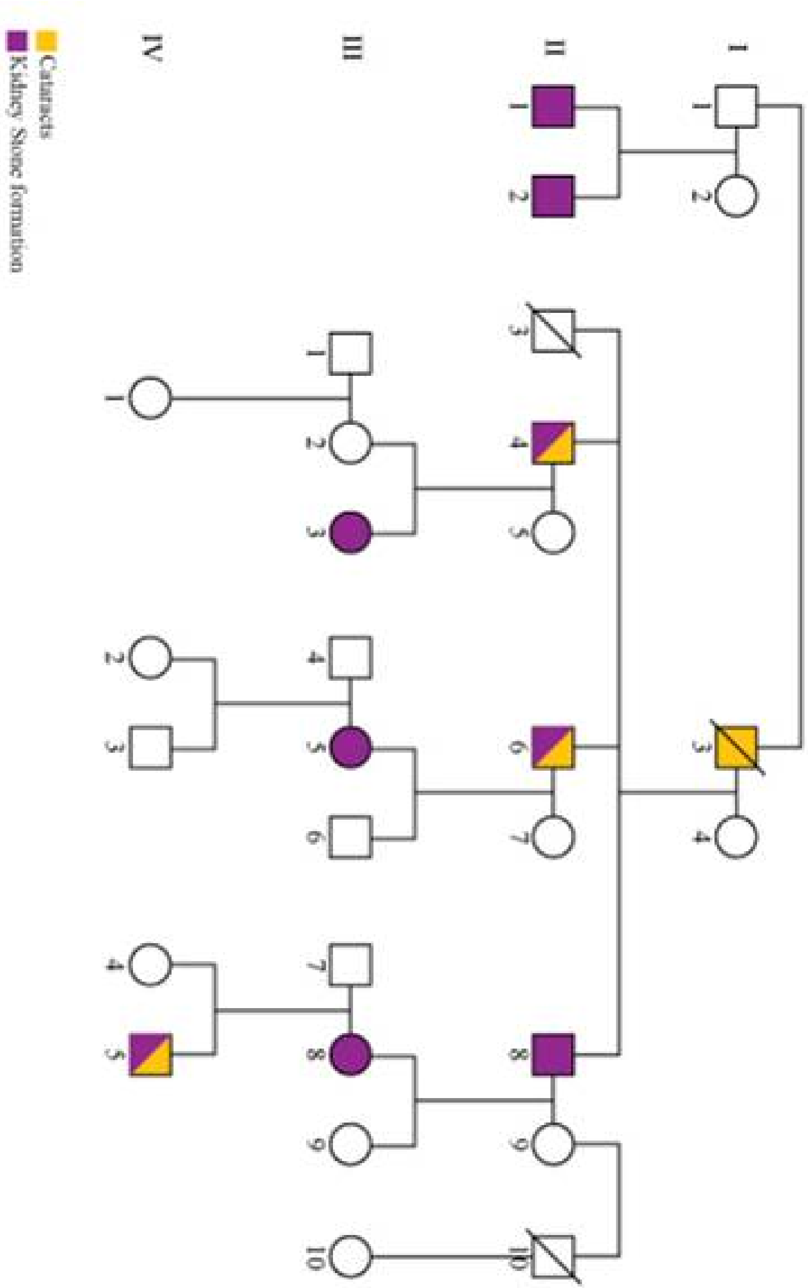

BIBLIOGRAPHY

Abecasis GR, Cherny SS, Cookson WO, Cardon LR (2002) Merlin--rapid analysis of dense genetic maps using sparse gene flow trees. Nat Genet 30: 97-101

Abinun M, Spickett G, Appleton AL, Flood T, Cant AJ (1996) Anhidrotic ectodermal dysplasia associated with specific antibody deficiency. Eur J Pediatr 155: 146-7

Ades LC, Rogers M, Sillence DO (1993) An X-linked reticulate pigmentary disorder with systemic manifestations: report of a second family. Pediatr Dermatol 10: 344-51

Allderdice PW, Davis JG, Miller OJ, Klinger HP, Warburton D, Miller DA, Allen FH, Jr., Abrams CA, McGilvray E (1969) The 13q-deletion syndrome. Am J Hum Genet 21: 499-512

Allen RC, Zoghbi HY, Moseley AB, Rosenblatt HM, Belmont JW (1992) Methylation of HpaII and HhaI sites near the polymorphic CAG repeat in the human androgen-receptor gene correlates with X chromosome inactivation. Am J Hum Genet 51: 1229-39

Anderson RC, Zinn AR, Kim J, Carder KR (2005) X-linked reticulate pigmentary disorder with systemic manifestations: report of a third family and literature review. Pediatr Dermatol 22: 122-6

Arsic D, Qi BQ, Beasley SW (2002) Hedgehog in the human: a possible explanation for the VATER association. J Paediatr Child Health 38: 117-21

Baldini A (2002) DiGeorge syndrome: the use of model organisms to dissect complex genetics. Hum Mol Genet 11: 2363-9

Ballif BC, Sulpizio SG, Lloyd RM, Minier SL, Theisen A, Bejjani BA, Shaffer LG (2007) The clinical utility of enhanced subtelomeric coverage in array CGH. Am J Med Genet A 143A: 1850-7

Bamforth JS, Lin CC (1997) DK phocomelia phenotype (von Voss-Cherstvoy syndrome) caused by somatic mosaicism for del(13q). Am J Med Genet 73: 408-11

Barrientos A (2002) In vivo and in organello assessment of OXPHOS activities. Methods 26: 307-16

Bartsch O, Kuhnle U, Wu LL, Schwinger E, Hinkel GK (1996) Evidence for a critical region for penoscrotal inversion, hypospadias, and imperforate anus within chromosomal region 13q32.2q34. Am J Med Genet 65: 218-21

Bassett AS, Chow EW, Husted J, Weksberg R, Caluseriu O, Webb GD, Gatzoulis MA (2005) Clinical features of 78 adults with 22q11 Deletion Syndrome. Am J Med Genet A 138: 307-13

Berlin AL, Paller AS, Chan LS (2002) Incontinentia pigmenti: a review and update on the molecular basis of pathophysiology. J Am Acad Dermatol 47: 169-87; quiz 188-90

Bernstein D (2004) Evaluation of the cardiovascular system, 17th edn. Saunders, Philadelphia

Bhoj EJ, Romeo S, Baroni MG, Bartov G, Schultz RA, Zinn AR (2009) MODY-like diabetes associated with an apparently balanced translocation: possible involvement of MPP7 gene and cell polarity in the pathogenesis of diabetes. Mol Cytogenet 2: 5

Bignell GR, Warren W, Seal S, Takahashi M, Rapley E, Barfoot R, Green H, Brown C, Biggs PJ, Lakhani SR, Jones C, Hansen J, Blair E, Hofmann B, Siebert R, Turner G, Evans DG, Schrander-Stumpel C, Beemer FA, van Den Ouweland A, Halley D, Delpech B, Cleveland MG, Leigh I, Leisti J, Rasmussen S (2000) Identification of the familial cylindromatosis tumour-suppressor gene. Nat Genet 25: 160-5

Bird LM, Mascarello JT (2001) Chromosome 2q duplications: case report of a de novo interstitial duplication and review of the literature. Am J Med Genet 100: 13-24

Boduroglu K, Alikasifoglu M, Tuncbilek E, Uludogan S (1998) Ring chromosome 13 in an infant with multiple congenital anomalies and penoscrotal transposition. Clin Dysmorphol 7: 299-301

Bose J, Grotewold L, Ruther U (2002) Pallister-Hall syndrome phenotype in mice mutant for Gli3. Hum Mol Genet 11: 1129-35

Brown S, Gersen S, Anyane-Yeboa K, Warburton D (1993) Preliminary definition of a "critical region" of chromosome 13 in q32: report of 14 cases with 13q deletions and review of the literature. Am J Med Genet 45: 52-9

Brown S, Russo J, Chitayat D, Warburton D (1995) The 13q- syndrome: the molecular definition of a critical deletion region in band 13q32. Am J Hum Genet 57: 859-66

Calvo S, Jain M, Xie X, Sheth SA, Chang B, Goldberger OA, Spinazzola A, Zeviani M, Carr SA, Mootha VK (2006) Systematic identification of human mitochondrial disease genes through integrative genomics. Nat Genet 38: 576-82

Carey JC (2003) Chromosomal Disorders. In: Rudolph CD, and Rudolph, A.M (ed) Rudolph's Pediatrics, 21st Edition edn. McGraw-Hill Medical Publishing Division, New York, pp 731-741

Cason AL, Ikeguchi Y, Skinner C, Wood TC, Holden KR, Lubs HA, Martinez F, Simensen RJ, Stevenson RE, Pegg AE, Schwartz CE (2003) X-linked spermine synthase gene (SMS) defect: the first polyamine deficiency syndrome. Eur J Hum Genet 11: 937-44

CDC CfDCaP (2006) Improved National Prevalence Estimates for 18 Selected Major Birth Defects-United States, 1999-2001. vol 54. U.S. Government Printing Office, Washington, DC, pp 1301-1305

Ceci JD (1994) Mouse chromosome 8. Mamm Genome 5 Spec No: S124-38

Christensen K, Madsen CM, Hauge M, Kock K (1990) An epidemiological study of congenital anorectal malformations: 15 Danish birth cohorts followed for 7 years. Paediatr Perinat Epidemiol 4: 269-75

Chung JL, Choi JR, Park MS, Choi SH (2001) A case of del(13)(q22) with multiple major congenital anomalies, imperforate anus and penoscrotal transposition. Yonsei Med J 42: 558-62

Cohen E, Chow EW, Weksberg R, Bassett AS (1999) Phenotype of adults with the 22q11 deletion syndrome: A review. Am J Med Genet 86: 359-65

Copeland WC (2008) Inherited mitochondrial diseases of DNA replication. Annu Rev Med 59: 131-46

Courtois G, Smahi A (2006) NF-kappaB-related genetic diseases. Cell Death Differ 13: 843-51

Craig JE, Friend KL, Gecz J, Rattray KM, Troski M, Mackey DA, Burdon KP (2008) A novel locus for X-linked congenital cataract on Xq24. Mol Vis 14: 721-6

de Ravel TJ, Devriendt K, Fryns JP, Vermeesch JR (2007) What's new in karyotyping? The move towards array comparative genomic hybridisation (CGH). Eur J Pediatr 166: 637-43

de Santa Barbara P, Roberts DJ (2002) Tail gut endoderm and gut/genitourinary/tail development: a new tissue-specific role for Hoxa13. Development 129: 551-61

Debray FG, Lambert M, Mitchell GA (2008) Disorders of mitochondrial function. Curr Opin Pediatr 20: 471-82

Dimauro S, Davidzon G (2005) Mitochondrial DNA and disease. Ann Med 37: 222-32

Douglas C. Wallace GM, Katrina Waymire, Shawn E. Levy, James E. Sligh and Jason E. Kokoszka (2002) Ant2 Conditional Knockout Mouse and Methods
In: **Office UP** (ed). Emory University, United States

Dravis C, Yokoyama N, Chumley MJ, Cowan CA, Silvany RE, Shay J, Baker LA, Henkemeyer M (2004) Bidirectional signaling mediated by ephrin-B2 and EphB2 controls urorectal development. Dev Biol 271: 272-90 du Manoir S, Speicher MR, Joos S, Schrock E, Popp S, Dohner H, Kovacs G, Robert-Nicoud M, Lichter P, Cremer T (1993) Detection of complete and partial chromosome gains and losses by comparative genomic in situ hybridization. Hum Genet 90: 590-610

Edelmann L, Hirschhorn K (2009) Clinical utility of array CGH for the detection of chromosomal imbalances associated with mental retardation and multiple congenital anomalies. Ann N Y Acad Sci 1151: 157-66

Ellison JW, Salido EC, Shapiro LJ (1996) Genetic mapping of the adenine nucleotide translocase-2 gene (Ant2) to the mouse proximal X chromosome. Genomics 36: 369-71

Ferencz C, Boughman JA, Neill CA, Brenner JI, Perry LW (1989) Congenital cardiovascular malformations: questions on inheritance. Baltimore-Washington Infant Study Group. J Am Coll Cardiol 14: 756-63

Fisher JS (2004) Environmental anti-androgens and male reproductive health: focus on phthalates and testicular dysgenesis syndrome. Reproduction 127: 305-15

Friend SH, Bernards R, Rogelj S, Weinberg RA, Rapaport JM, Albert DM, Dryja TP (1986) A human DNA segment with properties of the gene that predisposes to retinoblastoma and osteosarcoma. Nature 323: 643-6

Frix CD, 3rd, Bronson DM (1986) Acute miliary tuberculosis in a child with anhidrotic ectodermal dysplasia. Pediatr Dermatol 3: 464-7

Froese N, Schwarzer M, Niedick I, Frischmann U, Koster M, Kroger A, Mueller PP, Nourbakhsh M, Pasche B, Reimann J, Staeheli P, Hauser H (2006) Innate immune responses in NF-kappaB-repressing factor-deficient mice. Mol Cell Biol 26: 293-302

Fryns JP, Peeters R, Petit P, Van den Berghe H (1980) New chromosomal syndromes. III. The 13q deletion syndrome. Acta Paediatr Belg 33: 261-4

Garcia NM, Allgood J, Santos LJ, Lonergan D, Batanian JR, Henkemeyer M, Bartsch O, Schultz RA, Zinn AR, Baker LA (2006) DELETION MAPPING OF CRITICAL REGION FOR HYPOSPADIAS, PENOSCROTAL TRANSPOSITION AND IMPERFORATE ANUS ON HUMAN CHROMOSOME 13. J Pediatr Urol 2: 233-242

Garg V (2006) Insights into the genetic basis of congenital heart disease. Cell Mol Life Sci 63: 1141-8

Gatzoulis MA (2004) Adult congenital heart disease: a cardiovascular area of growth in urgent need of additional resource allocation. Int J Cardiol 97 Suppl 1: 1-2

Gedeon AK, Mulley JC, Kozman H, Donnelly A, Partington MW (1994) Localisation of the gene for X-linked reticulate pigmentary disorder with systemic manifestations (PDR), previously known as X-linked cutaneous amyloidosis. Am J Med Genet 52: 75-8

Gershoni-Baruch R, Zekaria D (1996) Deletion (13)(q22) with multiple congenital anomalies, hydranencephaly and penoscrotal transposition. Clin Dysmorphol 5: 289-94

Gimelli G, Giglio S, Zuffardi O, Alhonen L, Suppola S, Cusano R, Lo Nigro C, Gatti R, Ravazzolo R, Seri M (2002) Gene dosage of the spermidine/spermine N(1)-acetyltransferase (SSAT) gene with putrescine accumulation in a patient with a Xp21.1p22.12 duplication and keratosis follicularis spinulosa decalvans (KFSD). Hum Genet 111: 235-41

Golalipour MJ, Mobasheri E, Hoseinpour KR, Keshtkar AA (2007) Gastrointestinal malformations in Gorgan, North of Iran: epidemiology and associated malformations. Pediatr Surg Int 23: 75-9

Gurkan C, Lapp H, Hogenesch JB, Balch WE (2005) Exploring trafficking GTPase function by mRNA expression profiling: use of the SymAtlas web-application and the Membrome datasets. Methods Enzymol 403: 1-10

Gutierrez J, Sepulveda W, Saez R, Carstens E, Sanchez J (2001) Prenatal diagnosis of 13q-syndrome in a fetus with holoprosencephaly and thumb agenesis. Ultrasound Obstet Gynecol 17: 166-8

Haitina T, Lindblom J, Renstrom T, Fredriksson R (2006) Fourteen novel human members of mitochondrial solute carrier family 25 (SLC25) widely expressed in the central nervous system. Genomics 88: 779-90

Halestrap AP, Brennerb C (2003) The adenine nucleotide translocase: a central component of the mitochondrial permeability transition pore and key player in cell death. Curr Med Chem 10: 1507-25

Haraguchi R, Mo R, Hui C, Motoyama J, Makino S, Shiroishi T, Gaffield W, Yamada G (2001) Unique functions of Sonic hedgehog signaling during external genitalia development. Development 128: 4241-50

Haraguchi R, Suzuki K, Murakami R, Sakai M, Kamikawa M, Kengaku M, Sekine K, Kawano H, Kato S, Ueno N, Yamada G (2000) Molecular analysis of external genitalia formation: the role of fibroblast growth factor (Fgf) genes during genital tubercle formation. Development 127: 2471-9

Hayden MS, Ghosh S (2004) Signaling to NF-kappaB. Genes Dev 18: 2195-224

Higgins SS, Reid A (1994) Common congenital heart defects. Long-term follow-up. Nurs Clin North Am 29: 233-48

Hoffman JI, Kaplan S (2002) The incidence of congenital heart disease. J Am Coll Cardiol 39: 1890-900

Holder JL, Jr., Zhang L, Kublaoui BM, DiLeone RJ, Oz OK, Bair CH, Lee YH, Zinn AR (2004) Sim1 gene dosage modulates the homeostatic feeding response to increased dietary fat in mice. Am J Physiol Endocrinol Metab 287: E105-13

Hoye AT, Davoren JE, Wipf P, Fink MP, Kagan VE (2008) Targeting mitochondria. Acc Chem Res 41: 87-97

Iafolla AK, McConkie-Rosell A, Chen YT (1991) VATER and hydrocephalus: distinct syndrome? Am J Med Genet 38: 46-51

James LM (1993) Maps of birth defects occurrence in the U.S., Birth Defects Monitoring Program (BDMP)/CPHA, 1970-1987. Teratology 48: 551-646

Jin DY, Chae HZ, Rhee SG, Jeang KT (1997) Regulatory role for a novel human thioredoxin peroxidase in NF-kappaB activation. J Biol Chem 272: 30952-61

Kallioniemi A, Kallioniemi OP, Sudar D, Rutovitz D, Gray JW, Waldman F, Pinkel D (1992) Comparative genomic hybridization for molecular cytogenetic analysis of solid tumors. Science 258: 818-21

Karin M, Ben-Neriah Y (2000) Phosphorylation meets ubiquitination: the control of NF-[kappa]B activity. Annu Rev Immunol 18: 621-63

Kessel A, Yehudai D, Peri R, Pavlotzky E, Bamberger E, Tov N, Toubi E (2006) Increased susceptibility of cord blood B lymphocytes to undergo spontaneous apoptosis. Clin Exp Immunol 145: 563-70

Kiesewetter WB, Chang JH (1977) Imperforate Anus: a five to thirty year follow-up perspective. Prog Pediatr Surg 10: 111-20

Kim J, Kim P, Hui CC (2001) The VACTERL association: lessons from the Sonic hedgehog pathway. Clin Genet 59: 306-15

Kimmel SG, Mo R, Hui CC, Kim PC (2000) New mouse models of congenital anorectal malformations. J Pediatr Surg 35: 227-30; discussion 230-1

Kiss AM, Jady BE, Bertrand E, Kiss T (2004) Human box H/ACA pseudouridylation guide RNA machinery. Mol Cell Biol 24: 5797-807

Klingenberg M (2008) The ADP and ATP transport in mitochondria and its carrier. Biochim Biophys Acta 1778: 1978-2021

Kochanek KD, Murphy SL, Anderson RN, Scott C (2004) Deaths: final data for 2002. Natl Vital Stat Rep 53: 1-115

Krishnan KJ, Bender A, Taylor RW, Turnbull DM (2007) A multiplex real-time PCR method to detect and quantify mitochondrial DNA deletions in individual cells. Anal Biochem 370: 127-9

Kuhnle U, Bartsch O, Werner W, Schuster T (2000) Penoscrotal inversion, hypospadias, imperforate anus, facial anomalies, and developmental delay: definition of a new clinical syndrome. Pediatr Surg Int 16: 396-9

Kumar AaF (2005) Robbins and Cotran PATHOLOGIC BASIS OF DISEASE

In: **VINAY KUMAR AKA, NELSON FAUSTO** (ed) Robbins and Cotran PATHOLOGIC BASIS OF DISEASE, 7th edn. ELSEVIER SAUNDERS

Philadelphia

Lee C, Iafrate AJ, Brothman AR (2007) Copy number variations and clinical cytogenetic diagnosis of constitutional disorders. Nat Genet 39: S48-54

Leong FT, Freeman LJ, Keavney BD (2009) Fresh fields and pathways new: recent genetic insights into cardiac malformation. Heart 95: 442-7

Lerone M, Bolino A, Martucciello G (1997) The genetics of anorectal malformations: a complex matter. Semin Pediatr Surg 6: 170-9

Levy SE, Chen YS, Graham BH, Wallace DC (2000) Expression and sequence analysis of the mouse adenine nucleotide translocase 1 and 2 genes. Gene 254: 57-66

Lizard G, Chardonnet Y, Chignol MC, Thivolet J (1990) Evaluation of mitochondrial content and activity with nonyl-acridine orange and rhodamine 123: flow cytometric analysis and comparison with quantitative morphometry. Comparative analysis by flow cytometry and quantitative morphometry of mitochondrial content and activity. Cytotechnology 3: 179-88

Luciakova K, Barath P, Poliakova D, Persson A, Nelson BD (2003) Repression of the human adenine nucleotide translocase-2 gene in growth-arrested human diploid cells: the role of nuclear factor-1. J Biol Chem 278: 30624-33

Lunardi J, Hurko O, Engel WK, Attardi G (1992) The multiple ADP/ATP translocase genes are differentially expressed during human muscle development. J Biol Chem 267: 15267-70

Luo J, Balkin N, Stewart JF, Sarwark JF, Charrow J, Nye JS (2000) Neural tube defects and the 13q deletion syndrome: evidence for a critical region in 13q33-34. Am J Med Genet 91: 227-30

Maclean K, Field MJ, Colley AS, Mowat DR, Sparrow DB, Dunwoodie SL, Kirk EP (2004) Kousseff syndrome: a causally heterogeneous disorder. Am J Med Genet A 124A: 307-12

Mancuso M, Filosto M, Choub A, Tentorio M, Broglio L, Padovani A, Siciliano G (2007) Mitochondrial DNA-related disorders. Biosci Rep 27: 31-7

Martin JA, Kochanek KD, Strobino DM, Guyer B, MacDorman MF (2005) Annual summary of vital statistics--2003. Pediatrics 115: 619-34

McMillin JB, Pauly DF (1988) Control of mitochondrial respiration in muscle. Mol Cell Biochem 81: 121-9

Megarbane H, Boehm N, Chouery E, Bernard R, Salem N, Halaby E, Levy N, Megarbane A (2005) X-linked reticulate pigmentary layer. Report of a new patient and demonstration of a skewed X-inactivation. Genet Couns 16: 85-9

Menten B, Maas N, Thienpont B, Buysse K, Vandesompele J, Melotte C, de Ravel T, Van Vooren S, Balikova I, Backx L, Janssens S, De Paepe A, De Moor B, Moreau Y, Marynen P, Fryns JP, Mortier G, Devriendt K, Speleman F, Vermeesch JR (2006) Emerging patterns of cryptic chromosomal imbalance in patients with idiopathic mental retardation and multiple congenital anomalies: a new series of 140 patients and review of published reports. J Med Genet 43: 625-33

Metts JC, 3rd, Kotkin L, Kasper S, Shyr Y, Adams MC, Brock JW, 3rd (1997) Genital malformations and coexistent urinary tract or spinal anomalies in patients with imperforate anus. J Urol 158: 1298-300
Miller DC, Saigal CS, Litwin MS (2009) The demographic burden of urologic diseases in America. Urol Clin North Am 36: 11-27, v
Mitchell JR, Wood E, Collins K (1999) A telomerase component is defective in the human disease dyskeratosis congenita. Nature 402: 551-5
Mo R, Kim JH, Zhang J, Chiang C, Hui CC, Kim PC (2001) Anorectal malformations caused by defects in sonic hedgehog signaling. Am J Pathol 159: 765-74
Moore SW (2008) Down syndrome and the enteric nervous system. Pediatr Surg Int 24: 873-83
Morcuende JA, Weinstein SL (2003) Developmental skeletal anomalies. Birth Defects Res C Embryo Today 69: 197-207
Morgan EA, Nguyen SB, Scott V, Stadler HS (2003) Loss of Bmp7 and Fgf8 signaling in Hoxa13-mutant mice causes hypospadia. Development 130: 3095-109
Munnich A, Rustin P (2001) Clinical spectrum and diagnosis of mitochondrial disorders. Am J Med Genet 106: 4-17
Nelson K, Holmes LB (1989) Malformations due to presumed spontaneous mutations in newborn infants. N Engl J Med 320: 19-23
Nichols D, Chmiel J, Berger M (2008) Chronic inflammation in the cystic fibrosis lung: alterations in inter- and intracellular signaling. Clin Rev Allergy Immunol 34: 146-62
Nicoletti I, Migliorati G, Pagliacci MC, Grignani F, Riccardi C (1991) A rapid and simple method for measuring thymocyte apoptosis by propidium iodide staining and flow cytometry. J Immunol Methods 139: 271-9
Nijhuis-van der Sanden MW, Eling PA, Otten BJ (2003) A review of neuropsychological and motor studies in Turner Syndrome. Neurosci Biobehav Rev 27: 329-38
Nora JJ (1993) Causes of congenital heart diseases: old and new modes, mechanisms, and models. Am Heart J 125: 1409-19
Nussbaum Robert L. MRR, Willard Huntington F. (2007) Thompson and Thompson Genetics in Medicine, 7 edn. Saunders Elsevier, Philadelphia
Ogino Y, Suzuki K, Haraguchi R, Satoh Y, Dolle P, Yamada G (2001) External genitalia formation: role of fibroblast growth factor, retinoic acid signaling, and distal urethral epithelium. Ann N Y Acad Sci 948: 13-31
Paduch DA, Fine RG, Bolyakov A, Kiper J (2008) New concepts in Klinefelter syndrome. Curr Opin Urol 18: 621-7
Parida SK, Hall BD, Barton L, Fujimoto A (1995) Penoscrotal transposition and associated anomalies: report of five new cases and review of the literature. Am J Med Genet 59: 68-75
Partington MW, Marriott PJ, Prentice RS, Cavaglia A, Simpson NE (1981) Familial cutaneous amyloidosis with systemic manifestations in males. Am J Med Genet 10: 65-75
Partington MW, Prentice RS (1989) X-linked cutaneous amyloidosis: further clinical and pathological observations. Am J Med Genet 32: 115-9
Paulozzi LJ (1999) International trends in rates of hypospadias and cryptorchidism. Environ Health Perspect 107: 297-302
Perriton CL, Powles N, Chiang C, Maconochie MK, Cohn MJ (2002) Sonic hedgehog signaling from the urethral epithelium controls external genital development. Dev Biol 247: 26-46
Peshavariya HM, Dusting GJ, Selemidis S (2007) Analysis of dihydroethidium fluorescence for the detection of intracellular and extracellular superoxide produced by NADPH oxidase. Free Radic Res 41: 699-712
Pietila M, Pirinen E, Keskitalo S, Juutinen S, Pasonen-Seppanen S, Keinanen T, Alhonen L, Janne J (2005) Disturbed keratinocyte differentiation in transgenic mice and organotypic

keratinocyte cultures as a result of spermidine/spermine N-acetyltransferase overexpression. J Invest Dermatol 124: 596-601
Poblete Gutierrez P, Eggermann T, Holler D, Jugert FK, Beermann T, Grussendorf-Conen EI, Zerres K, Merk HF, Frank J (2002) Phenotype diversity in familial cylindromatosis: a frameshift mutation in the tumor suppressor gene CYLD underlies different tumors of skin appendages. J Invest Dermatol 119: 527-31
Pollex RL, Hegele RA (2007) Copy number variation in the human genome and its implications for cardiovascular disease. Circulation 115: 3130-8
Post LC, Innis JW (1999) Infertility in adult hypodactyly mice is associated with hypoplasia of distal reproductive structures. Biol Reprod 61: 1402-8
Ramalho-Santos M, Melton DA, McMahon AP (2000) Hedgehog signals regulate multiple aspects of gastrointestinal development. Development 127: 2763-72
Ravnan JB, Tepperberg JH, Papenhausen P, Lamb AN, Hedrick J, Eash D, Ledbetter DH, Martin CL (2006) Subtelomere FISH analysis of 11 688 cases: an evaluation of the frequency and pattern of subtelomere rearrangements in individuals with developmental disabilities. J Med Genet 43: 478-89
Raymond FL, Tarpey P (2006) The genetics of mental retardation. Hum Mol Genet 15 Spec No 2: R110-6
Reers M, Smiley ST, Mottola-Hartshorn C, Chen A, Lin M, Chen LB (1995) Mitochondrial membrane potential monitored by JC-1 dye. Methods Enzymol 260: 406-17
Richards AA, Santos LJ, Nichols HA, Crider BP, Elder FF, Hauser NS, Zinn AR, Garg V (2008) Cryptic chromosomal abnormalities identified in children with congenital heart disease. Pediatr Res 64: 358-63
Rozen S, Skaletsky H (2000) Primer3 on the WWW for general users and for biologist programmers. Methods Mol Biol 132: 365-86
Ryan AK, Goodship JA, Wilson DI, Philip N, Levy A, Seidel H, Schuffenhauer S, Oechsler H, Belohradsky B, Prieur M, Aurias A, Raymond FL, Clayton-Smith J, Hatchwell E, McKeown C, Beemer FA, Dallapiccola B, Novelli G, Hurst JA, Ignatius J, Green AJ, Winter RM, Brueton L, Brondum-Nielsen K, Scambler PJ, et al. (1997) Spectrum of clinical features associated with interstitial chromosome 22q11 deletions: a European collaborative study. J Med Genet 34: 798-804
Satoh M, Yasuda T, Higaki T, Goto M, Tanuma S, Ide T, Furuichi Y, Sugimoto M (2003) Innate apoptosis of human B lymphoblasts transformed by Epstein-Barr virus: modulation by cellular immortalization and senescence. Cell Struct Funct 28: 61-70
Schweizer P, Kalhoff H, Horneff G, Wahn V, Diekmann L (1999) [Polysaccharide specific humoral immunodeficiency in ectodermal dysplasia. Case report of a boy with two affected brothers]. Klin Padiatr 211: 459-61
Sebat J, Lakshmi B, Malhotra D, Troge J, Lese-Martin C, Walsh T, Yamrom B, Yoon S, Krasnitz A, Kendall J, Leotta A, Pai D, Zhang R, Lee YH, Hicks J, Spence SJ, Lee AT, Puura K, Lehtimaki T, Ledbetter D, Gregersen PK, Bregman J, Sutcliffe JS, Jobanputra V, Chung W, Warburton D, King MC, Skuse D, Geschwind DH, Gilliam TC, Ye K, Wigler M (2007) Strong association of de novo copy number mutations with autism. Science 316: 445-9
Sebold CD, Romie S, Szymanska J, Torres-Martinez W, Thurston V, Muesing C, Vance GH (2005) Partial trisomy 2q: report of a patient with dup (2)(q33.1q35). Am J Med Genet A 134A: 80-3
Sefiani A, Abel L, Heuertz S, Sinnett D, Lavergne L, Labuda D, Hors-Cayla MC (1989) The gene for incontinentia pigmenti is assigned to Xq28. Genomics 4: 427-9

Selzer RR, Richmond TA, Pofahl NJ, Green RD, Eis PS, Nair P, Brothman AR, Stallings RL (2005) Analysis of chromosome breakpoints in neuroblastoma at sub-kilobase resolution using fine-tiling oligonucleotide array CGH. Genes Chromosomes Cancer 44: 305-19

Sharer JD (2005) The adenine nucleotide translocase type 1 (ANT1): a new factor in mitochondrial disease. IUBMB Life 57: 607-14

Sharpe RM (2003) The 'oestrogen hypothesis'- where do we stand now? Int J Androl 26: 2-15

Shaw-Smith C, Redon R, Rickman L, Rio M, Willatt L, Fiegler H, Firth H, Sanlaville D, Winter R, Colleaux L, Bobrow M, Carter NP (2004) Microarray based comparative genomic hybridisation (array-CGH) detects submicroscopic chromosomal deletions and duplications in patients with learning disability/mental retardation and dysmorphic features. J Med Genet 41: 241-8

Sitton JE, Reimund EL (1992) Extramedullary hematopoiesis of the cranial dura and anhidrotic ectodermal dysplasia. Neuropediatrics 23: 108-10

Smahi A, Courtois G, Vabres P, Yamaoka S, Heuertz S, Munnich A, Israel A, Heiss NS, Klauck SM, Kioschis P, Wiemann S, Poustka A, Esposito T, Bardaro T, Gianfrancesco F, Ciccodicola A, D'Urso M, Woffendin H, Jakins T, Donnai D, Stewart H, Kenwrick SJ, Aradhya S, Yamagata T, Levy M, Lewis RA, Nelson DL (2000) Genomic rearrangement in NEMO impairs NF-kappaB activation and is a cause of incontinentia pigmenti. The International Incontinentia Pigmenti (IP) Consortium. Nature 405: 466-72

Smahi A, Hyden-Granskog C, Peterlin B, Vabres P, Heuertz S, Fulchignoni-Lataud MC, Dahl N, Labrune P, Le Marec B, Piussan C, et al. (1994) The gene for the familial form of incontinentia pigmenti (IP2) maps to the distal part of Xq28. Hum Mol Genet 3: 273-8

Smith ED (1988) Incidence, frequency of types, and etiology of anorectal malformations. Birth Defects Orig Artic Ser 24: 231-46

Spouge D, Baird PA (1986) Imperforate anus in 700,000 consecutive liveborn infants. Am J Med Genet Suppl 2: 151-61

Stepien G, Torroni A, Chung AB, Hodge JA, Wallace DC (1992) Differential expression of adenine nucleotide translocator isoforms in mammalian tissues and during muscle cell differentiation. J Biol Chem 267: 14592-7

Sunyaev S, Ramensky V, Koch I, Lathe W, 3rd, Kondrashov AS, Bork P (2001) Prediction of deleterious human alleles. Hum Mol Genet 10: 591-7

Suzuki K, Ogino Y, Murakami R, Satoh Y, Bachiller D, Yamada G (2002) Embryonic development of mouse external genitalia: insights into a unique mode of organogenesis. Evol Dev 4: 133-41

Tarpey PS, Stevens C, Teague J, Edkins S, O'Meara S, Avis T, Barthorpe S, Buck G, Butler A, Cole J, Dicks E, Gray K, Halliday K, Harrison R, Hills K, Hinton J, Jones D, Menzies A, Mironenko T, Perry J, Raine K, Richardson D, Shepherd R, Small A, Tofts C, Varian J, West S, Widaa S, Yates A, Catford R, Butler J, Mallya U, Moon J, Luo Y, Dorkins H, Thompson D, Easton DF, Wooster R, Bobrow M, Carpenter N, Simensen RJ, Schwartz CE, Stevenson RE, Turner G, Partington M, Gecz J, Stratton MR, Futreal PA, Raymond FL (2006) Mutations in the gene encoding the Sigma 2 subunit of the adaptor protein 1 complex, AP1S2, cause X-linked mental retardation. Am J Hum Genet 79: 1119-24

Thienpont B, Mertens L, de Ravel T, Eyskens B, Boshoff D, Maas N, Fryns JP, Gewillig M, Vermeesch JR, Devriendt K (2007) Submicroscopic chromosomal imbalances detected by array-CGH are a frequent cause of congenital heart defects in selected patients. Eur Heart J 28: 2778-84

Thuresson AC, Bondeson ML, Edeby C, Ellis P, Langford C, Dumanski JP, Anneren G (2007) Whole-genome array-CGH for detection of submicroscopic chromosomal imbalances in children with mental retardation. Cytogenet Genome Res 118: 1-7

Tollervey D, Kiss T (1997) Function and synthesis of small nucleolar RNAs. Curr Opin Cell Biol 9: 337-42

Trask BJ (2002) Human cytogenetics: 46 chromosomes, 46 years and counting. Nat Rev Genet 3: 769-78

Urban AE, Korbel JO, Selzer R, Richmond T, Hacker A, Popescu GV, Cubells JF, Green R, Emanuel BS, Gerstein MB, Weissman SM, Snyder M (2006) High-resolution mapping of DNA copy alterations in human chromosome 22 using high-density tiling oligonucleotide arrays. Proc Natl Acad Sci U S A 103: 4534-9

Venkatraman ES, Olshen AB (2007) A faster circular binary segmentation algorithm for the analysis of array CGH data. Bioinformatics 23: 657-63

von Kleist-Retzow JC, Schauseil-Zipf U, Michalk DV, Kunz WS (2003) Mitochondrial diseases--an expanding spectrum of disorders and affected genes. Exp Physiol 88: 155-66

Walsh LE, Vance GH, Weaver DD (2001) Distal 13q Deletion Syndrome and the VACTERL association: case report, literature review, and possible implications. Am J Med Genet 98: 137-44

Wang HU, Chen ZF, Anderson DJ (1998) Molecular distinction and angiogenic interaction between embryonic arteries and veins revealed by ephrin-B2 and its receptor Eph-B4. Cell 93: 741-53

Warnes CA, Liberthson R, Danielson GK, Dore A, Harris L, Hoffman JI, Somerville J, Williams RG, Webb GD (2001) Task force 1: the changing profile of congenital heart disease in adult life. J Am Coll Cardiol 37: 1170-5

Warot X, Fromental-Ramain C, Fraulob V, Chambon P, Dolle P (1997) Gene dosage-dependent effects of the Hoxa-13 and Hoxd-13 mutations on morphogenesis of the terminal parts of the digestive and urogenital tracts. Development 124: 4781-91

Wei F, Cheng S, Badie N, Elder F, Scott C, Jr., Nicholson L, Ross JL, Zinn AR (2001) A man who inherited his SRY gene and Leri-Weill dyschondrosteosis from his mother and neurofibromatosis type 1 from his father. Am J Med Genet 102: 353-8

Williams DL (2008) Oxidative stress and the eye. Vet Clin North Am Small Anim Pract 38: 179-92, vii

Xing C, Sestak AL, Kelly JA, Nguyen KL, Bruner GR, Harley JB, Gray-McGuire C (2007) Localization and replication of the systemic lupus erythematosus linkage signal at 4p16: interaction with 2p11, 12q24 and 19q13 in European Americans. Hum Genet 120: 623-31

Yagi H, Furutani Y, Hamada H, Sasaki T, Asakawa S, Minoshima S, Ichida F, Joo K, Kimura M, Imamura S, Kamatani N, Momma K, Takao A, Nakazawa M, Shimizu N, Matsuoka R (2003) Role of TBX1 in human del22q11.2 syndrome. Lancet 362: 1366-73

Yan SD, Zhu H, Zhu A, Golabek A, Du H, Roher A, Yu J, Soto C, Schmidt AM, Stern D, Kindy M (2000) Receptor-dependent cell stress and amyloid accumulation in systemic amyloidosis. Nat Med 6: 643-51

Yan Y, Dalmasso G, Nguyen HT, Obertone TS, Charrier-Hisamuddin L, Sitaraman SV, Merlin D (2008) Nuclear factor-kappaB is a critical mediator of Ste20-like proline-/alanine-rich kinase regulation in intestinal inflammation. Am J Pathol 173: 1013-28

Zhang MQ (1998) Statistical features of human exons and their flanking regions. Hum Mol Genet 7: 919-32

Zinn AR, Roeltgen D, Stefanatos G, Ramos P, Elder FF, Kushner H, Kowal K, Ross JL (2007) A Turner syndrome neurocognitive phenotype maps to Xp22.3. Behav Brain Funct 3: 24